Sensitivity Analysis for Oil Fate and Exposure Modeling of a Subsea Blowout – Data Report

By: Deborah French-McCay and Deborah Crowley
RPS Ocean Science
55 Village Square, South Kingstown, Rhode Island 02879, USA
T +1 401 789-6224
Debbie.McCay@rpsgroup.com
www.rpsgroup.com | www.asascience.com

Prepared For:
American Petroleum Institute (API)
Washington, DC
API Project 2015- 110161

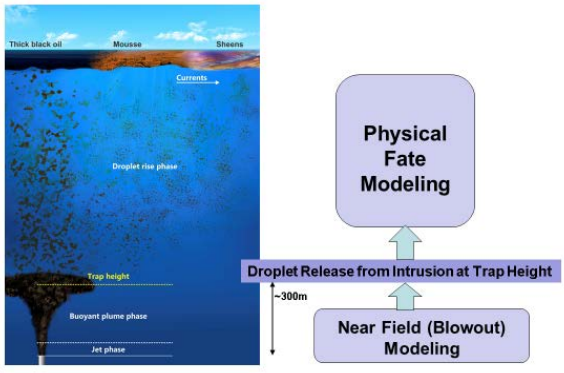

June 2018

Table of Contents

List of Figures

List of Tables

Summary

The objectives for using subsea dispersant injection (SSDI) on an uncontrolled blowout in deep water are to reduce the amount of oil reaching the water surface, where it could oil wildlife and shorelines, and to reduce the exposure of humans and wildlife to volatile hydrocarbons released from surfaced oil. The amount of oil reaching the surface is primarily a function of the oil droplet size distribution and SSDI reduces oil droplet sizes released to the water column. In prior work, French-McCay et al. (2018d) performed oil spill transport and fate modeling of a hypothetical example blowout at 1400 m in DeSoto Canyon in the Gulf of Mexico, which was used to predict the volume of water that would contain oil above specified concentrations, the amount and distribution of surface oil, and the amount and locations of oil that would strand on shorelines with and without SSDI application. The purpose was to inform the decision-making process related to subsea dispersant use by developing a quantitative Comparative Risk Assessment (CRA) of alternative response options.

As the CRA approach developed in the original study (French-McCay et al. 2018d; Bock et al. 2018; Walker et al. 2018) was tested with just one spill scenario (one spill site, discharge volume, oil type), the next step was to evaluate the sensitivity of the oil spill model results quantifying exposure to key inputs. The objectives of the analysis herein are to evaluate the sensitivity of model results to model inputs and to explore the applicability of the CRA modeling results to blowouts of other spill sizes, water depths, etc.

The model results show that modeled mass balance (i.e., fraction of oil in each environmental compartment, such as water surface, atmosphere, water column and sediments) of a subsurface release is most sensitive to the droplet size distribution of the oil released at depth and the depth of the release. The residence time of oil droplets in the water column, and the fraction of the released oil dissolved and degraded in the water column, increased substantially with decreasing droplet size. The assumed biodegradation rates in deep water affected the ratio between non-degraded dissolved and particulate oil hydrocarbons and biodegradation products (i.e., breakdown products and microbial biomass), but the fraction of oil surfacing, evaporating and affecting shorelines was not sensitive to the assumed biodegradation rates. The mass of oil hydrocarbons on the surface, emitted to the atmosphere and stranding on shorelines was controlled by the droplet size distribution of the released oil. Other model inputs had much less influence on the overall mass balance and fate of the oil.

The droplet size distribution and fraction of the oil surfacing was directly related to the exit velocity from the release orifice. Exit velocity was calculated from the total oil and gas flow rate and cross-sectional area of the orifice, accounting for gas compression at depth. Thus, keeping exit velocity constant, the surfacing oil mass was approximately proportional to oil flow rate, but the percent distribution of the mass balance was similar regardless of the oil flow rate. These findings allow extrapolation of the reported results from the sensitivity analysis to other oil spill volumes and gas-to-oil ratios.

For a given droplet size distribution, the rise rates of oil droplets were a function of the changing oil density as the oil weathered during the rise and the ambient water density profile. The modeled oil was a light crude, typical of many other light crude oils produced globally. Deep water density profiles are similar throughout the Gulf of Mexico to the modeled spill site. Thus, the modeled mass balance and other results are applicable to other deep water releases with similar droplet size distributions from the same water depths.

The implications of this work are that the benefits of SSDI use on deep water releases are demonstrable through its reduction of the oil droplet size distribution of oil released to the ambient water column.

Reduction in oil droplet size from a deep water blowout would disperse more oil into a larger water volume at depth; enhance biodegradation; reduce surface water, nearshore and shoreline exposure to floating oil and entrained/dissolved oil in the upper water column, and reduce human and wildlife exposure to volatile hydrocarbons.

1 Introduction

In 2010 during the Deepwater Horizon (DWH) oil spill, subsea dispersant injection (SSDI) was utilized at the source to mitigate the overall impact of the released oil. Among the concerns driving the decision to utilize SSDI were the amount of oil reaching the water surface, where it could oil wildlife and shorelines, and the exposure of humans and wildlife to volatile hydrocarbons released from surfaced oil. The objective for using SSDI was to reduce the droplet sizes of oil released into the water column so that less oil would surface and more of the oil would "weather" at depth (OSAT 2010). Oil weathering includes dissolution of soluble and semi-soluble components and biodegradation, both of which are facilitated by breaking up oil into smaller droplet sizes with higher surface area-to-volume ratios (Mackay et al. 1982; NRC 1989, 2003, 2005; Reed et al. 1999; French-McCay 2002, 2003, 2004; Venosa and Holder 2007; Lee et al. 2015). The additional weathering at depth by use of SSDI would reduce the amount of volatiles reaching the surface and evaporating, particularly in the area of active response near the wellhead where benzene and other hydrocarbon levels in the atmosphere have been considered a human health risk.

In prior work (French-McCay et al. 2018d; Bock et al. 2018; Walker et al. 2018) an approach was developed, which combined predictions from an oil spill fate model with a novel method of quantifying valued ecosystem component (VEC) exposures and recovery, to perform a Comparative Risk Assessment (CRA)of various response options. The CRA approach was used to evaluate an example hypothetical offshore deepwater well-control incident in order to identify an oil spill response strategy (including considering SSDI) that would minimize ecological risks, reduce exposure of surface dwelling wildlife and response workers to volatile organic compounds (VOCs), and minimize socioeconomic disturbance. The approach was used to evaluate the implications of various response strategies, i.e., no intervention, mechanical recovery, in-situ burning (ISB), surface dispersant application, and SSDI at the source, individually and in combination. Stakeholders typically accept the use of mechanical recovery equipment when it is feasible and available. However, both the use of ISB and dispersants usually require more in-depth analysis of potential trade-offs. The study endeavored to inform that decision-making process, specifically with respect to SSDI for deep-sea blowouts, using a quantitative approach based on state-of-the-art scientific understanding and oil spill modeling. The oil spill transport and fate modeling was used to predict the volume of water that would contain oil above specified concentrations, the amount and distribution of surface oil, and the amount and locations of oil that could strand on shorelines with and without SSDI application.

As the CRA approach developed in the original study (French-McCay et al. 2018d; Bock et al. 2018; Walker et al. 2018) was tested with just one spill scenario (one spill site, discharge volume, oil type), the next step was to evaluate the sensitivity of the oil spill model results quantifying exposure to key inputs. The objective was to explore the applicability of the CRA modeling results to blowouts of other spill sizes, water depths, etc. Incorporating sensitivity analyses provides an opportunity to identify the factors that control the results (Kaplan and Garrick, 1981).

During a subsea blowout in deep water, an oil jet and buoyant plume carries oil and gas upwards to a water depth (or depths) where, due to the ambient density gradient in the ocean, the buoyant plume is arrested, or "trapped" and forms an intrusion (Socolofsky et al. 2011, 2015). Oil droplets are released

from the intrusion to the water column above, where they subsequently rise and are transported by ambient currents. Based on test cases using several models, the trap height is typically a few hundred meters above the release depth (Socolofsky et al. 2015). Thus, we focused our study on releases at >400 m depth.

Based on prior studies (French-McCay 2002; NRC 2005; Chen and Yapa 2007; Johansen et al. 2013; Zhao et al. 2014, 2015; North et al. 2015; French-McCay et al. 2015, 2016, 2018a,c,d; Buchholz et al. 2016; Nissanka and Yapa. 2016; Testa et al. 2016; Spaulding et al. 2017; Daae et al. 2018), oil fate and the modeled mass balance (i.e., fraction of oil in each environmental compartment, such as water surface, atmosphere, water column and sediments) of a subsurface release is highly sensitive to the droplet size distribution of the oil released at depth and the depth of the release. In the present work, nearfield modeling was first performed to evaluate potential trap heights and droplet size distributions that might be released from an uncontrolled well blowout. Then far field modeling of released oil droplets was performed varying oil droplet size distribution and release depth, along with other variables, to examine the sensitivity of the modeled oil mass balance, as well as several exposure metrics used in the CRA analysis, to model inputs.

This data report contains a summary of model inputs and outputs for the model sensitivity analyses. The findings will be synthesized and implications discussed in a later publication.

2 Methods

2.1 Models

Following the methods of Spaulding et al. (2017) and French-McCay et al. (2018a,b,c,d), we have modeled deepwater blowouts using two sequential models: OILMAP DEEP (OIL Model Application Package for DEEPwater releases; Crowley et al. 2014; Spaulding et al. 2015, 2017) and the SIMAP (Spill Impact Model Application Package) oil fate model (French-McCay 2003, 2004; French-McCay et al. 2015, 2016, 2018b). OILMAP DEEP evaluates the nearfield dynamics of a blowout plume, and the droplet sizes produced subject to the turbulent energy involved and the oil properties, with and without the application of dispersants (Spaulding et al. 2000; Crowley et al. 2014; Spaulding et al. 2015, 2017; Li et al. 2017). This determines the initial conditions for the SIMAP model, which calculates transport and fate of the oil in the far field after release from the near-field buoyant plume.

Based on modeling analyses by Spaulding et al. (2015, 2017), as well as field observation following the DWH spill (Valentine et al. 2010; Reddy et al. 2012), most of the gas dissolves in the nearfield plume of a deepwater oil and gas release such as those modeled here. Furthermore, gas hydrocarbons (molecules with $\leq$ 5 carbons, C1 to C5) are much less toxic than the oil hydrocarbons (molecules with $\geq$ 6 carbons, C6+) to aquatic biota (McGrath et al. 2005; Redman and Parkerton 2015), and so are not of interest for evaluation of oil spill environmental effects. Therefore, the far field modeling tracked so-called “dead oil”, i.e., oil that no longer includes gases (<C6) within it. The oil mass and droplet size distribution in the trapped plume intrusion is used as input to SIMAP, which then simulates the buoyant rise of the oil droplets (as a function of droplet size and density which is dependent on weathering state), dissolution (which is faster for smaller droplets), current transport, dilution and biodegradation (which is faster for releases with smaller droplet sizes because of increased dissolution and therefore bioavailability for microbes), as well as the dynamics and fate of surfaced oil.

The far field model SIMAP quantifies oil trajectory, concentrations of 18 oil hydrocarbon pseudo-components as droplet and dissolved phases in the water column, areas swept by floating oil of varying

mass concentrations and thicknesses, shorelines oiled to varying degrees, and amount of oil settling to sediments. Processes simulated by SIMAP include spreading (gravitational and by shearing), evaporation of 17 volatile oil components from surface oil, transport on the surface and in the water column, randomized dispersion from small-scale motions (mixing), emulsification, entrainment of oil as droplets into the water column due to waves (either without or facilitated by dispersant application), dissolution of 9 soluble and semi-soluble hydrocarbon (S/SS HC) components, volatilization of dissolved hydrocarbons from the surface water, adherence of oil droplets to suspended particulate matter (SPM), adsorption of semi-soluble hydrocarbons to SPM, sedimentation, stranding on shorelines, and degradation (based on component-specific first-order biodegradation and photo-oxidation rates). The model tracks soluble and semi-soluble components of the oil (i.e., monoaromatic hydrocarbons (MAHs, such as benzene, toluene, ethylbenzene and xylene, BTEX), polycyclic aromatic hydrocarbons (PAHs), and soluble alkanes; i.e., S/SS HCs), as well as insoluble volatile aliphatic hydrocarbons, separately from high-molecular weight non-volatile and insoluble components of the oil. Sublots of the discharged oil are represented by Lagrangian Elements ("spillets"), each characterized by location, state (floating, droplet in water, sedimented, ashore), mass of the various hydrocarbon components, water content, thickness, diameter, density, viscosity, and associated SPM mass. A separate set of Lagrangian Elements is used to track mass and movements of the dissolved hydrocarbons. (See French-McCay et al. (2018b,d) for a description of the model algorithms and assumptions.)

The SIMAP model has been validated with data from >20 large oil spills, including the *Exxon Valdez*, *North Cape* and Deepwater Horizon (DWH) oil spills (French and Rines 1997; French-McCay 2003, 2004; French-McCay and Rowe 2004; French-McCay et al. 2015, 2015, 2018a,c), as well as test spills designed to verify the model (French et al. 1997). These studies showed that the accuracy of oil trajectories depended on the accuracy of the current and wind data input to the model, and that, given reasonably accurate input data for transport (as evidenced by floating oil trajectory and shoreline oiling distributions as compared to observations), predicted concentrations of oil hydrocarbons in water and sediments agreed within an order of magnitude with measurements.

2.2 General Approach

The scenarios examined were for oil and gas blowouts in the northern Gulf of Mexico. In the original CRA study (French-McCay et al. 2018d), a hypothetical spill site in the northeastern Gulf of Mexico (in De Soto Canyon) was modeled assuming varying response strategies:

1. No intervention (natural attenuation);
2. Mechanical recovery;
3. Mechanical recovery (M), *in-situ* burning (B), and surface dispersant (SD) application (MBSD);
4. Subsea dispersant injection (SSDI), in addition to MBSD; and
5. SSDI alone.

The spill sites for the sensitivity analysis were moved much closer to shore than the original CRA site, to near Mississippi Canyon, which allows evaluation of the effects of using SSDI for reducing shoreline oiling, as well as reducing floating oil and VOC emissions. Two water depths were used for the discharge location (Figure 1). In the original CRA study, the release was assumed to be at 1400 m at the location noted in Figure 1.

- Release at 500m in a location 63 km from the nearest shoreline in southern Louisiana, where the bathymetry is about 550 m: 89.168 W, 28.476 N
- Release at 1400m in a location 92 km from the nearest shoreline in southern Louisiana, where the bathymetry is about 1450 m: 88.830 W, 28.274 N

The following steps were taken in the present work.

- A matrix of nearfield model runs, varying oil and gas discharge rates, water depth and other variables, was performed using the OILMAP-Deep model (Spaulding et al. 2017). Results of this modeling provided estimates of:
  - Trap height for release of oil droplets to the far field from the buoyant plume, and
  - Median droplet size of oil released from the intrusion (i.e., at the trap height).
- Probabilistic (stochastic) modeling was performed using the far field oil fate model SIMAP (French-McCay 2004; French-McCay et al. 2018b) to examine likely oil trajectories under varying meteorological and oceanic (metocean) conditions. A typical metocean condition (i.e., that resulting in near median exposure to floating oil, shoreline oiling and water column contamination) was selected as the base case for far field analyses varying model inputs.
- A far field modeling matrix for SIMAP model runs was designed and run, varying the oil droplet size distribution and other inputs.
- Results of the far field modeling were compiled and presented in terms of mass balance and indicative exposure metrics.

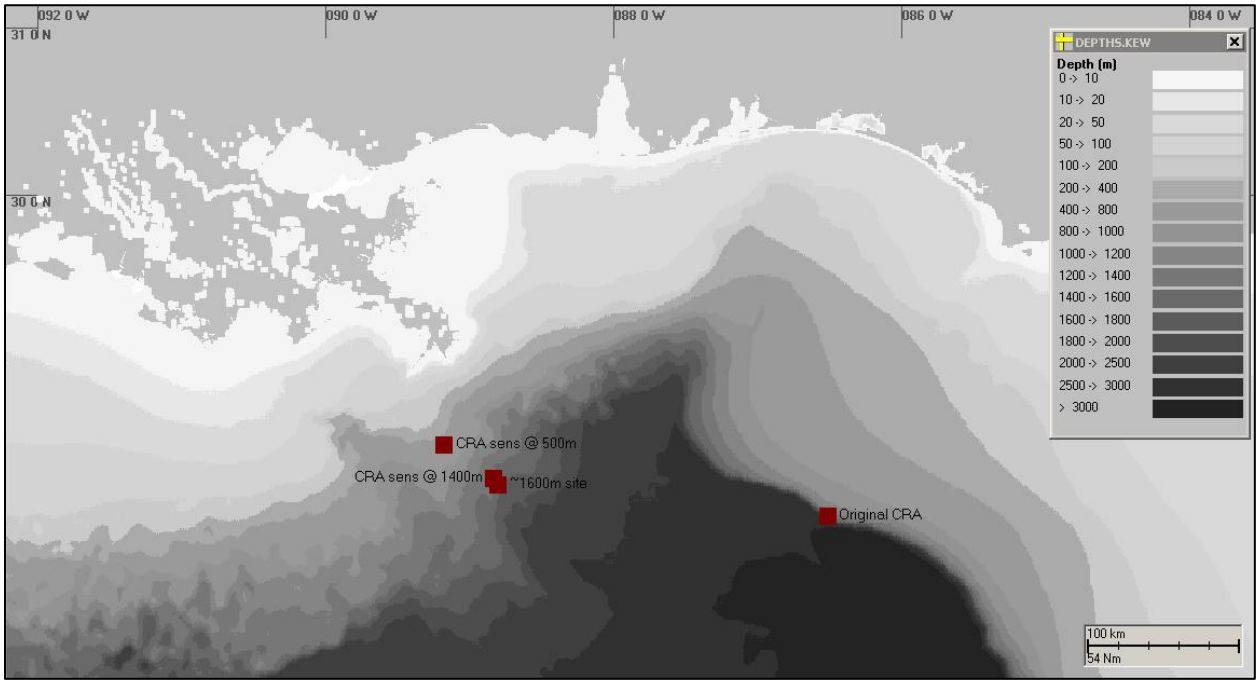

Figure 1. Assumed spill sites for original CRA (French-McCay et al. 2018d) and sensitivity ("sens") model runs at 500m or 1400m below the surface. The ~1600 m site was used for the initial probabilistic modeling.

2.3 Nearfield (OILMAP-Deep) Modeling Matrix

In order to evaluate the sensitivity of oil spill modeling results to oil droplet sizes (specifically the median diameter, taken as the mean of a lognormal distribution of droplet diameters, d_{50}) to spill scenario assumptions, a matrix of nearfield calculations was run using OILMAP-Deep (Spaulding et al. 2017), which was based on the inputs most influential to the results. The variables were:

- Two water depths, i.e.,1400m and 500m (1400 m was used in the CRA modeling)

- Two orifice sizes from which oil and gas flow, i.e., circular, with 18 ¾ inch (476 mm) inside diameter (as assumed for CRA modeling) and with a 6 inch inside diameter
- Seven oil flow rates: 10k, 20k, 45k, 60k, 80k, 100k and 120k bbl/day (1590-19,078 m^3/day; 45k = 45,000 bbl/day = 7154 m^3/day was assumed for CRA modeling)
- Two gas-to-oil ratios (GOR), e.g., 500 scf/stb (standard cubic foot per stock tank barrel; 2807 standard m^3 per m^3, sm^3/sm^3) and 2000 scf/stb (11,229 sm^3/sm^3; 2000 scf/stb was assumed for CRA modeling)

Assumptions and data inputs were the same as for the CRA modeling (French-McCay et al. 2018d), except as noted in the following.

Annual mean salinity/temperature/density profiles for the spill sites were taken from the World Ocean Atlas 2001 (WOA01, Boyer et al. 2004), compiled and maintained by the US National Oceanographic Data Center (www.nodc.noaa.gov). Figure 1 shows the profiles used, which are very similar at the two spill sites. The temperatures at the 500-m and 1400-m release depths were 8.27 ºC and 4.35ºC, respectively.

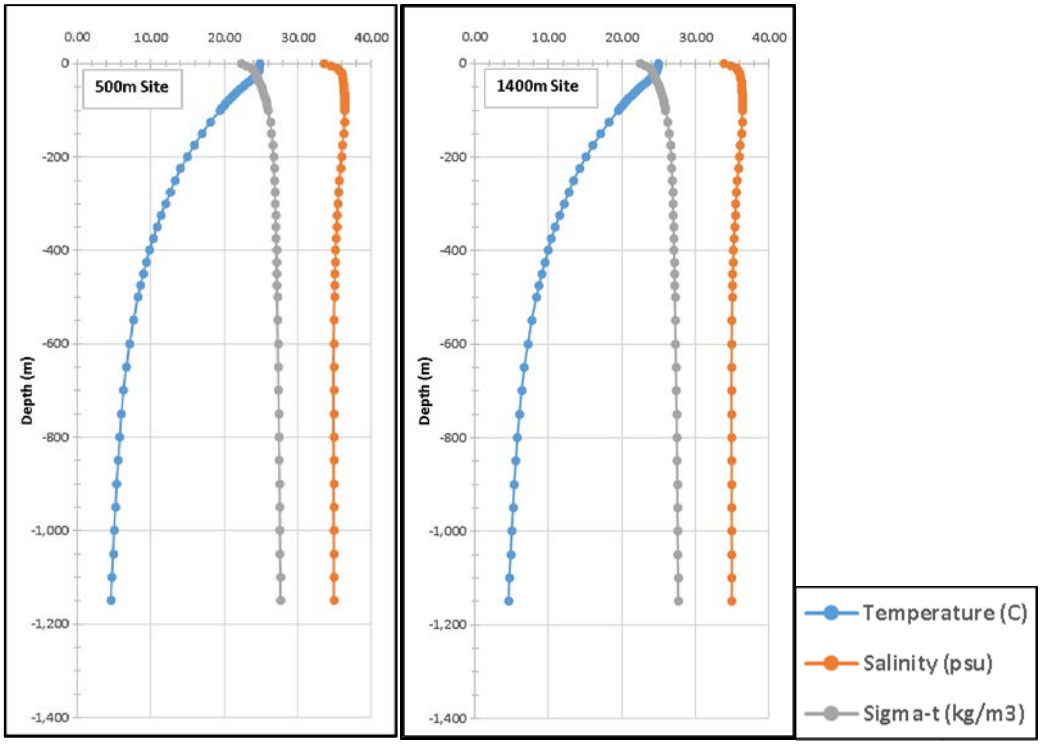

Figure 2. Temperature, salinity and density (sigma-t) profiles at the spill sites modeled.

The oil is assumed HOOPS crude oil (ExxonMobil 2016), as used for the CRA modeling (French-McCay et al. 2018d):

- The oil density (for dead oil) at 16ºC is 0.854 g/cm^3 (API 34.2). Using a general regression for crude oil density versus temperature (French-McCay et al. 2015, 2018b), the dead oil density at 4.35ºC (for the 1400 m depth) is 0.8620 g/cm^3 and oil density at 8.27ºC (at 500 m depth) is 0.8592 g/cm^3.

- Dynamic viscosity (at standard shear rate 10/s; on dead oil) is 8.43 cP at 20°C and 5.02 cP at 40°C. Using these data and a viscosity-temperature curve (Arrhenius equation) fit to these two measurements (French-McCay et al. 2015, 2018b), viscosity is 13.34 cP at 4.35°C (for the 1400 m depth) and 11.84 cP at 8.27°C (at 500 m depth)
- Interfacial tension (oil-brine, IFT) of untreated oil is 16.6 mN/m (French-McCay et al. 2018d). For treated oil, the dispersant-to-oil ratios are (based on measurements by Venkataraman et al. 2013):
    - DOR = 100 or 1% dispersant, 0.194 mN/m
    - DOR = 50 or 2% dispersant, 0.121 mN/m
    - DOR = 200 or 0.5% dispersant, 2.89 mN/m

The release temperature of the oil and gas discharge is assumed 85°C. Gas compression was calculated assuming the gas is methane and using the Soave-Reldich-Kwong equation of state (Spaulding et al. 2015, 2017).

Model calculations and results related to the droplet size distribution modeling include:

- Exit velocity at the orifice (based on total volume of oil and gas flow at the release depth, divided by the cross-sectional area of the orifice)
- Median droplet size (d_{50})
- Maximum stable droplet size (d_{max}) for the orifice diameter and IFT (Li et al. 2017).

In addition, the nearfield plume trap heights above the release depths (500 m and 1400 m) were calculated for a range of release conditions, assuming the appropriate temperature-salinity profile (Figure 1).

2.4 Probabilistic Modeling

Probabilistic oil spill modeling has been employed for oil spill risk analyses in many studies to evaluate the likely trajectories of floating and subsurface oil (e.g., Spaulding et al. 1983; Al-Rabeh et al.1989; Price et al. 2003; Skognes and Johansen 2004; French-McCay et al. 2004, 2005; Buchholz et al. 2016). As performed in French-McCay et al. (2018d), in order to characterize the effects of natural variability in environmental conditions and to select a base-case set of metocean conditions (i.e., start date and time) for all the sensitivity analysis model runs (at both spill depths noted above), a single set of probabilistic (stochastic) model simulations was run. The probabilistic set involved 100 model runs, varying the spill date and time, and so wind, currents and other metocean conditions, assuming a spill of 45,000 bbl/day (7154 m^3/day) for 21 days and no response intervention (no SSDI, mechanical removal, in situ burning, or surface dispersant use). The droplet size distribution used for the probabilistic model simulations was the same as for the original CRA, assuming untreated oil. The far field release depth (i.e., trap height) used in these model runs was 1015 m below the surface, which was the modeled trap height in the CRA modeling analysis. From these results, a median case for surface floating and shoreline exposure was selected to be used as the base case metocean conditions for the far field modeling.

2.5 Farfield (SIMAP) Modeling Matrix

Thirty-seven SIMAP model cases were run to evaluate the change in mass balance with various assumed inputs, including those characterizing different spill response options:

1) No intervention (i.e., the base case)
2) MBSD only
3) SSDI without MBSD
4) SSDI combined with MBSD

Based on the nearfield modeling results, a range of representative median droplet sizes (d_{50}s) were selected for far field model runs with SIMAP (Table1). In addition, some cases were run with an alternative standard deviation of the assumed lognormal droplet size distribution (s_d = standard deviation of ln(d), where d is droplet diameter and d_{50} is the mean of ln(d)), which defines the breadth of the droplet size distribution. The model cases, each with unique d_{50} as well as other key inputs such as s_d, were selected based on the nearfield model results to provide a range of far field model inputs at each of the assumed trap-height release depths. Varying droplet sizes in the range of 1mm to 10mm (or more) has little effect on model results, as the oil surfaces rapidly from these depths. Fewer no-treatment cases (with d_{50} >1mm) were performed than cases with d_{50} <1mm (which could represent SSDI-treated cases or untreated releases with high exit velocities) and to gain more information. Thus, various permutations were modeled, representing a range of d_{50}, to examine in the far field results. The d_{50}s were selected at intervals to cover the possible sizes of oil droplets that could be produced.

Additionally, because of known sensitivity to oil droplet size, most of the model runs were performed varying the median droplet size (which shifts the entire droplet size distribution) initialized in the far field modeling to simulate various assumptions regarding the use and effectiveness of SSDI, but with no surface response activities (M, B, SD, and combinations thereof). However, some runs were made including MBSD. Additionally, the response activities were assumed to begin immediately at the start of the spill, to simplify the interpretation of results. In the original CRA study, response activities were assumed not to begin until needed resources could be deployed (i.e., after 2 days for MBSD, 6 days for SSDI).

Alternative assumed degradation (biodegradation and photo-oxidation) rates were also examined. The base case biodegradation and photo-oxidation rates used for most cases were those used for the original CRA (French-McCay et al. 2018d). The biodegradation rates had been developed as part of the the research for modeling the DWH oil spill (French-McCay et al., 2015, 2018b,c). Alternative rates used were 50% of the base rate, and zero degradation in the water column. The degradation rates of floating, shoreline and sediment oil were not changed.

For all model runs except one, the oil flow rate was assumed 45,000 bbl/day (7154 m^3/day). One run with a higher oil flow rate, i.e., 100,000 bbl/day (15,899 m^3/day), was run to demonstrate that the surfacing mass is approximately proportional to oil flow rate (keeping exit velocity constant), but the percent distribution of the mass balance is similar regardless of the oil flow rate. In addition, two cases were run including mechanical, *in situ* burning and surface dispersant (MBSD, assumptions as for the CRA): one for the 500-m release depth and one for the 1400-m release depth.

The d_{50} assumptions listed in Table 1 and used as input to the far field modeling would be predicted by the oil droplet size distribution model in OILMAP-Deep assuming the listed DOR and exit velocity. The associated oil flow rate was used as input to the far field model SIMAP. Other droplet size models might predict the listed d_{50}s using other assumptions and conditions. If so, the oil flow rate used in the far field modeling should match the assumed conditions. However, comparing the results for the 100,000 bbl/day (15,899 m^3/day) oil flow rate case to the 45,000 bbl/day (7154 m^3/day) case with the same d_{50} and s_d, the surfacing mass is proportional to oil flow rate and the percent distribution of the mass balance is similar regardless of the oil flow rate (see Section 7 below for discussion of results).

Table 1. Inputs for SIMAP far field model runs evaluating various droplet size distributions, in-water degradation rates, use or not of SSDI, and inclusion of MBSD with or without SSDI.

Case #	Release Depth (m)	Median Diameter d_{50} (um)	Standard Deviation (s_d)	SSDI Treatment*	Exit Velocity (m/s)*	Include MBSD?	Oil Flow Rate (bbl/day)	In-Water Degradation Rates**
1	1400	100	0.5	DOR=100	5.4	No	45,000	Base
2	1400	250	0.5	DOR=100	2.1	No	45,000	Base
3	1400	400	0.5	DOR=100	1.3	No	45,000	Base
4	1400	550	0.5	DOR=100	0.9	No	45,000	Base
5	1400	700	0.5	DOR=100	0.7	No	45,000	Base
6	1400	900	0.5	DOR=100	0.6	No	45,000	Base
7	1400	2000	0.5	Untreated	3.0	No	45,000	Base
8	1400	5000	0.5	Untreated	1.2	No	45,000	Base
9	1400	5000	0.5	Untreated	1.2	**Yes**	45,000	Base
10	1400	250	0.5	DOR=100	2.1	No	**100,000**	Base
11	1400	550	**0.8**	DOR=100	0.9	No	45,000	Base
12	500	100	0.5	DOR=100	5.4	No	45,000	Base
13	500	250	0.5	DOR=100	2.1	No	45,000	Base
13-BD50	500	250	0.5	DOR=100	2.1	No	45,000	**50% of Base**
13-BD0	500	250	0.5	DOR=100	2.1	No	45,000	**0**
14	500	400	0.5	DOR=100	1.3	No	45,000	Base
15	500	550	0.5	DOR=100	0.9	No	45,000	Base
16	500	700	0.5	DOR=100	0.7	No	45,000	Base
16-BD50	500	700	0.5	DOR=100	0.7	No	45,000	**50% of Base**
16-BD0	500	700	0.5	DOR=100	0.7	No	45,000	**0**
17	500	900	0.5	DOR=100	0.6	No	45,000	Base
18	500	2000	0.5	Untreated	3.0	No	45,000	Base
19	500	5000	0.5	Untreated	1.2	No	45,000	Base
19-BD50	500	5000	0.5	Untreated	1.2	No	45,000	**50% of Base**
19-BD0	500	5000	0.5	Untreated	1.2	No	45,000	**0**
20	500	5000	0.5	Untreated	1.2	**Yes**	45,000	Base
21	500	550	**0.8**	DOR=100	0.9	No	45,000	Base
22	**100**	250	0.5	DOR=100	2.1	No	45,000	Base
23	1400	50	**0.25**	DOR=100	11.0	No	45,000	Base
24	1400	50	**0.8**	DOR=100	11.0	No	45,000	Base
25	1400	175	0.5	DOR=100	3.0	No	45,000	Base
26	500	50	0.5	DOR=100	11.0	No	45,000	Base
27	500	50	**0.25**	DOR=100	11.0	No	45,000	Base
28	500	50	**0.8**	DOR=100	11.0	No	45,000	Base
29	1400	50	0.5	DOR=100	11.0	No	45,000	Base
30	1400	250	**0.8**	DOR=100	2.1	No	45,000	Base
31	500	250	**0.8**	DOR=100	2.1	No	45,000	Base

*The d_{50} listed and used as input to the far field modeling is predicted by the oil droplet size distribution model (Li et al. 2017) assuming the listed DOR and exit velocity. The associated oil flow rate was used as input to the far field model SIMAP.

** Base degradation rates were as used by French-McCay et al. (2018d).

3 Results

3.1 Nearfield Droplet Size Modeling

Figure 3 shows the calculated maximum stable oil droplet size (diameter) as a function of IFT for the HOOPS oil modeled and median water density at 500 -1400 m (1027 kg/m^3). The maximum stable droplet size ranges from ~1 mm for HOOPS oil treated with dispersant at DOR=100 to ~13 mm for untreated oil.

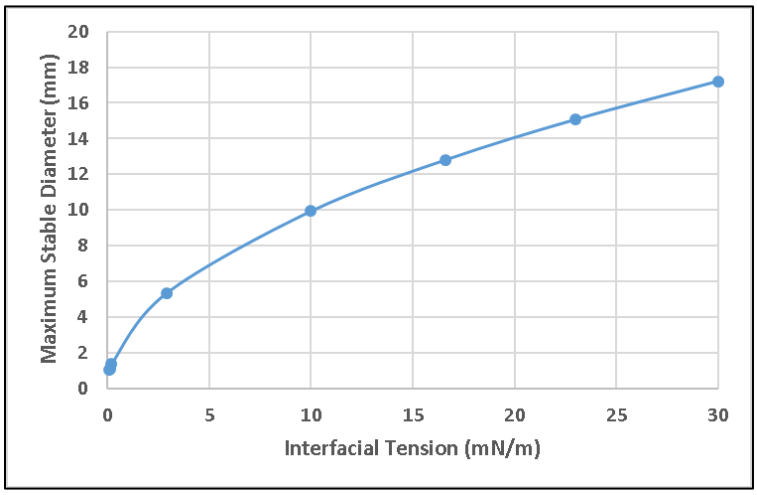

Figure 3. Maximum stable droplet diameter as a function of IFT for HOOPS oil released at the depths (500m, 1400m) and locations (Figure 1) modeled.

Results of the nearfield modeling are summarized in Tables 2-3 and Figures 4-6. The results for combinations of release depth, oil flow rate and GOR, assuming an 18.75-inch (476 mm) orifice, are presented in Table 2. Table 3 presents results for a 6-inch orifice. The results indicate:

- The estimated d_{50} declines with increasing exit velocity and decreasing IFT.
- The change in oil properties based on conditions at the two release depths of 1400m and 500m have a relatively insignificant influence on the droplet size prediction.
- The IFT change from untreated to DOR=100 is substantial (a factor 86 decrease), but the change in IFT from DOR=100 to DOR=50 is small (a factor 1.6 decrease). Therefore, reducing DOR from 100 to 50 (i.e., from 1% to 0.5% dispersant) has only a small effect on d_{50}. The IFT changes from untreated to DOR=200 (factor 5.7 decrease) and DOR=200 to DOR=100 (factor 15 decrease) do affect the d_{50} substantially.
- The estimated d_{50} is sensitive to IFT. However, the IFT relationship to DOR is somewhat uncertain.
- The exit velocity needs to be on the order of 60 m/s to reduce d_{50} of untreated oil to <100 μm. For a 6-inch orifice, the oil flow rate would need to be over 60,000 bbl/day (9539 m^3/day) at 500 m and GOR=2000 scf/stb (11,229 sm^3/sm^3), and higher for deeper depths and lower GOR. For an 18.75-inch (476 mm) orifice, the oil flow rate would need to be over 1.3 million bbl/day (212 thousand m^3/day) to reduce d_{50} to <100 μm.

Since the d_{50} is scaled to the exit velocity of the oil and gas coming through the orifice (Li et al. 2017), the same (oil plus gas) volume flow rate through an orifice with half the surface area would result in the same d_{50} as twice the flow through the same orifice size. Note that the gas volume flow rate is corrected for compression at depth, and so the same combination of oil flow rate and gas-to-oil ratio (GOR) at standard conditions (1 atm) would have different exit velocities (slower with increasing depth) and d_{50}s (larger with increasing depth) at different discharge depths (all other conditions being the same).

Table 2. Model inputs and and calculated exit velocity for 18.75-inch (476 mm) orifice. Median diameters (d_{50}) that were replaced by maximum stable droplet size are shown in red italicized font.

Depth (m)	Oil Rate (bbl /day)	Oil Rate (m^3/day)	GOR (scf/stb)	GOR at Release Depth (m^3/m^3)	Exit Velocity (m/s)	d_{50} (µm) at IFT = 16.6 mN/m	d_{50} (µm) at IFT = 2.89 mN/m	d_{50} (µm) at IFT = 0.194 mN/m	d_{50} (µm) at IFT = 0.121 mN/m
1400	10,000	1,590	500	0.80	0.19	*12,810*	*5345*	*1385*	*1094*
1400	20,000	3,180	500	0.80	0.37	*12,810*	*5345*	*1385*	*1094*
1400	45,000	7,154	500	0.80	0.84	7736	2580	665	539
1400	60,000	9,539	500	0.80	1.11	5743	1915	494	400
1400	80,000	12,719	500	0.80	1.49	4263	1421	367	297
1400	100,000	15,899	500	0.80	1.86	3383	1128	291	236
1400	120,000	19,078	500	0.80	2.23	2801	934	241	195
1400	10,000	1,590	2000	3.19	0.43	*12,810*	5100	1315	1066
1400	20,000	3,180	2000	3.19	0.87	7458	2487	641	520
1400	45,000	7,154	2000	3.19	1.95	3219	1073	277	224
1400	60,000	9,539	2000	3.19	2.60	2389	797	205	167
1400	80,000	12,719	2000	3.19	3.46	1774	591	153	124
1400	100,000	15,899	2000	3.19	4.33	1408	469	121	98
1400	120,000	19,078	2000	3.19	5.19	1165	389	100	81
500	10,000	1,590	500	2.26	0.34	*12,810*	*5345*	*1385*	*1094*
500	20,000	3,180	500	2.26	0.67	9528	3129	791	641
500	45,000	7,154	500	2.26	1.51	4113	1351	342	277
500	60,000	9,539	500	2.26	2.02	3053	1003	254	205
500	80,000	12,719	500	2.26	2.69	2266	744	188	152
500	100,000	15,899	500	2.26	3.36	1798	591	149	121
500	120,000	19,078	500	2.26	4.04	1489	489	124	100
500	10,000	1,590	2000	9.03	1.04	6094	2001	506	410
500	20,000	3,180	2000	9.03	2.07	2972	976	247	200
500	45,000	7,154	2000	9.03	4.66	1283	421	107	86
500	60,000	9,539	2000	9.03	6.22	952	313	79	64
500	80,000	12,719	2000	9.03	8.29	707	232	59	48
500	100,000	15,899	2000	9.03	10.36	561	184	47	38
500	120,000	19,078	2000	9.03	12.43	464	152	39	31

Table 3. Inputs and model results for 6-inch (152 mm) orifice.

Depth (m)	Oil Rate (bbl /day)	Oil Rate (m^3/day)	GOR (scf/stb)	GOR at Release Depth (m^3/m^3)	Exit Velocity (m/s)	d_{50} (µm) at IFT = 16.6 mN/m	d_{50} (µm) at IFT = 2.89 mN/m	d_{50} (µm) at IFT = 0.194 mN/m	d_{50} (µm) at IFT = 0.121 mN/m
1400	10,000	1,590	500	0.80	1.81	3467	1156	298	242
1400	20,000	3,180	500	0.80	3.63	1691	564	145	118
1400	45,000	7,154	500	0.80	8.16	730	243	63	51
1400	60,000	9,539	500	0.80	10.88	542	181	47	38
1400	80,000	12,719	500	0.80	14.51	402	134	35	28
1400	100,000	15,899	500	0.80	18.13	319	106	27	22
1400	120,000	19,078	500	0.80	21.76	264	88	23	18
1400	10,000	1,590	2000	3.19	4.23	1443	481	124	101
1400	20,000	3,180	2000	3.19	8.45	704	235	60	49
1400	45,000	7,154	2000	3.19	19.02	304	101	26	21
1400	60,000	9,539	2000	3.19	25.36	225	75	19	16
1400	80,000	12,719	2000	3.19	33.82	167	56	14	12
1400	100,000	15,899	2000	3.19	42.27	133	44	11	9
1400	120,000	19,078	2000	3.19	50.72	110	37	9	8
500	10,000	1,590	500	2.26	3.29	1843	605	153	124
500	20,000	3,180	500	2.26	6.57	899	295	75	60
500	45,000	7,154	500	2.26	14.79	388	127	32	26
500	60,000	9,539	500	2.26	19.72	288	95	24	19
500	80,000	12,719	500	2.26	26.29	214	70	18	14
500	100,000	15,899	500	2.26	32.86	170	56	14	11
500	120,000	19,078	500	2.26	39.43	140	46	12	9
500	10,000	1,590	2000	9.03	10.12	575	189	48	39
500	20,000	3,180	2000	9.03	20.23	280	92	23	19
500	45,000	7,154	2000	9.03	45.53	121	40	10	8
500	60,000	9,539	2000	9.03	60.70	90	29	7	6
500	80,000	12,719	2000	9.03	80.94	67	22	6	4
500	100,000	15,899	2000	9.03	101.17	53	17	4	4
500	120,000	19,078	2000	9.03	121.41	44	14	4	3

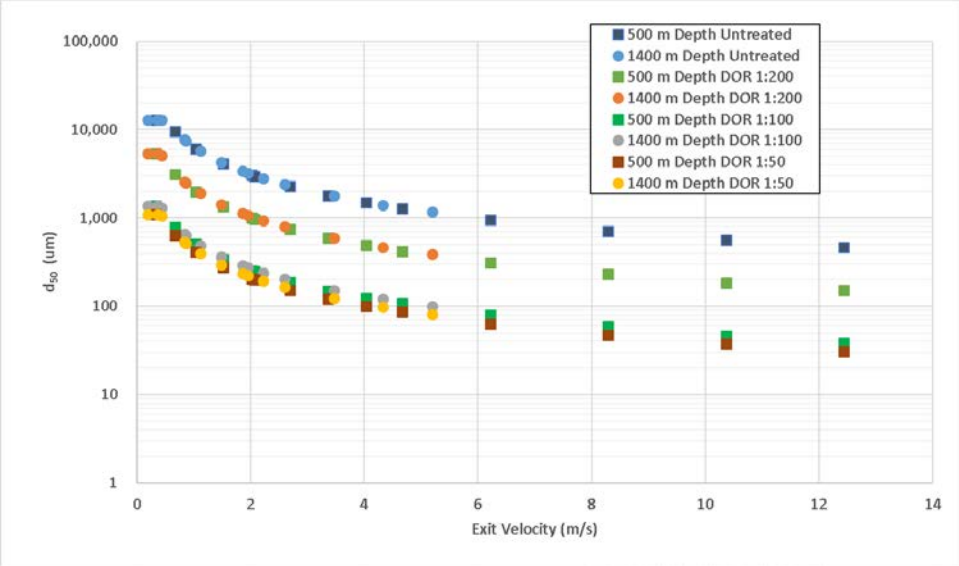

Figure 4. Median diameter (d_{50}) versus exit velocity for two release depths and various treatment properties (DOR and associated oil-water IFT), assuming an orifice of 18.75 in (476 mm). The d_{50} is capped by the maximum stable size for any given IFT.

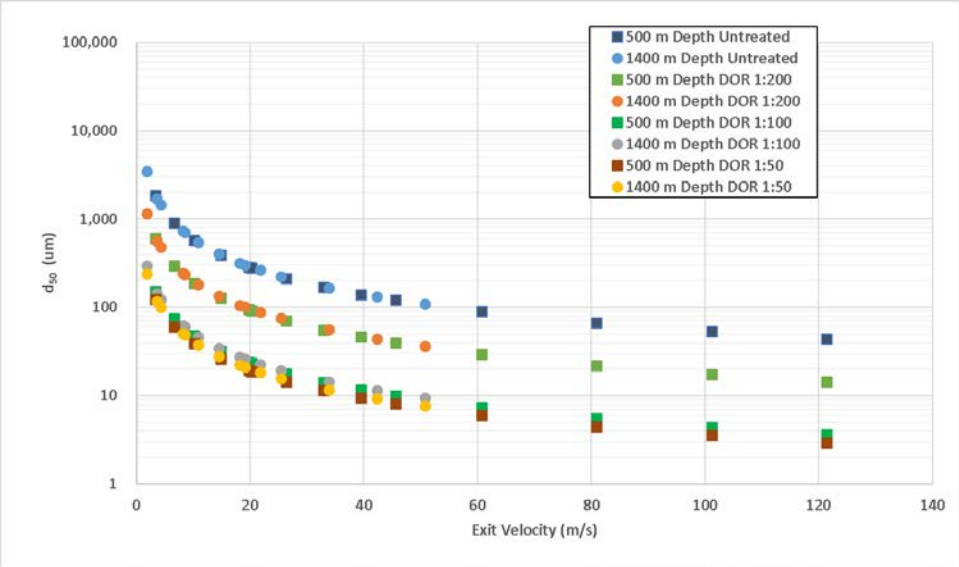

Figure 5. Estimated d_{50} versus exit velocity for two release depths and various treatment properties (DOR and associated IFT), assuming an orifice of 6 in (152 mm).

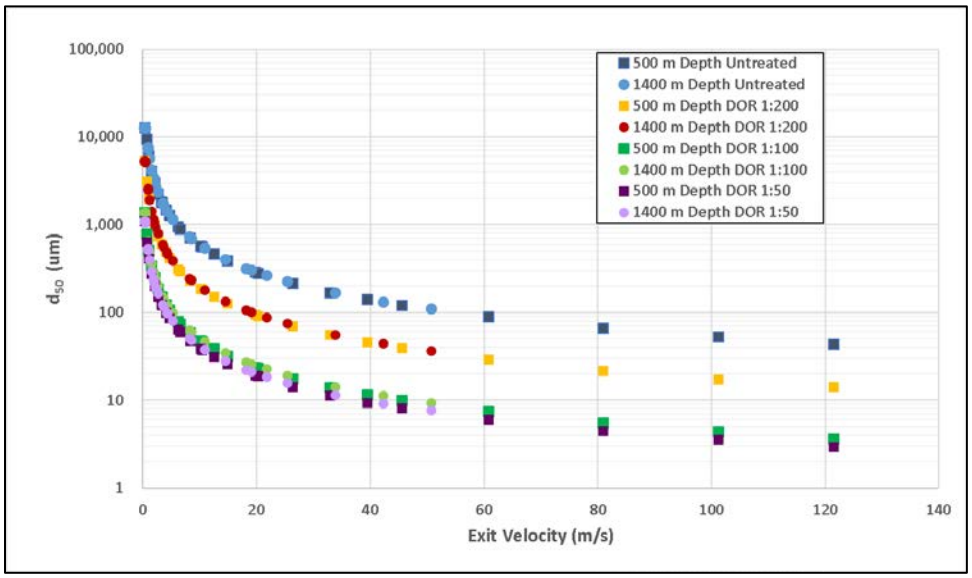

Figure 6. Estimated d_{50} versus exit velocity for two release depths and various treatment properties (DOR and associated IFT), plotting results for both orifices (6 in = 152 mm; 18.75 in = 476 mm).

3.2 Nearfield Modeling Estimates of Trap Height

The nearfield plume trap height above the release depth 500 m (at 89.168ºW, 28.476ºN) was calculated for a range of release conditions (Table 4). Two assumptions were tested for the gas bubble sizes: (1) variable model-predicted bubble sizes (exit velocity dependent; using Li et al. 2017 model) and (2) assuming a constant gas bubble diameter of 10 mm. Figure 7 shows that the gas flow rate is the primary control of the trap height. The results were not as sensitive to the bubble size assumptions tested. Assuming the variable gas bubble sizes, the trap height averages about 280 m above the discharge depth and varies by < ~33% within the range of flow conditions examined. The depth of 220 m below the surface was used as the release depth into the far field model for spill cases at 500 m.

The trap height for a range of release conditions at a release depth of 1400 m (or more generally, between 1000 and 2000 m) is about 300 m above the release depth (i.e. 1100 m below the surface) based on several analyses of the Deepwater Horizon (Spaulding et al. 2015, 2017; Zhao et al. 2015), a sensitivity study by Socolofsky et al. (2015), and the CRA modeling performed by French-McCay et al. (2018). This depth (1100 m) was used as the release depth into the far field model for spill cases at 1400 m.

Table 4. Model-estimated nearfield plume trap heights based on indicated assumptions and an 18.75 in (476 mm) orifice. Calculations were made under two assumptions: variable model-predicted gas bubble sizes (exit velocity dependent) and a constant bubble size of 10 mm diameter.

Depth (m)	Oil Flow Rate (bbl/day)	Oil Flow Rate (m^3/day)	GOR (scf/ stb)	GOR (sm^3/ sm^3)	Trap Height Above Discharge Depth (m) – Assuming All Bubbles 10 mm Diameter	Trap Height Above Discharge Depth (m) – Modeled Bubble Sizes	Trap Height as Depth Below Surface (m) – Modeled Bubble Sizes
500	20,000	3,180	500	2,807	200	185	315
500	20,000	3,180	1200	6,737	252	232	268
500	20,000	3,180	2000	11,229	292	267	233
500	45,000	7,154	500	2,807	252	235	265
500	45,000	7,154	1200	6,737	317	292	208
500	45,000	7,154	2000	11,229	357	317	183
500	90,000	14,309	500	2,807	307	282	218
500	90,000	14,309	1200	6,737	372	322	178
500	90,000	14,309	2000	11,229	415	357	143
500	45,000		mean		309	281	219
500	all		mean		307	277	223

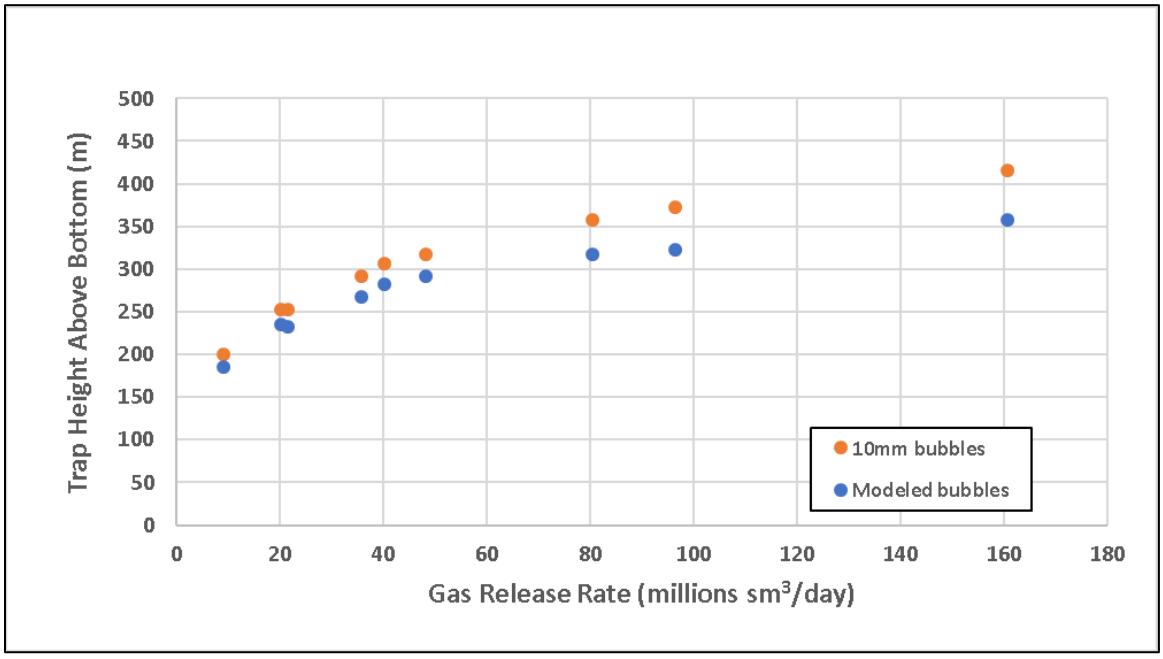

Figure 7. Trap height estimates from OILMAP-Deep as a function of gas flow rate and for a range of oil flow rates at a discharge depth of 500 m below the surface.

3.3 Probabilistic Modeling

Exposure indices for the 100 probabilistic model runs are summarized in Table 5, using the following metrics:

- Length (km) of shoreline oiled by >1g/m^2 (~1um)
- Cumulative area-days (m^2-days) of surface oil exposure above various thresholds (1g/m^2 ~= 1um)
    - m^2-days >1000um
    - m^2-days >100um
    - m^2-days >10um
    - m^2-days >1um
    - m^2-days >0.1um
    - m^2-days >0.01um
- Cumulative area (m^2) exposed to floating oil (summed over the 66-day simulation), summed over all time steps (similar information to above)
    - m^2 >100um
    - m^2 >10um
    - m^2 >1um
    - m^2 >0.1um
    - m^2 >0.01um
- Maximum water column exposure to total hydrocarbons (THC) over the 66-day simulation
    - Volume (m^3) where THC > 1 ppm at any time
    - Volume (m^3) where THC > 10 ppm at any time
    - Maximum mass of hydrocarbons (MT) in the water at any time

From these results, an approximately median case for surface floating and shoreline exposure was selected to be used as the base case metocean conditions. Based on the indices, sorted by shoreline length oiled by > 1 g/m^2, floating oil exposure above 10 g/m^2, and water column exposure (volume (m^3) where total hydrocarbon concentrations exceeded 10 μg/L), runs # 71 and 45 are a near median cases, considering all three of these exposure indices. (Run 71 is 50th for m^2-days floating oil exposure, 46th for shoreline oiling and 55th for water column exposure. Run # 45 is 47th for m^2-days floating oil exposure, 59th for shoreline oiling and 60th for water column exposure. Other percentile combinations are identified in the table. For example, in the original CRA analysis two runs were used: the 97th percentile for shore oiling and a near median case for surface oil exposure. In this sensitivity analysis set of runs, run # 47 is 31st for m^2-days floating oil exposure, 95th for shoreline oiling and 46th for water column exposure. This would be an extreme case. Figures 8 to 14 show these three and other example trajectories. Run #45 (Figure 10; spill start May 25, 2006 at 19:09 CDT) was selected as the base case for the sensitivity analysis, as it was near median for all three exposure indices and included enough shoreline oiling for evaluating effectiveness of SSDI on that exposure metric.

Table 5. Start times and exposure indices for the 100 probabilistic model runs (assuming untreated oil).

Order by Water Column Volume THC >10ppm	Average of 3 Surface-Oil Order Scores	Average Order (Float +Shore) /2	Order for Floating Oil Area >10um	Order for Floating Oil m^2-days >10um	Order for Shore Oiled	*Run #*	Start Date	Start Time	Shore Length (km) >1um	Floating Oil m^2-days >10um	Floating Oil m^2 >10um	Volume (m^3) where THC > 10 ppm
35	6.7	8.0	4	4	12	***25***	9/29/2007	10:39	2	6.23E+10	2.96E+12	2.20E+07
78	7.0	6.5	8	8	5	***40***	10/9/2008	1:13	0	6.54E+10	3.10E+12	3.04E+07
74	7.3	6.5	9	9	4	***36***	10/9/2008	0:24	0	6.68E+10	3.16E+12	2.99E+07
32	8.7	10.5	5	5	16	***79***	9/27/2007	9:38	4	6.37E+10	3.02E+12	2.02E+07
20	9.0	10.5	6	6	15	***46***	9/9/2007	23:15	4	6.43E+10	3.07E+12	1.80E+07
37	12.0	11.0	14	14	8	***65***	7/29/2008	2:48	0	7.88E+10	3.76E+12	2.23E+07
33	12.3	9.5	18	18	1	***2***	9/23/2008	10:34	0	8.48E+10	4.04E+12	2.05E+07
84	13.0	14.3	11	10	18	***51***	10/12/2007	19:21	10	6.84E+10	3.27E+12	3.25E+07
15	15.0	14.0	17	17	11	***32***	9/15/2008	4:06	1	8.22E+10	3.93E+12	1.64E+07
87	15.0	17.3	10	11	24	***37***	10/13/2006	10:06	70	6.84E+10	3.26E+12	3.30E+07
9	16.7	21.5	7	7	36	***90***	9/7/2007	17:36	123	6.44E+10	3.07E+12	1.53E+07
41	16.7	17.3	16	15	19	***94***	7/20/2008	11:41	17	7.95E+10	3.81E+12	2.29E+07
27	18.3	26.0	3	3	49	***50***	9/5/2007	10:11	197	6.14E+10	2.93E+12	1.91E+07
11	19.0	28.0	1	1	55	***97***	8/23/2008	2:22	302	5.73E+10	2.73E+12	1.56E+07
21	19.3	28.0	2	2	54	***96***	8/27/2008	6:31	290	5.79E+10	2.77E+12	1.82E+07
42	21.3	25.8	13	12	39	***11***	8/18/2005	7:36	142	7.52E+10	3.61E+12	2.36E+07
83	23.0	20.5	28	28	13	***30***	11/9/2006	14:32	2	9.42E+10	4.48E+12	3.19E+07
49	23.3	23.3	24	23	23	***26***	9/10/2006	19:23	68	8.81E+10	4.21E+12	2.45E+07
73	25.3	23.3	30	29	17	***20***	11/13/2006	11:42	5	9.48E+10	4.51E+12	2.98E+07
38	26.0	32.8	12	13	53	***99***	9/1/2005	2:10	233	7.55E+10	3.60E+12	2.24E+07
17	27.0	29.8	22	21	38	***85***	8/16/2005	7:20	138	8.67E+10	4.17E+12	1.70E+07
99	31.7	28.8	38	37	20	***92***	11/29/2006	1:14	30	1.00E+11	4.77E+12	3.95E+07

22	33.0	39.8	20	19	60	***18***	6/17/2005	13:04	407	8.53E+10	4.08E+12	1.82E+07
54	33.0	30.0	40	38	21	***16***	1/4/2007	21:09	33	1.01E+11	4.79E+12	2.55E+07
97	40.3	41.0	39	39	43	***77***	12/13/2006	16:06	153	1.01E+11	4.79E+12	3.72E+07
12	40.7	53.3	15	16	91	***33***	3/21/2008	11:31	1,209	7.96E+10	3.77E+12	1.56E+07
45	41.7	49.5	26	26	73	***83***	4/23/2006	0:39	656	9.15E+10	4.31E+12	2.40E+07
79	41.7	38.3	48	49	28	***84***	1/11/2007	21:18	83	1.05E+11	4.92E+12	3.07E+07
18	42.0	50.8	25	24	77	***57***	4/18/2008	21:59	702	8.88E+10	4.21E+12	1.70E+07
64	42.7	42.0	43	45	40	***12***	12/23/2006	11:20	146	1.03E+11	4.81E+12	2.83E+07
31	43.0	47.8	33	34	62	***98***	3/19/2007	15:54	427	9.78E+10	4.64E+12	1.97E+07
92	43.7	54.8	21	22	88	***24***	4/14/2006	3:23	1,053	8.70E+10	4.11E+12	3.45E+07
26	44.0	49.3	34	33	65	***58***	8/27/2007	7:00	479	9.68E+10	4.68E+12	1.90E+07
28	45.3	34.5	68	66	2	***4***	7/10/2006	7:54	0	1.14E+11	5.52E+12	1.91E+07
81	46.0	55.5	27	27	84	***78***	4/6/2008	15:29	831	9.41E+10	4.45E+12	3.08E+07
90	46.3	59.8	19	20	100	***1***	3/5/2007	12:18	1,469	8.62E+10	4.08E+12	3.35E+07
67	46.7	44.3	50	53	37	***14***	1/1/2007	8:39	129	1.07E+11	5.01E+12	2.86E+07
95	47.0	36.8	66	69	6	***60***	5/3/2006	15:47	0	1.16E+11	5.50E+12	3.67E+07
8	48.3	53.0	42	36	67	***44***	5/12/2007	8:39	504	1.00E+11	4.80E+12	1.48E+07
77	48.7	61.0	23	25	98	***56***	3/1/2007	5:40	1,452	8.93E+10	4.20E+12	3.04E+07
40	49.7	48.3	53	52	44	***23***	6/25/2008	14:27	168	1.06E+11	5.05E+12	2.27E+07
55	50.0	49.0	54	50	46	***71***	6/24/2008	20:35	176	1.06E+11	5.06E+12	2.55E+07
60	51.0	53.0	47	47	59	***45***	5/25/2006	19:09	334	1.04E+11	4.87E+12	2.66E+07
47	51.3	57.5	37	41	76	***64***	12/13/2007	12:04	694	1.02E+11	4.77E+12	2.43E+07
91	51.3	56.0	41	43	70	***67***	12/20/2007	19:21	621	1.02E+11	4.80E+12	3.40E+07
39	51.7	62.8	29	30	96	***82***	3/3/2008	19:35	1,342	9.49E+10	4.50E+12	2.25E+07
46	52.3	63.0	31	31	95	***47***	3/2/2008	9:58	1,289	9.67E+10	4.58E+12	2.41E+07
36	52.7	63.0	32	32	94	***70***	3/2/2008	22:41	1,282	9.68E+10	4.59E+12	2.22E+07
51	53.3	58.5	44	42	74	***73***	5/31/2008	15:15	681	1.02E+11	4.85E+12	2.48E+07
71	54.0	49.3	65	62	35	***19***	8/7/2006	22:45	118	1.12E+11	5.44E+12	2.94E+07

19	54.3	64.0	35	35	93	***93***	4/5/2007	14:09	1,281	9.94E+10	4.71E+12	1.73E+07
10	55.0	48.0	70	68	27	***10***	4/14/2005	6:45	82	1.15E+11	5.58E+12	1.56E+07
93	55.0	57.8	51	48	66	***13***	6/17/2006	6:07	494	1.05E+11	5.02E+12	3.45E+07
98	55.7	57.8	52	51	64	***38***	6/20/2006	7:11	464	1.06E+11	5.04E+12	3.75E+07
13	57.7	67.5	36	40	97	***7***	1/14/2008	18:07	1,442	1.01E+11	4.71E+12	1.58E+07
65	58.3	51.8	72	71	32	***22***	5/11/2006	12:05	105	1.18E+11	5.61E+12	2.83E+07
72	58.3	61.8	49	54	72	***35***	12/23/2007	14:06	651	1.07E+11	5.00E+12	2.95E+07
59	59.7	67.3	45	44	90	***95***	4/1/2007	1:45	1,201	1.03E+11	4.85E+12	2.64E+07
48	60.7	62.5	57	57	68	***5***	1/15/2006	6:54	569	1.10E+11	5.14E+12	2.44E+07
96	60.7	53.0	76	76	30	***63***	11/12/2007	10:17	97	1.20E+11	5.80E+12	3.70E+07
23	61.0	53.0	77	77	29	***43***	4/10/2005	14:30	90	1.20E+11	5.81E+12	1.83E+07
29	61.3	54.5	75	75	34	***6***	11/10/2007	23:31	110	1.19E+11	5.80E+12	1.93E+07
75	61.3	69.0	46	46	92	***59***	4/1/2007	1:45	1,236	1.03E+11	4.86E+12	3.00E+07
66	62.3	50.3	86	87	14	***27***	8/1/2005	18:04	4	1.45E+11	7.10E+12	2.84E+07
86	62.7	64.8	58	59	71	***31***	1/10/2006	18:00	645	1.10E+11	5.17E+12	3.28E+07
14	63.0	55.5	78	78	33	***49***	4/9/2005	15:00	108	1.23E+11	5.94E+12	1.58E+07
57	63.7	66.5	56	60	75	***3***	12/29/2007	8:01	682	1.11E+11	5.12E+12	2.62E+07
30	64.0	55.8	81	80	31	***76***	7/6/2005	4:10	105	1.32E+11	6.31E+12	1.95E+07
16	64.3	49.0	94	96	3	***28***	6/9/2007	23:50	0	1.71E+11	8.12E+12	1.69E+07
25	64.3	53.8	85	86	22	***75***	2/5/2005	9:06	60	1.43E+11	7.09E+12	1.90E+07
24	65.0	51.3	92	93	10	***8***	6/9/2007	6:42	1	1.67E+11	7.92E+12	1.87E+07
69	65.3	63.3	69	70	57	***17***	5/20/2006	11:02	314	1.18E+11	5.55E+12	2.91E+07
53	66.3	72.0	55	55	89	***80***	2/16/2008	3:14	1,123	1.08E+11	5.08E+12	2.52E+07
85	66.3	70.0	60	58	81	***21***	1/5/2006	12:45	765	1.10E+11	5.18E+12	3.28E+07
61	66.7	71.3	59	56	85	***68***	3/22/2006	18:09	843	1.09E+11	5.17E+12	2.69E+07
3	67.3	56.8	88	89	25	***39***	5/26/2005	2:44	77	1.53E+11	7.31E+12	1.31E+07
2	68.3	53.0	99	99	7	***62***	7/1/2007	9:27	0	2.16E+11	1.01E+13	1.31E+07
7	68.3	57.8	89	90	26	***100***	5/26/2005	20:29	78	1.54E+11	7.38E+12	1.42E+07

43	68.7	71.3	64	63	79	***53***	1/4/2006	3:04	724	1.12E+11	5.29E+12	2.37E+07
63	69.3	73.5	61	61	86	***89***	2/2/2008	14:25	908	1.12E+11	5.24E+12	2.73E+07
1	69.7	54.5	100	100	9	***88***	7/10/2007	15:43	0	2.23E+11	1.07E+13	1.28E+07
100	70.0	73.0	63	65	82	***91***	1/23/2006	1:54	777	1.13E+11	5.28E+12	4.20E+07
52	70.3	68.5	74	74	63	***69***	11/16/2007	7:36	451	1.19E+11	5.71E+12	2.49E+07
70	70.3	64.0	83	83	45	***72***	2/10/2005	19:53	171	1.39E+11	6.63E+12	2.92E+07
58	71.3	73.5	67	67	80	***74***	3/6/2006	18:32	729	1.15E+11	5.51E+12	2.64E+07
62	71.7	65.5	84	84	47	***55***	3/2/2005	22:41	179	1.40E+11	6.94E+12	2.70E+07
76	71.7	71.0	73	73	69	***41***	11/22/2007	18:19	577	1.19E+11	5.61E+12	3.02E+07
80	73.0	70.0	79	79	61	***52***	6/7/2005	14:10	415	1.27E+11	6.13E+12	3.07E+07
50	73.7	74.8	71	72	78	***61***	2/4/2008	23:36	715	1.19E+11	5.59E+12	2.46E+07
56	74.7	69.0	87	85	**52**	***66***	2/18/2005	21:43	229	1.43E+11	7.15E+12	2.60E+07
94	75.0	81.0	62	64	99	***15***	2/22/2007	23:41	1,466	1.13E+11	5.25E+12	3.61E+07
88	76.0	69.5	90	88	**50**	***87***	7/14/2005	18:11	212	1.51E+11	7.70E+12	3.30E+07
34	77.3	70.0	93	91	48	***86***	7/20/2005	10:36	194	1.54E+11	8.02E+12	2.16E+07
6	78.0	71.3	91	92	**51**	***9***	5/18/2005	13:55	220	1.60E+11	7.90E+12	1.40E+07
5	78.3	69.0	97	97	41	***42***	7/28/2007	19:57	148	1.76E+11	8.52E+12	1.36E+07
4	79.3	70.0	98	98	42	***48***	7/23/2007	14:28	151	2.12E+11	9.71E+12	1.36E+07
44	82.0	82.3	82	81	83	***29***	2/1/2006	15:36	821	1.34E+11	6.37E+12	2.37E+07
68	82.0	75.5	96	94	56	***34***	4/24/2007	22:56	312	1.69E+11	8.25E+12	2.91E+07
89	82.7	76.5	95	95	58	***54***	4/26/2007	15:42	331	1.69E+11	8.24E+12	3.33E+07
82	83.0	84.0	80	82	87	***81***	2/11/2007	3:22	1,009	1.35E+11	6.28E+12	3.18E+07

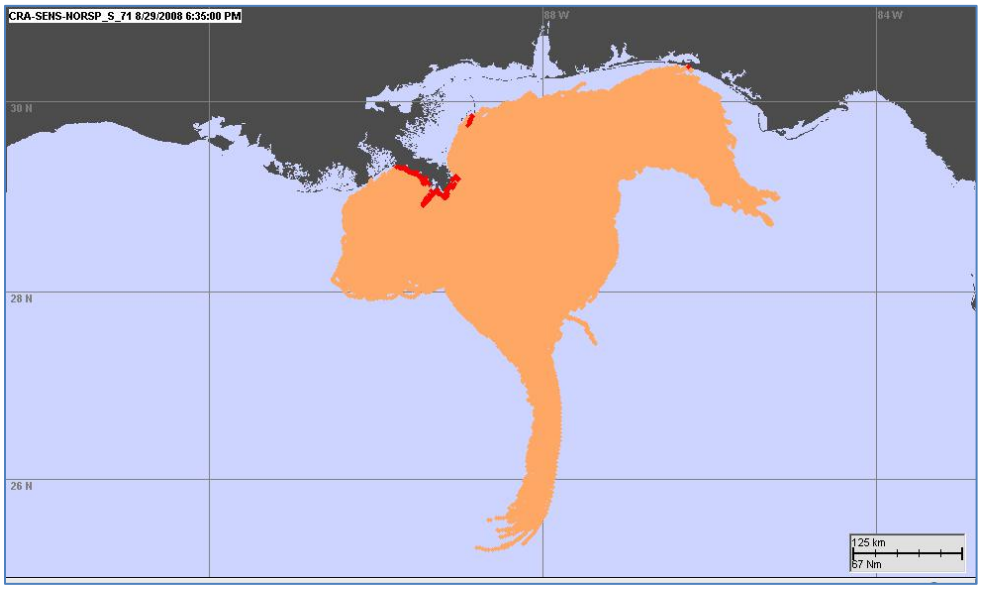

Figure 8. Cumulative floating oil trajectory (orange) and shore oiled (red) for Run # 71 (6/24/2008, 20:35), which is 50th for m^2-days floating oil exposure, 46th for shoreline oiling and 55th for water column exposure.

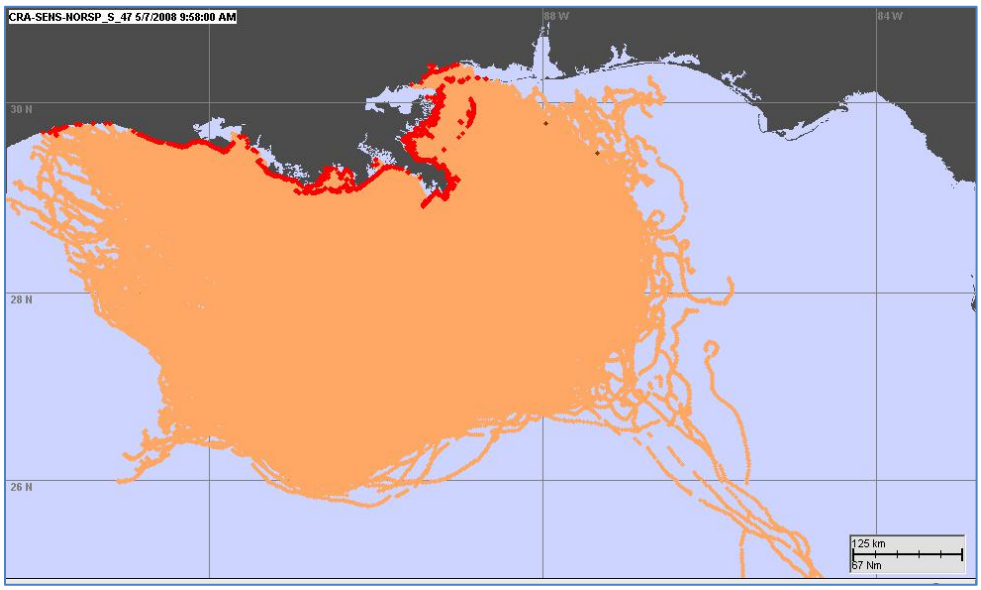

Figure 9. Cumulative floating oil trajectory (orange) and shore oiled (red) for Run # 47 (3/2/2008, 9:58), which is 31st for m^2-days floating oil exposure, 95th for shoreline oiling and 46th for water column exposure.

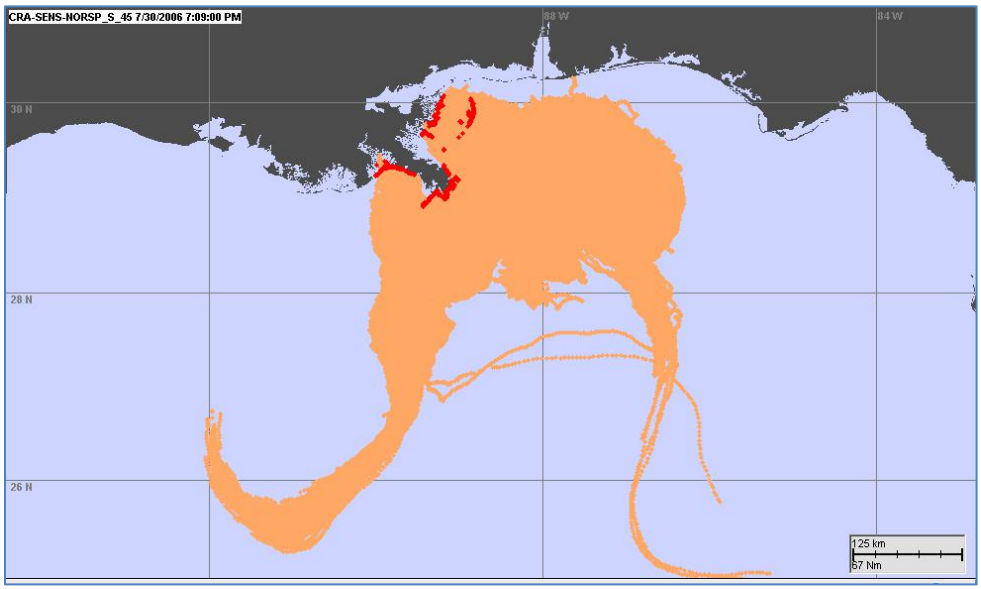

Figure 10. Cumulative floating oil trajectory (orange) and shore oiled (red) for Run # 45 (5/25/2006, 19:09), which is 47th for m^2-days floating oil exposure, 59th for shoreline oiling and 60th for water column exposure.

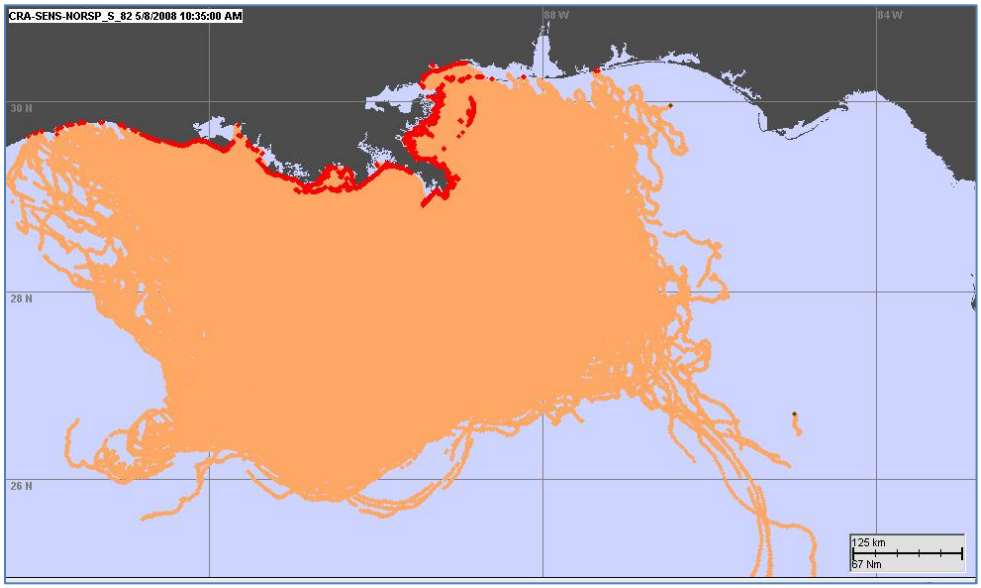

Figure 11. Cumulative floating oil trajectory (orange) and shore oiled (red) for Run # 82 (3/3/2008, 19:35), which is 30th for m^2-days floating oil exposure, 96th for shoreline oiling and 39th for water column exposure.

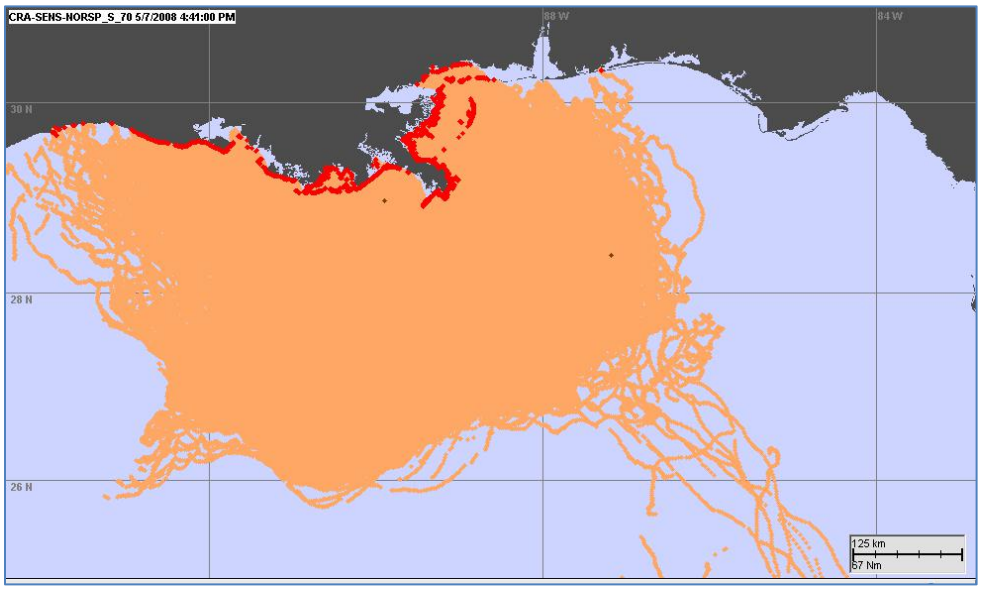

Figure 12. Cumulative floating oil trajectory (orange) and shore oiled (red) for Run # 70 (3/2/2008, 22:41), which is 32nd for m^2-days floating oil exposure, 94th for shoreline oiling and 36th for water column exposure.

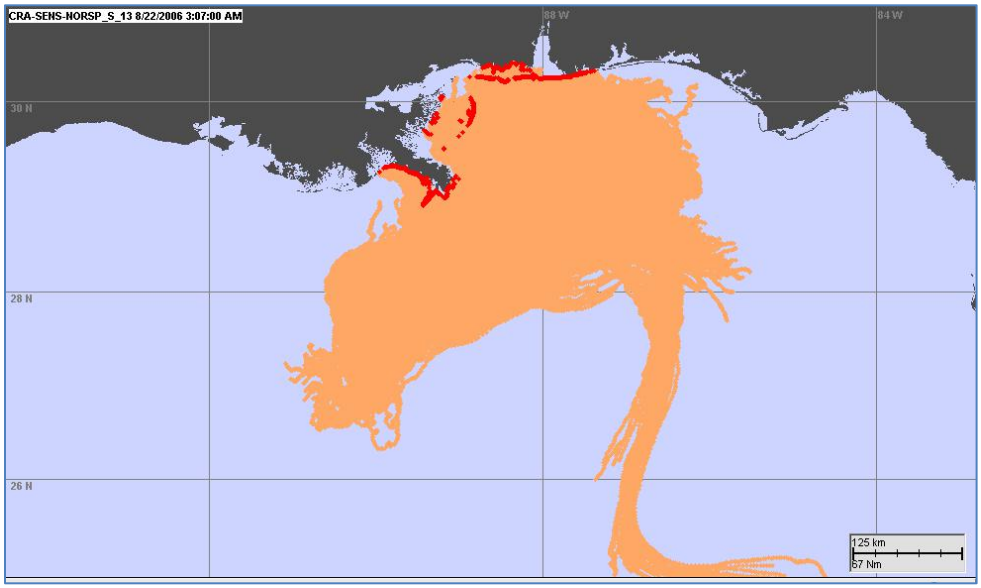

Figure 13. Cumulative floating oil trajectory (orange) and shore oiled (red) for Run # 13 (6/17/2006, 6:07), which is 48th for m^2-days floating oil exposure, 66th for shoreline oiling and 93rd for water column exposure.

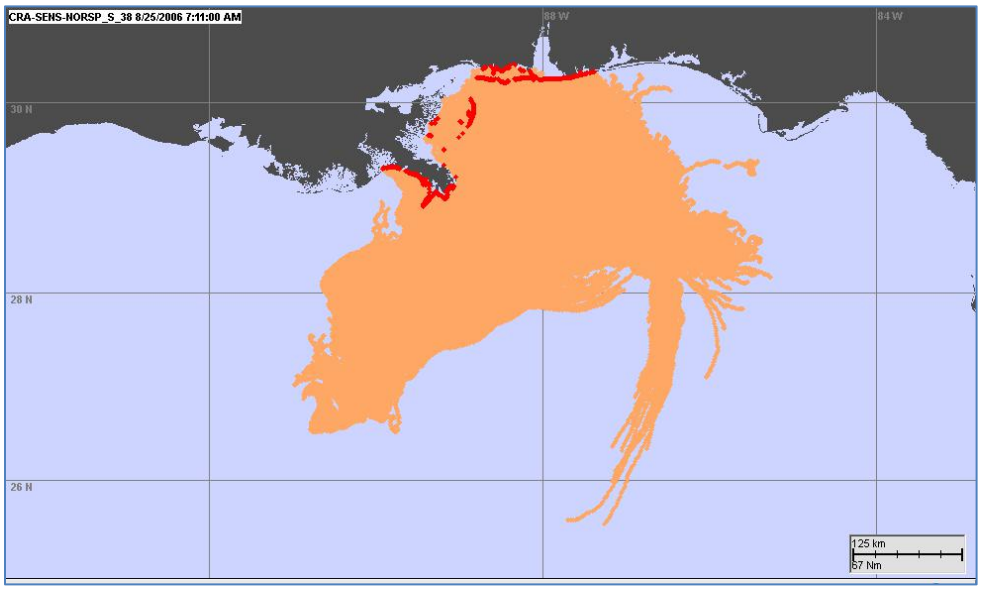

Figure 14. Cumulative floating oil trajectory (orange) and shore oiled (red) for Run # 38 (6/20/2006, 7:11), which is 51st for m^2-days floating oil exposure, 64th for shoreline oiling and 98th for water column exposure.

3.4 Far field Modeling

The matrix of inputs for the far-field model runs was summarized in Table 1. All cases were for spills starting May 25, 2006 at 19:09 CDT. Model results are summarized in Figures 15 to 42, and described in the following sections.

3.4.1 Overall Mass Balance and Exposure Indices

Case #2 and #10 were run with the same inputs (e.g., release depth 1400 m, d_{50} = 250 μm) except that the oil volume flow rate was 45,000 bbl/day (7154 m^3/day) for Case #2 and 100,000 bbl/day (15,899 m^3/day) for Case #10. These cases demonstrate that the mass balance, expressed as a percentage of the total oil mass *spilled to date*, is essentially the same (Figure 15). The mass (Figure 16) and areas/volumes exposed above particular thresholds (Appendix B) were greater for the larger spill volume, but the percentage of oil floating or in the water column was the same regardless of the spill volume. This result indicates that trends related to mass balance due to varying inputs listed in Table 1, for example d_{50}, that are seen in results assuming 45,000 bbl/day (7154 m^3/day), would be seen at larger and smaller spill volumes (released at similar depth and conditions). Plots of oil mass by environmental compartment over time for other cases are in Appendix A. Appendix B contains summary tables of mass balance and exposure metric results for all modeled cases.

Results of the far field modeling using SIMAP are summarized in Figures 17 to 23. In Figures 17,18 and 23, the maximum percentage of the *total released oil mass* (over 21 days) in each compartment at any time after the spill is plotted as a function of median droplet size. Note that for the atmospheric, shoreline, sediment, degradation and outside-the-model-boundary environmental compartments, the maximum is at the end of the 66-day model simulation. For floating oil and water column contamination, the maximum is some time prior to the end of the simulation, near the end of the release period at 21 days (Figure 16). One can see that the inferred benefits of SSDI increase substantially when d_{50} is decreased to below about 700 μm for the 1400-m discharge and when d_{50} is decreased to below about 300 μm for the 500-m discharge. This difference is because of the droplet rise times (Figure 24) from the 220-m intrusion (280 m being the trap height assumed for the 500-m discharge) being much shorter than those from 1100 m (for the 1400-m discharge). The droplet rise times in Figure 24 are based on modified Stokes Law (algorithm in French-McCay et al 2018b), increasing oil density and shrinking diameter as oil droplets weather (dissolves, biodegrades) over the rise period, and the changing ambient water density as the droplets rise higher in the water column. With longer rise times, the smaller oil droplets reach the surface farther from the release location. In Figure 24, the mean distances down current where oil droplets of various sizes reached the surface were calculated from the temporal and vertical mean current speed multiplied by the rise times. Because the currents varied in direction over time, the smaller droplets, which would be produced by use of SSDI, surfaced much farther apart in widely dispersed sheens, whereas (untreated) droplets >1mm surfaced within 4 km of the 1400-m release and within 1.4 km of the 500-m release in thick oil patches. The percentage of the spilled oil surfacing is inversely related to the rise time to the surface. Rise times of droplets <200 μm from below 1100 m are so long that much of the oil would dissolve and degrade before the droplets could rise to surface waters; hence they could be considered permanently dispersed in the water column. From 220 m, droplets <100 μm could be considered permanently dispersed in the water column.

In all cases, the fraction of the released oil degraded in the water column increases substantially with decreasing d_{50}. The degradation includes biodegradation of all hydrocarbons in water, surface floating, shoreline and sediment compartments, at compartments- and component-specific rates, and photo-oxidation of polycyclic aromatic hydrocarbons (PAHs) in the upper 20 m of the water column. Most of the biodegradation results from soluble and semi-soluble aromatic hydrocarbons as they dissolve into the water column and lower molecular weight aliphatic hydrocarbons in small dispersed oil droplets. Thus, there is more biodegradation for the deeper releases as compared to the shallower spills after 66 days. All the lower molecular weight compounds are highly volatile, so evaporate quickly when oil containing them surfaces.

The areas and lengths of shoreline affected above static thresholds expressed as g/m^2 do not for all cases scale linearly with the percentage of mass surfacing (areas are summarized by Figure 22). The areas and lengths of shoreline affected are mostly a function of where Lagrangian Elements come ashore. For cases where d_{50} is large enough such that oil comes up in about the same places, the oil piles up higher in the same places on shore. If the volume coming ashore is more than the local holding capacity (which is a function of viscosity, shore type and intertidal width, French-McCay et al. 2018b), some oil is sluffed off and moves alongshore in the model. This spreading is typically local, as there are many nearby shore cells. For the smaller d_{50}s (i.e., d_{50} = 250 μm and smaller), much less oil surfaces and it comes up much farther from the spill site and in different places. Also, given the noise in the random walk dispersion algorithm, the exact spots where oil comes ashore vary. In these cases, the oil is surfacing in different places than for the larger droplet cases, hence the patterns on shore are not the same. The intermediate-sized droplets come up farther afield and so come ashore farther afield at more dispersed locations (generally farther east to the Florida Panhandle for these cases; see maps of shoreline oiling in Appendix C). While the mass ashore is much less, it is still higher than the thresholds used for these very large spills. For smaller spill volumes, the dispersed mass ashore would fall below the thresholds, and the shore areas oiled would decrease with d_{50}. That trend is apparent for the 500-m spill results where much of the oil comes up in the same location and so shore oiling is focused on the same areas, whereas for the 1400-m spill the intermediate-sized droplets (175-900 μm) come up farther afield and so results for that d_{50} range show an inverse trend (Figure 22).

Figure 23 shows the maximum percentage of the released oil mass in each compartment at any time after the spill as a function of the standard deviation of the lognormal droplet size distribution (s_d), for releases with d_{50} = 50 μm and from 220 m below surface (the intrusion depth for the 500-m spill) and from 1100 m below surface (1400-m spill). The mass balance changes slightly with the change in s_d, with more oil surfacing at a given d_{50} when the s_d increases. Similar results were obtained for other d_{50} values.

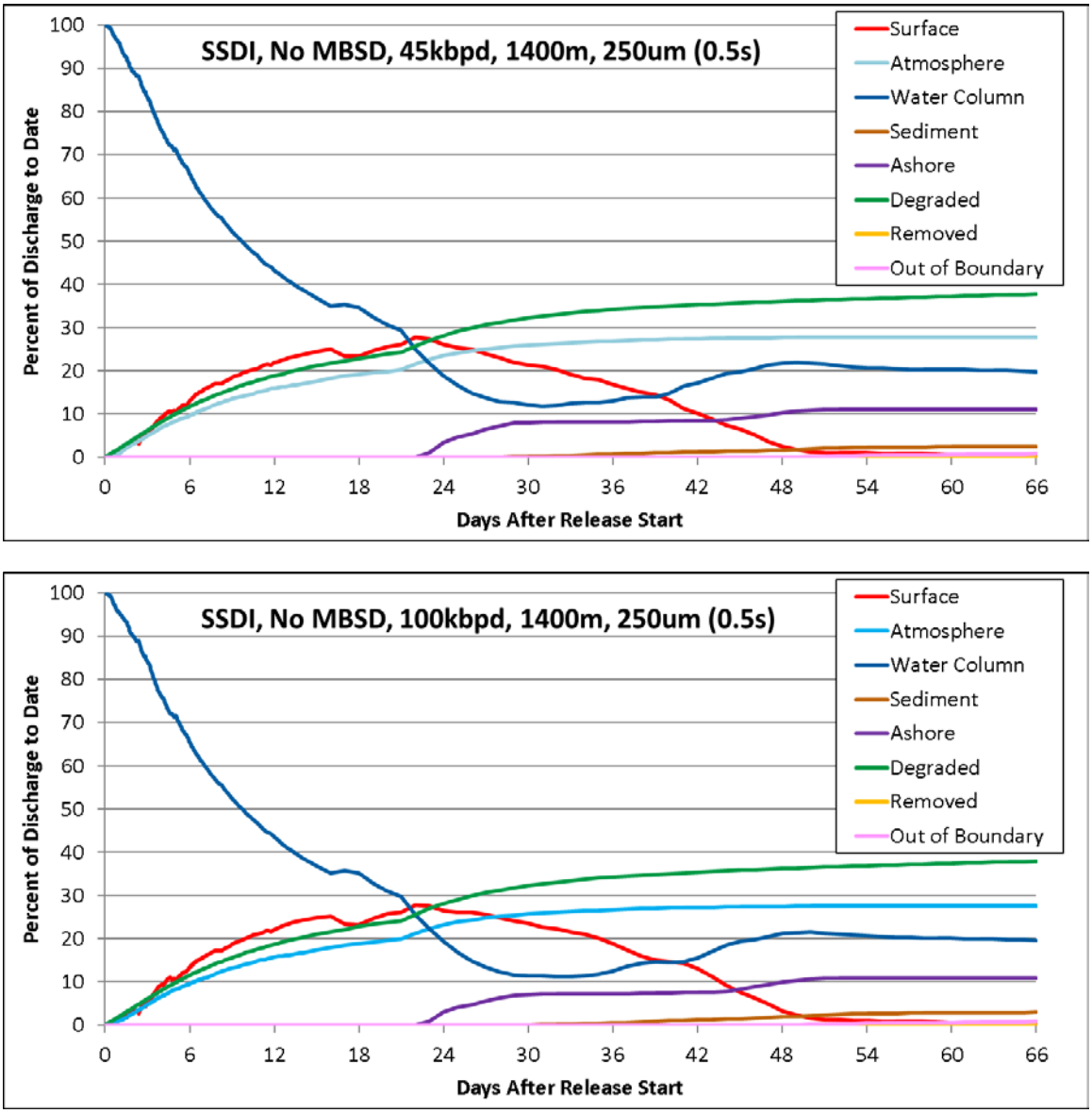

Figure 15. Percent of spilled mass to date in various environmental compartments for cases assuming d_{50} = 250 μm and s_d = 0.5, and other inputs as in Table 1. (Upper panel: Case #2, 45,000 bbl/day (7154 m3/day); lower panel: Case #10, 100,000 bbl/day (15,899 m^3/day)).

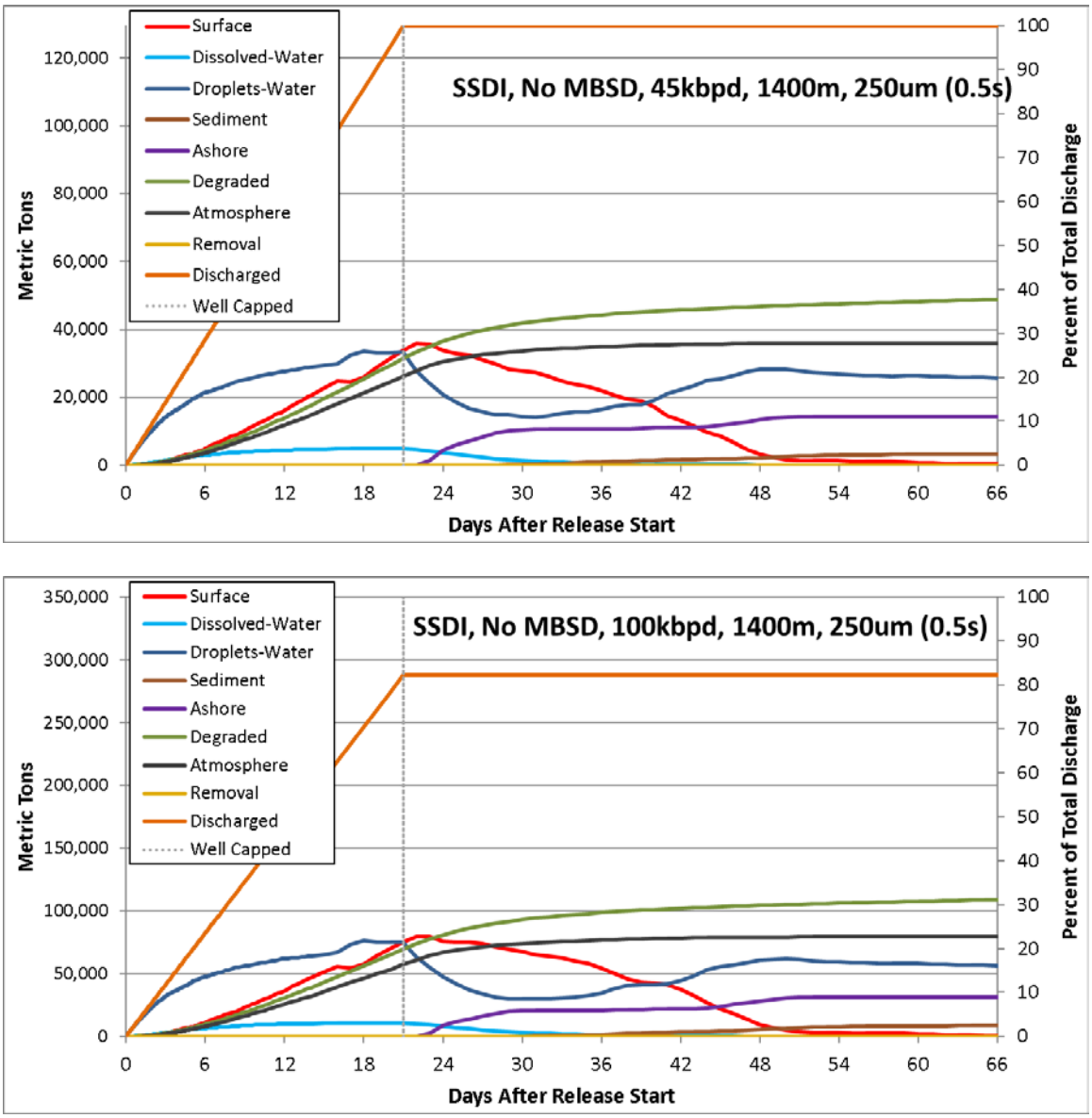

Figure 16. Spilled mass in various environmental compartments for cases assuming d_{50} = 250 µm and s_d = 0.5, and other inputs as in Table 1. (Upper panel: Case #2, 45,000 bbl/day (7154 m3/day); lower panel: Case #10, 100,000 bbl/day (15,899 m^3/day)).

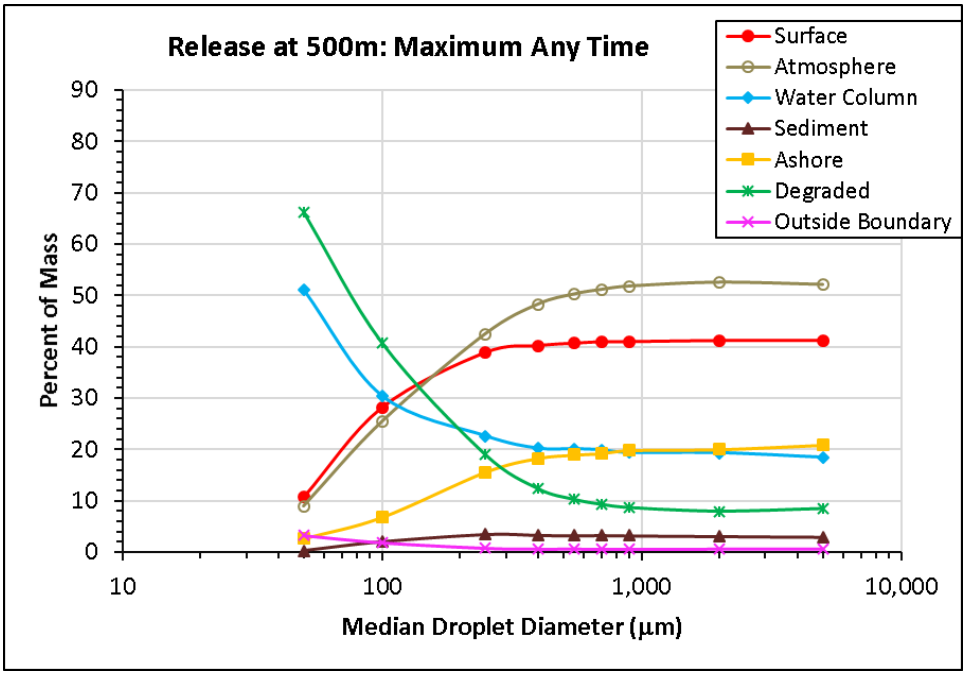

Figure 17. Maximum percent of the released oil mass in each compartment at any time after the spill as a function of median droplet size – 500-m spills with intrusion at 220 m below surface.

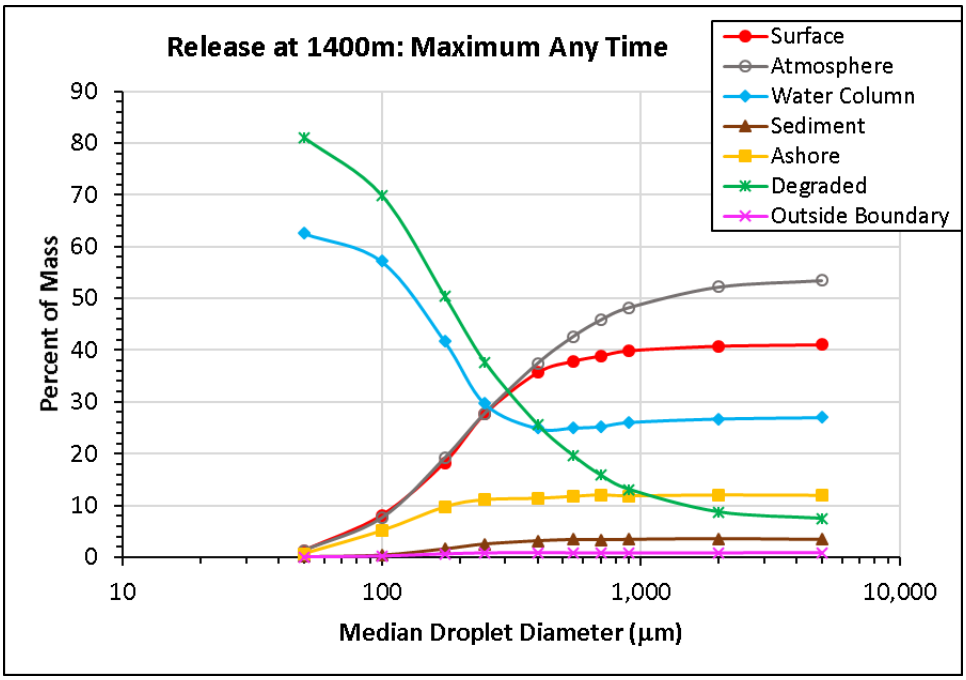

Figure 18. Maximum percent of the released oil mass in each compartment at any time after the spill as a function of median droplet size – 1400-m spills with intrusion at 1100 m below surface.

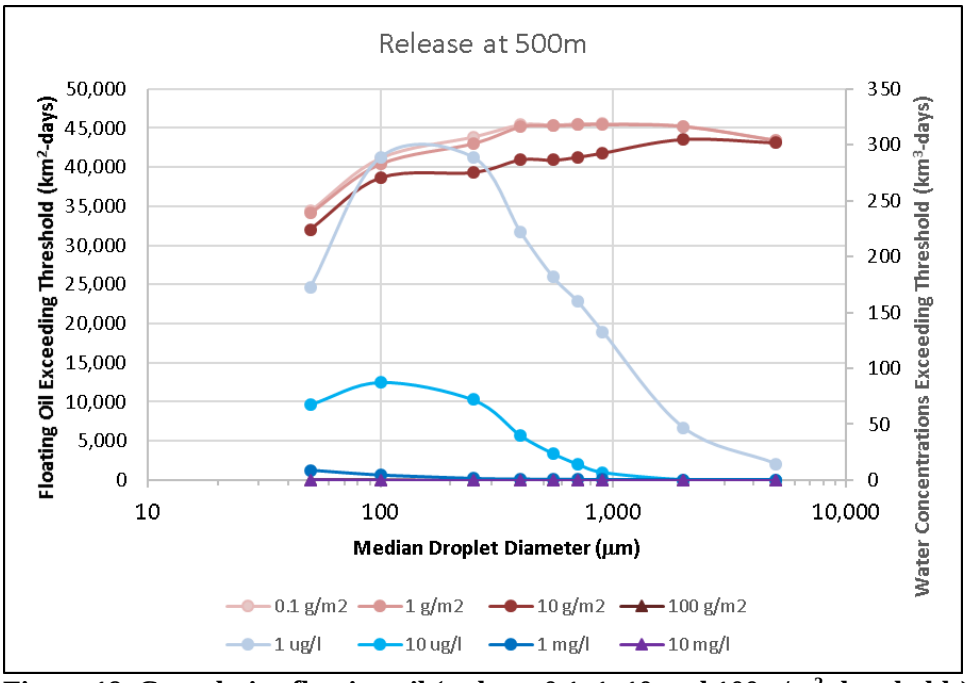

Figure 19. Cumulative floating oil (reds, at 0.1, 1, 10 and 100 g/m^2 thresholds) and water column (blues, dissolved hydrocarbons at 1 µg/l and 10 µg/l and total hydrocarbons in droplets at 1 mg/l and 10 mg/l thresholds) exposure indices as a function of median droplet size – 500-m spills with intrusion at 220 m below surface.

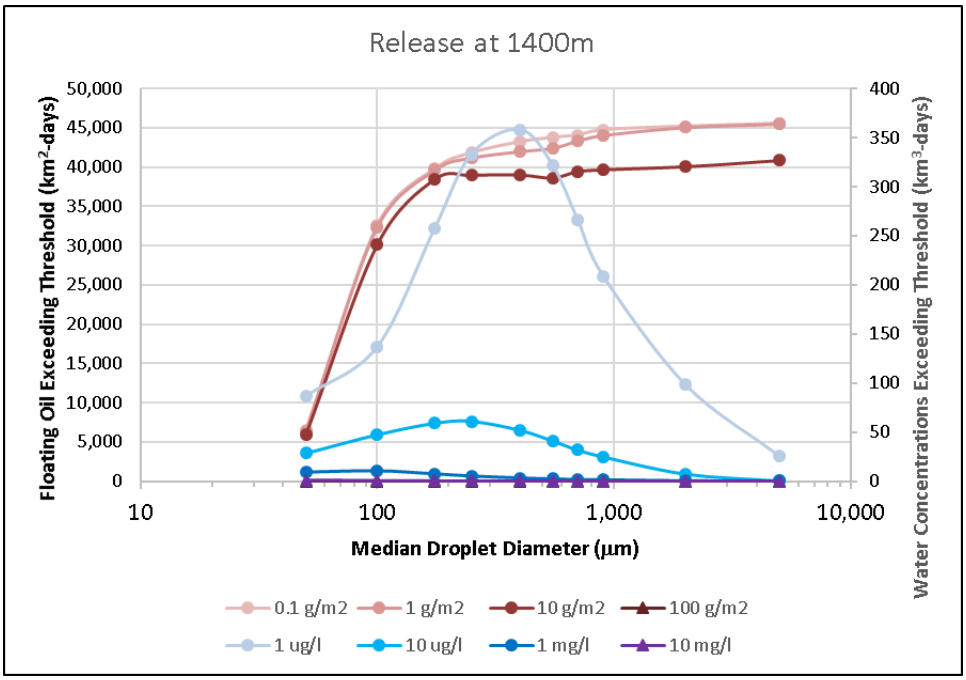

Figure 20. Cumulative floating oil (reds, at 0.1, 1, 10 and 100 g/m^2 thresholds) and water column (blues, dissolved hydrocarbons at 1 µg/l and 10 µg/l and total hydrocarbons in droplets at 1 mg/l and 10 mg/l thresholds) exposure indices as a function of median droplet size – 1400-m spills with intrusion at 1100 m below surface.

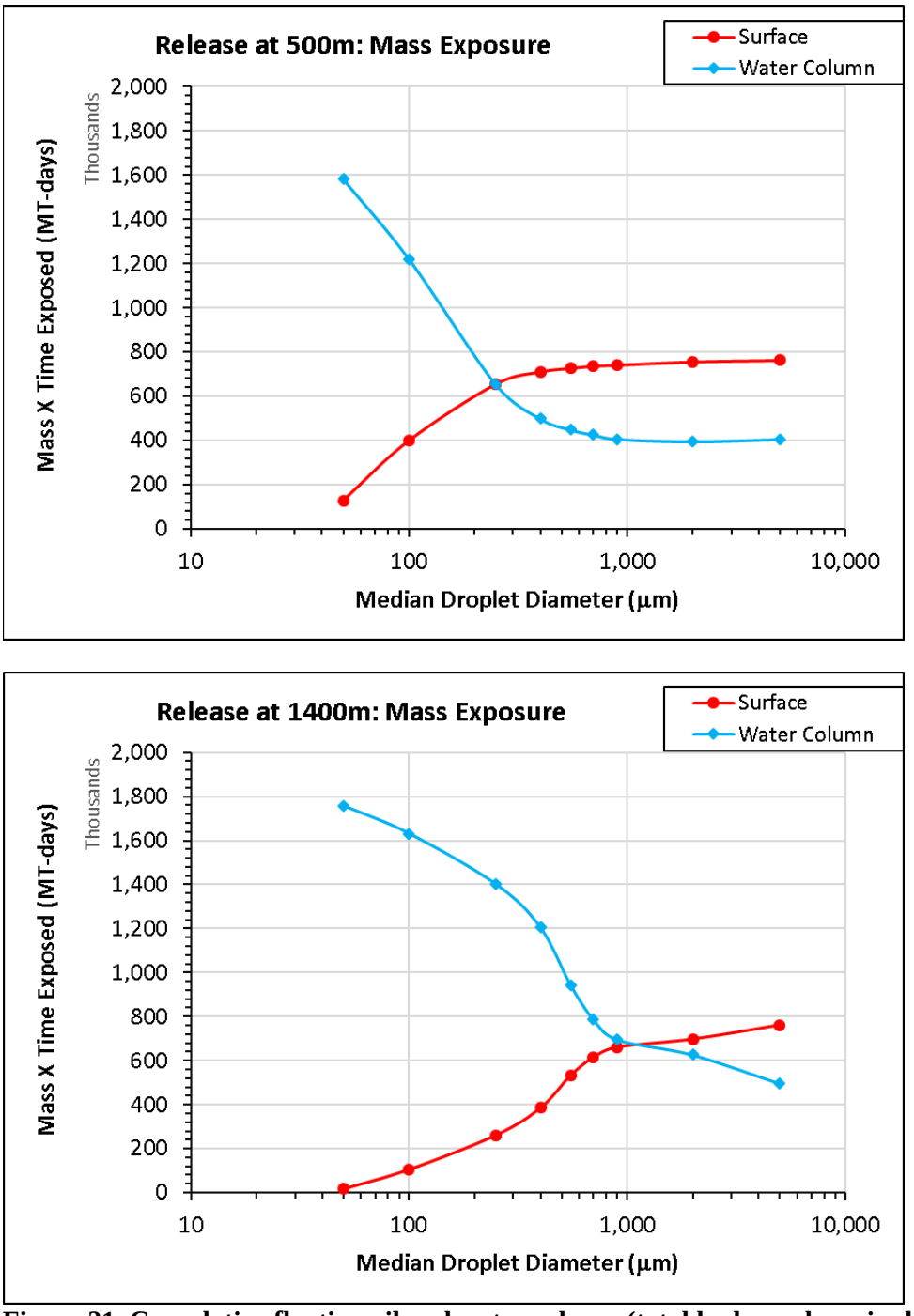

Figure 21. Cumulative floating oil and water column (total hydrocarbons in droplets and dissolved) exposure indices, expressed as metric ton-days, as a function of median droplet size – 500-m spills with intrusion at 220 m below surface (top) and 1400-m spills with intrusion at 1100 m below surface (bottom). Note that a normalized plot expressed as (fraction of spilled mass)-days would show the same relationship (but would be using less intuitive units).

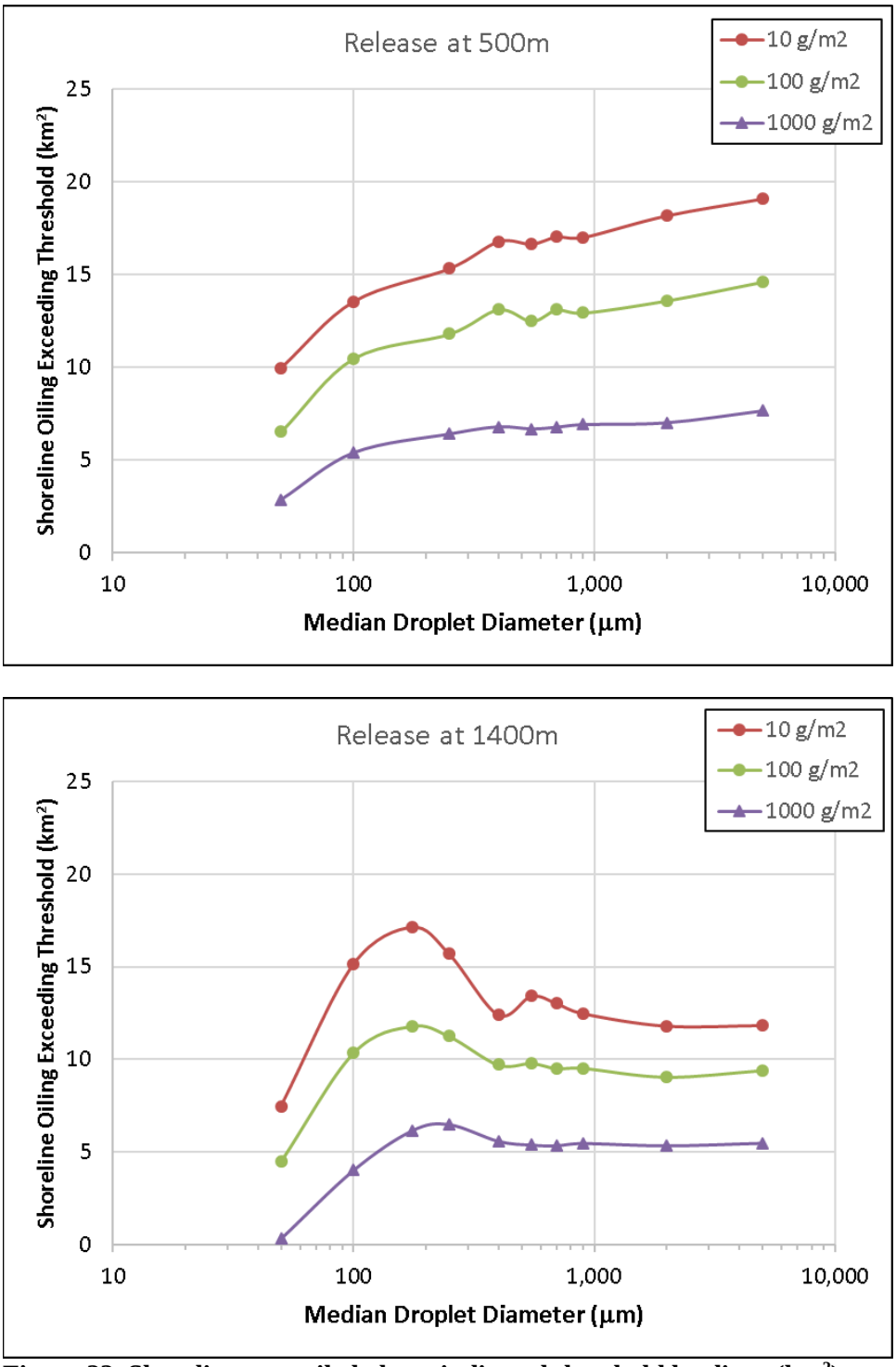

Figure 22. Shoreline area oiled above indicated threshold loadings (km^2) as a function of median droplet size – 500-m spills with intrusion at 220 m below surface (top) and 1400-m spills with intrusion at 1100 m below surface (bottom). Note that for d_{50} = 100 - 250 µm, oil droplets surface widely and come ashore in more dispersed locations but in lower amounts (Figures 17-18).

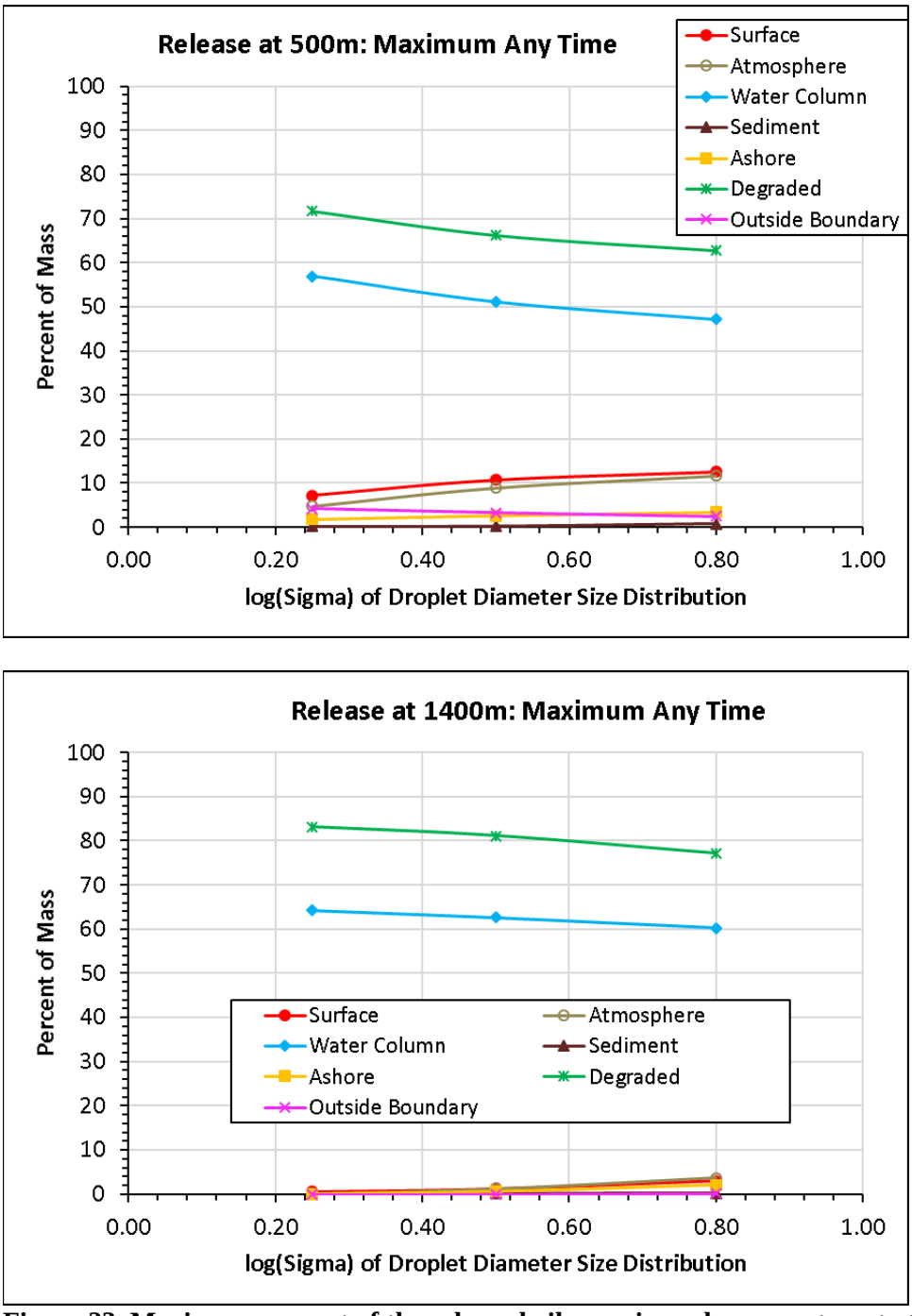

Figure 23. Maximum percent of the released oil mass in each compartment at any time after the spill as a function of the standard deviation of the lognormal droplet size distribution (s_d) for releases with d_{50} = 50 µm – 500-m spills with intrusion at 220 m below surface (top) and 1400-m spills with intrusion at 1100 m below surface (bottom).

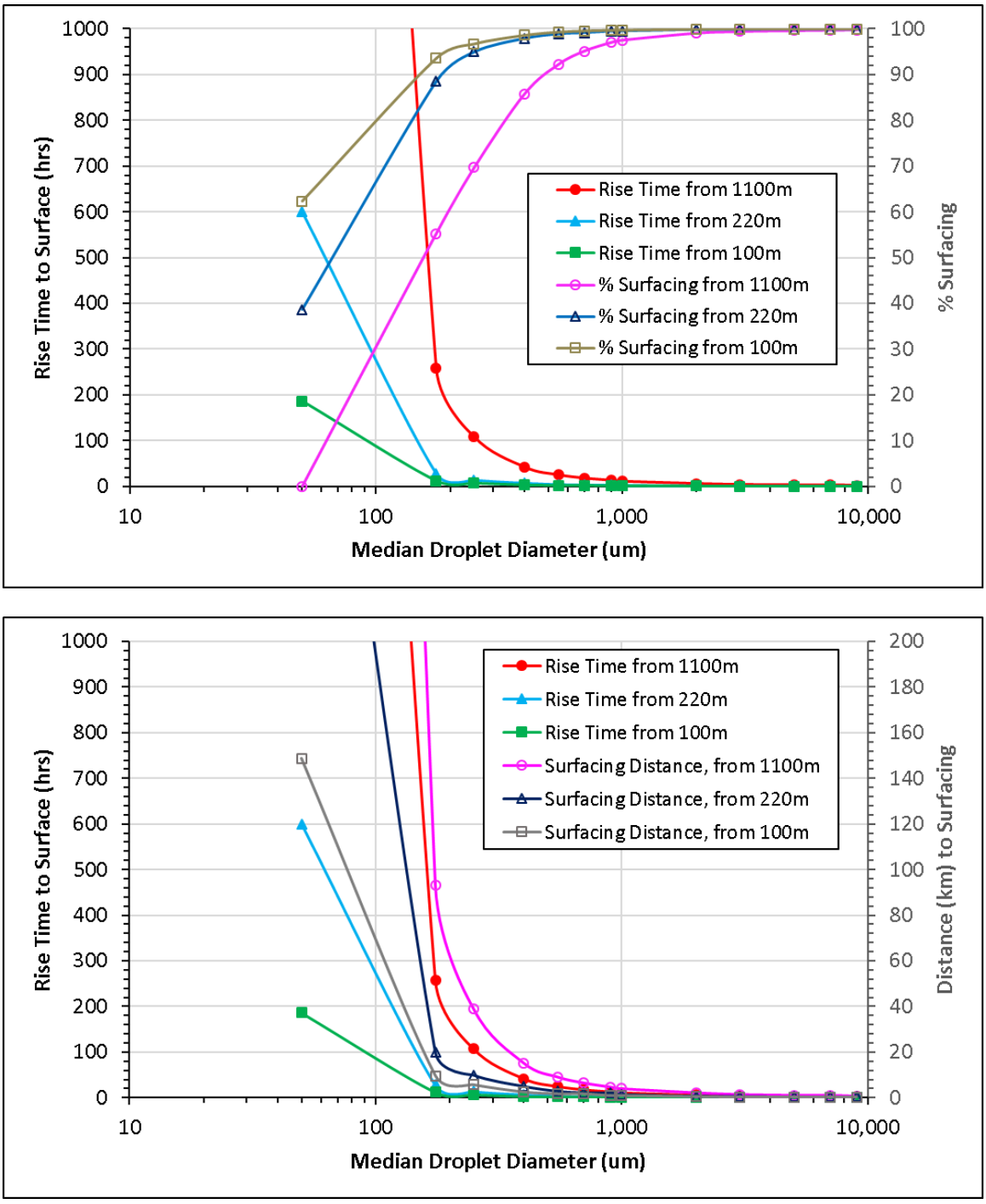

Figure 24. Rise time to the surface (1 m) as a function of initial droplet diameter released at the intrusion depth, compared to (A) percentage of mass reaching the surface (top panel) and (B) distance down current where the droplet size surfaced based on the temporally-averaged current profile (bottom panel).

3.4.2 Mass Balance of Pseudo-components

Figures 25 to 32 show the mass balance of modeled pseudo-components of the oil for case #2, the spill at 1400 m where d_{50} = 250 µm. The pseudo-components are differentiated by aromatic/aliphatic compounds, boiling point range (i.e., volatility), and for aromatics, the octanol-water partition coefficient (K_{ow}). The pseudo-components are defined in French-McCay et al. (2018a,b), as summarized in Appendix D. Figures 24-28 show the progressive changes from the most soluble AR1 (BTEX) to the least soluble aromatic pseudo-components (3-ring PAHs). BTEX rapidly dissolves at depth and biodegrades, whereas the 3-ring PAHs partially dissolve in the water column and biodegrade there, while the remaining 3-ring PAHs surface with the larger oil droplets and slowly evaporate. There are small differences between the mass balances of AR6, AR7 and AR8, with AR8 showing the most in surfaced oil and the atmosphere. Figures 29-32 show the progressive changes from the most volatile and labile AL1 to the least volatile and labile aliphatic pseudo-components AL6-AL8. The AL pseudo-components do not dissolve, and so the fraction in the water column is within oil droplets where they biodegrade. The lightest, most volatile pseudo-components AL1 and AL2 biodegraded faster than the other AL pseudo-components, based on rates estimated from the literature (see French-McCay et al. 2015, 2018a,b).

The patterns for other droplet size distributions are as follows. For smaller d_{50}, the less soluble PAHs dissolve more in deep water, whereas for larger d_{50}, the PAHs dissolve less and more incompletely in deep water. Similarly, the aliphatics degrade faster with smaller droplet sizes.

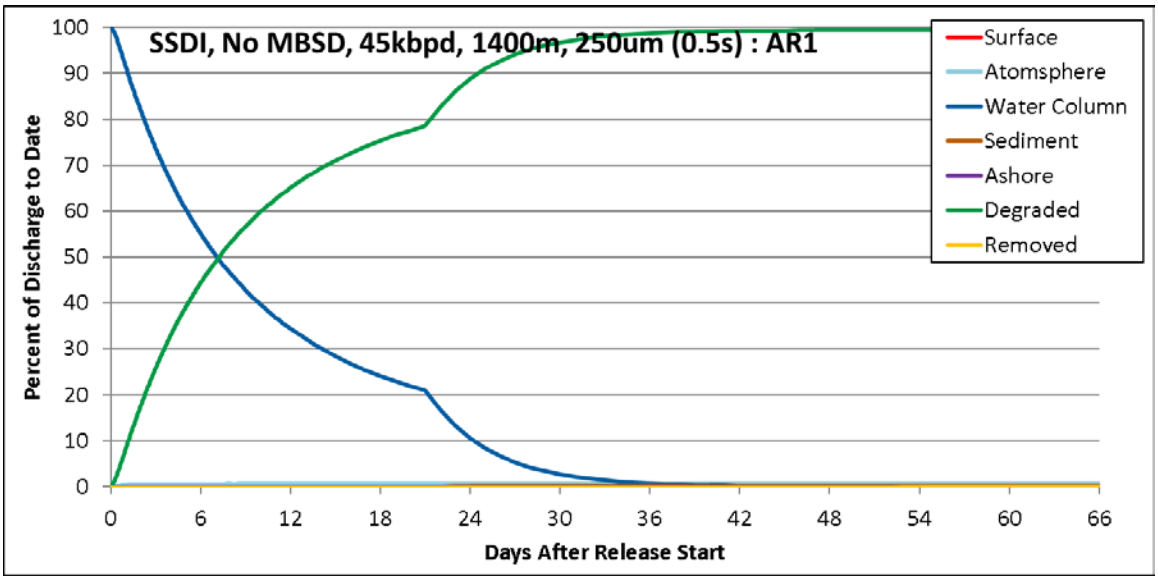

Figure 25. Percent of spilled mass of pseudo-component AR1 in various environmental compartments for case #2 (assuming d_{50} = 250 µm and s_d = 0.5).

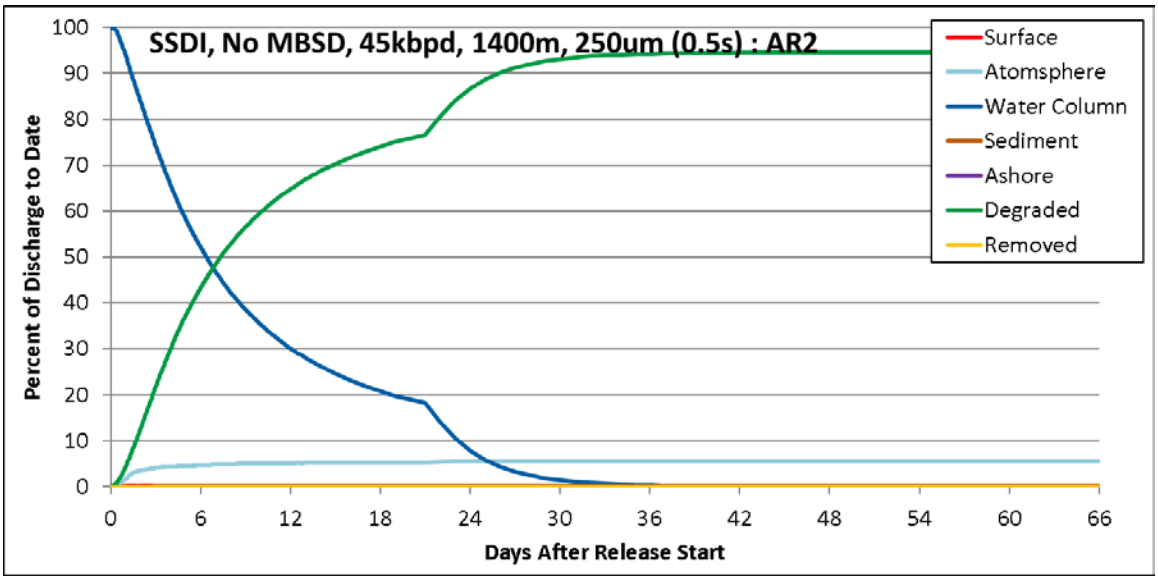

Figure 26. Percent of spilled mass of pseudo-component AR2 in various environmental compartments for case #2 (assuming d_{50} = 250 µm and s_d = 0.5).

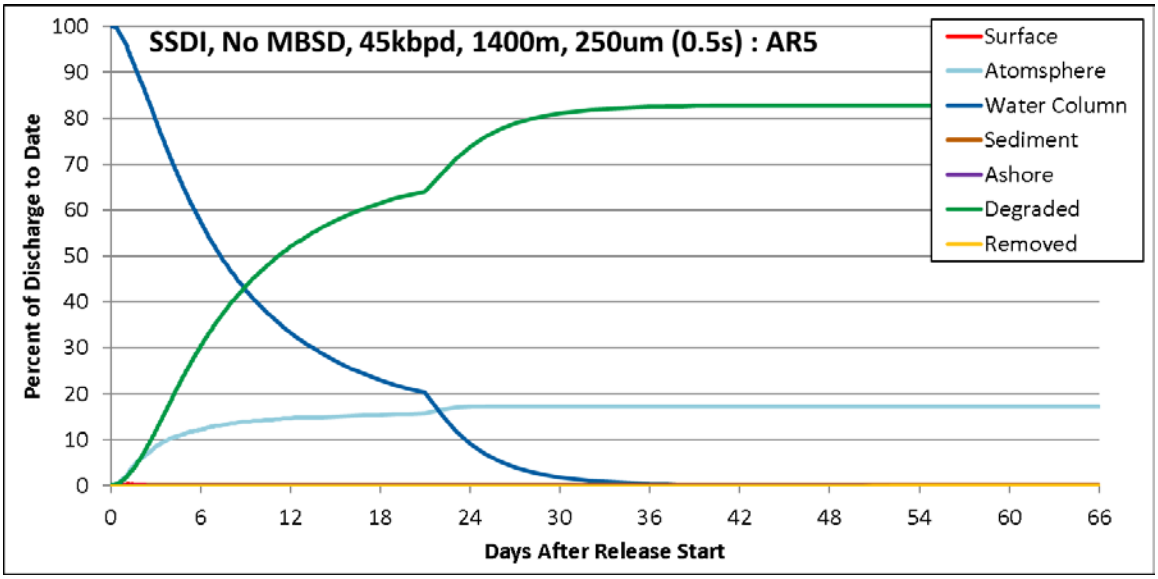

Figure 27. Percent of spilled mass of pseudo-component AR5 in various environmental compartments for case #2 (assuming d_{50} = 250 µm and s_d = 0.5). Results are similar for pseudo-component AR3.

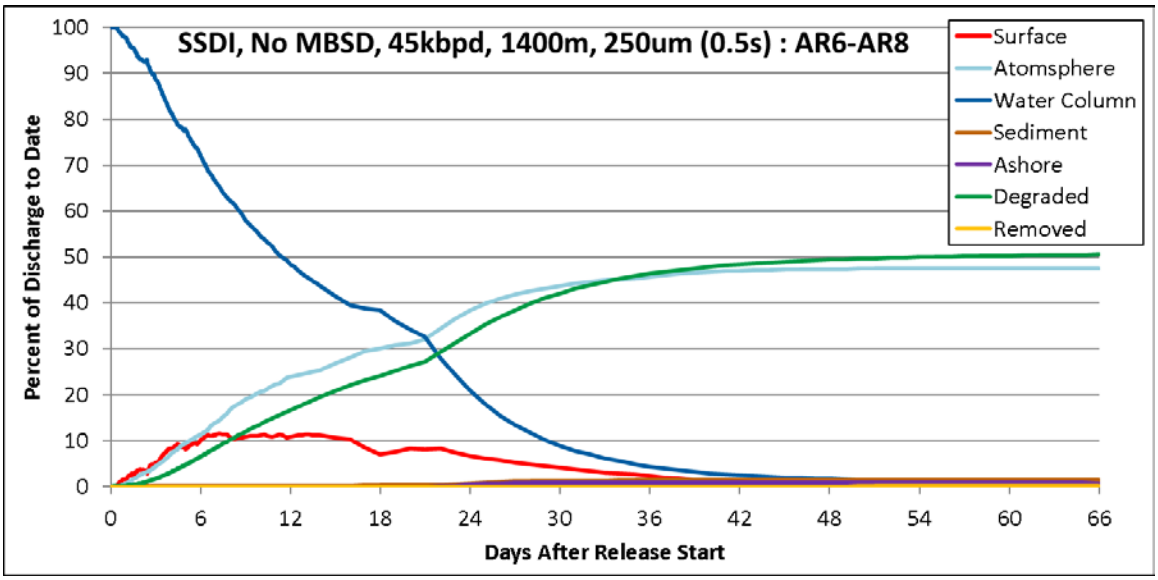

Figure 28. Percent of spilled mass of pseudo-components AR6, AR7 and AR8 (summed 3-ring PAHs) in various environmental compartments for case #2 (assuming d_{50} = 250 µm and s_d = 0.5).

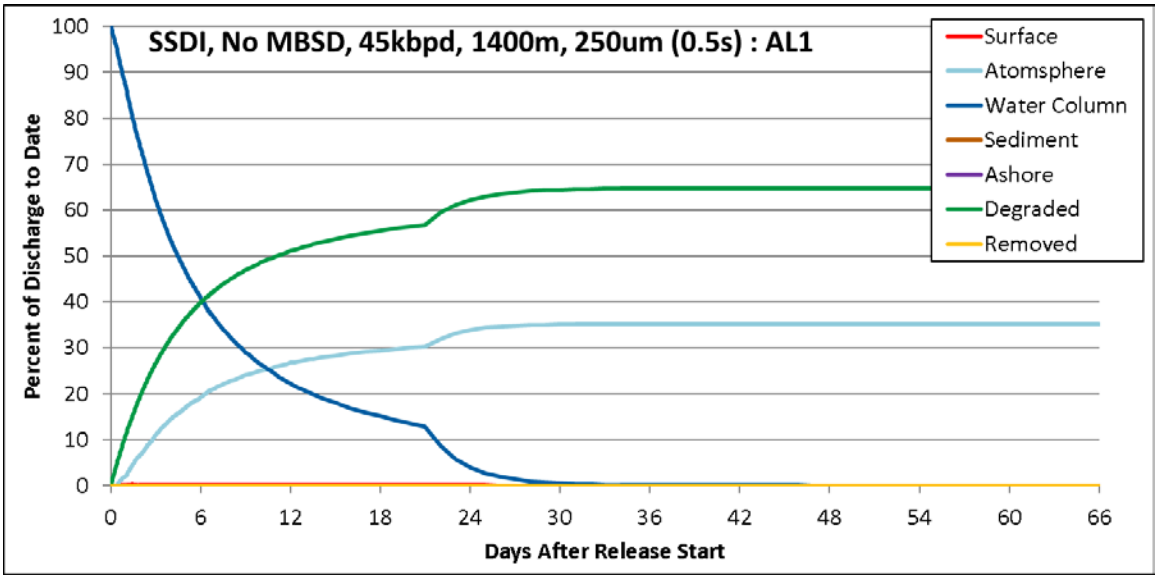

Figure 29. Percent of spilled mass of pseudo-component AL1 in various environmental compartments for case #2 (assuming d_{50} = 250 µm and s_d = 0.5).

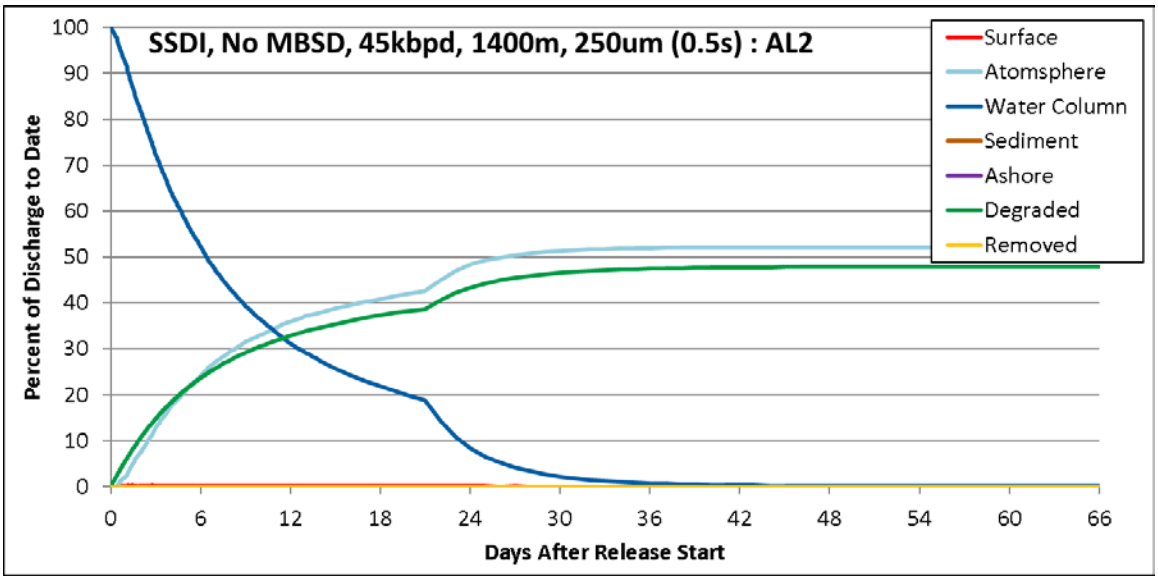

Figure 30. Percent of spilled mass of pseudo-component AL2 in various environmental compartments for case #2 (assuming d_{50} = 250 µm and s_d = 0.5).

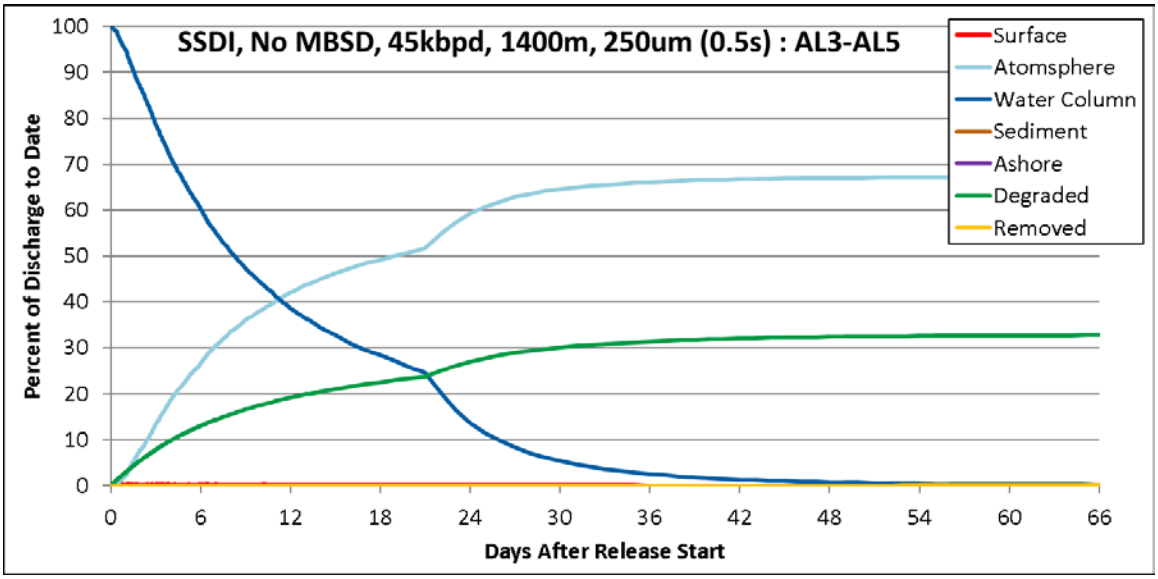

Figure 31. Percent of spilled mass of pseudo-components AL3, AL4 and AL5 (aliphatics summed over boiling range 180-280ºC) in various environmental compartments for case #2 (assuming d_{50} = 250 µm and s_d = 0.5).

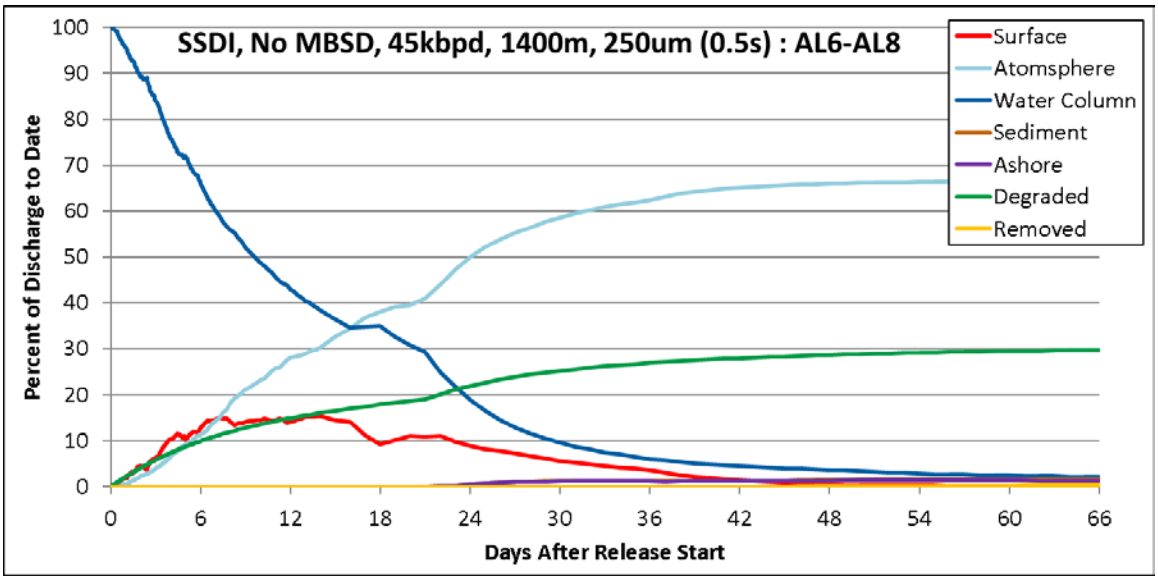

Figure 32. Percent of spilled mass of pseudo-components AL6, AL7 and AL8 (summed for boiling range 280-380ºC) in various environmental compartments for case #2 (assuming d_{50} = 250 µm and s_d = 0.5).

3.4.3 Fraction and Fate in Deep Water

Figures 33 to 40 show the fraction of the spilled oil reaching surface waters over time, as well as the distribution of the mass in the deeper water between dissolved, particulate (droplet), and degraded forms. Figures 33 to 36 show four assumed droplet size distributions for releases from an intrusion at 1100 m, and Figures 37 to 40 show the same four droplet size distributions for releases from an intrusion at 220 m. There is dramatic difference in the fraction of spilled oil rising to surface waters over the droplet size range from d_{50} = 50 μm to d_{50} = 700 μm, with most of the oil remaining in deep water when d_{50} = 50 μm and most oil rapidly surfacing when $d_{50} \geq$ 700 μm. For the cases assuming d_{50} = 250 μm, more mass rises to surface waters when the discharge is in shallower water. The dissolved fraction in deep water is always small because dissolved hydrocarbons are rapidly degraded. The fate of the hydrocarbons in deep water is for the most part to be biodegraded, but a small fraction settles to the sediments.

Figures 41 and 42 summarize the fate of the oil in deep water and the fraction reaching surface waters as a function of d_{50}. The results show a dramatic reduction of oil reaching surface waters below d_{50} = 700 μm for the 1100-m intrusion and below d_{50} = 500 μm for the 220-m intrusion.

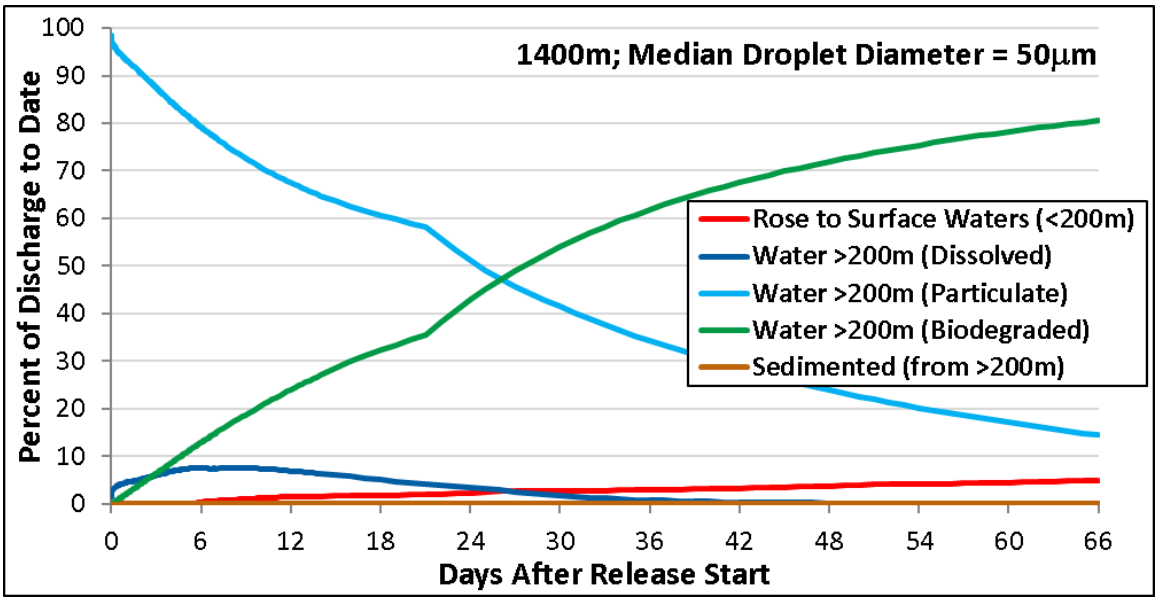

Figure 33. Percent of spilled mass to date by environmental compartment below 200m, as compared to percentage that rose into waters <200 m, for case #29: 1400-m spills with intrusion at 1100 m below surface, assuming d_{50} = 50 μm and s_d = 0.5, and other inputs as in Table 1.

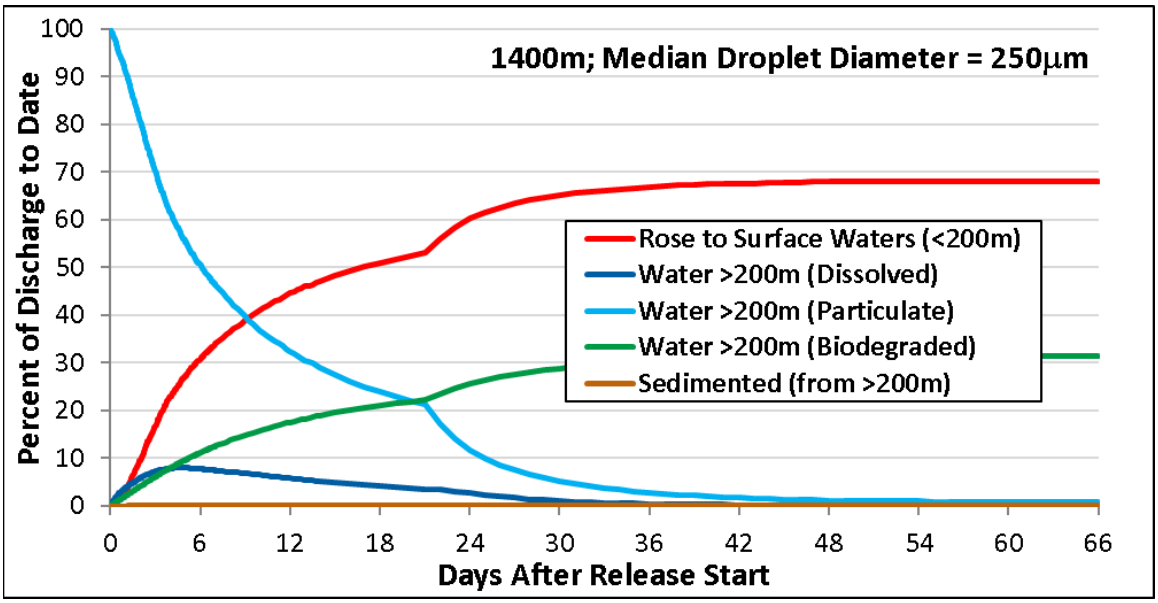

Figure 34. Percent of spilled mass to date by environmental compartment below 200m, as compared to percentage that rose into waters <200 m, for case #2: 1400-m spills with intrusion at 1100 m below surface, assuming d_{50} = 250 μm and s_d = 0.5, and other inputs as in Table 1.

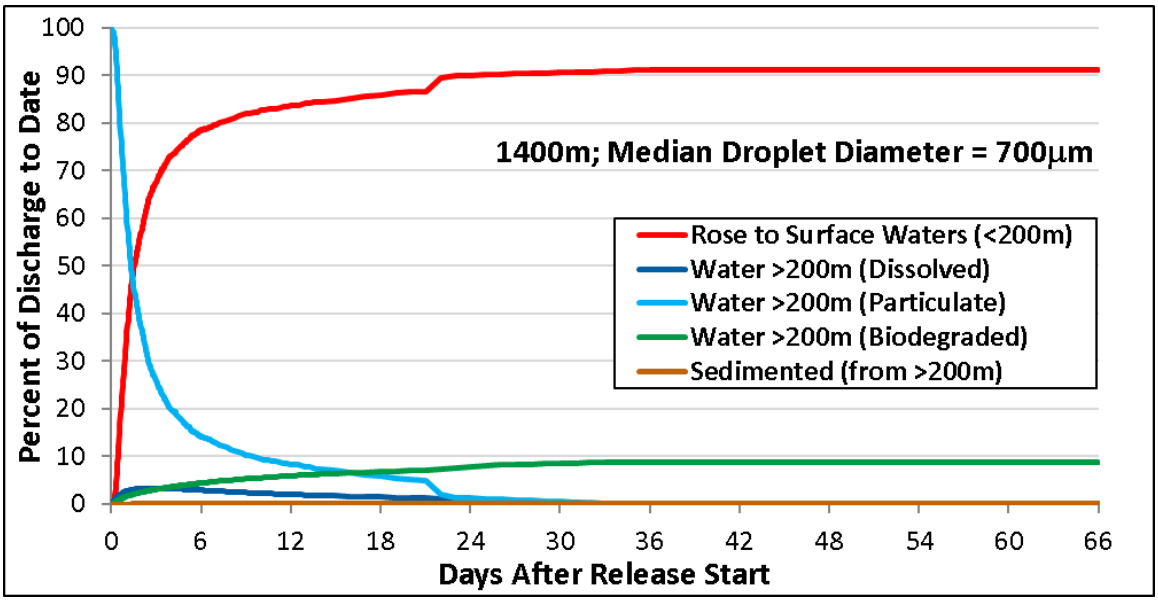

Figure 35. Percent of spilled mass to date by environmental compartment below 200m, as compared to percentage that rose into waters <200 m, for case #5: 1400-m spills with intrusion at 1100 m below surface, assuming d_{50} = 700 μm and s_d = 0.5, and other inputs as in Table 1.

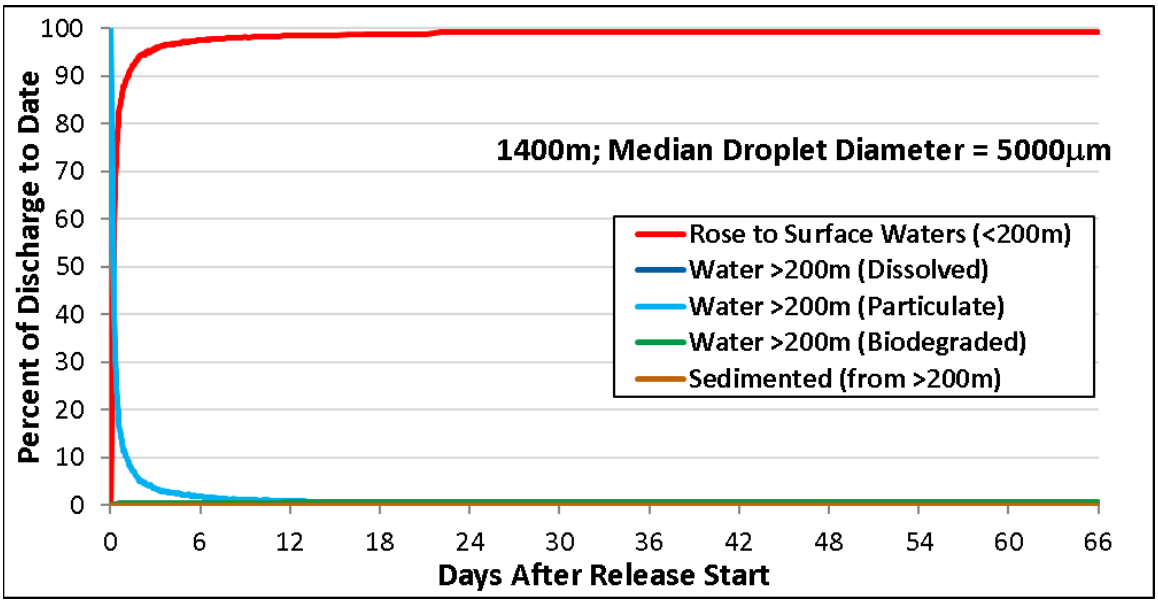

Figure 36. Percent of spilled mass to date by environmental compartment below 200m, as compared to percentage that rose into waters <200 m, for case #8: 1400-m spills with intrusion at 1100 m below surface, assuming d_{50} = 5000 μm and s_d = 0.5, and other inputs as in Table 1.

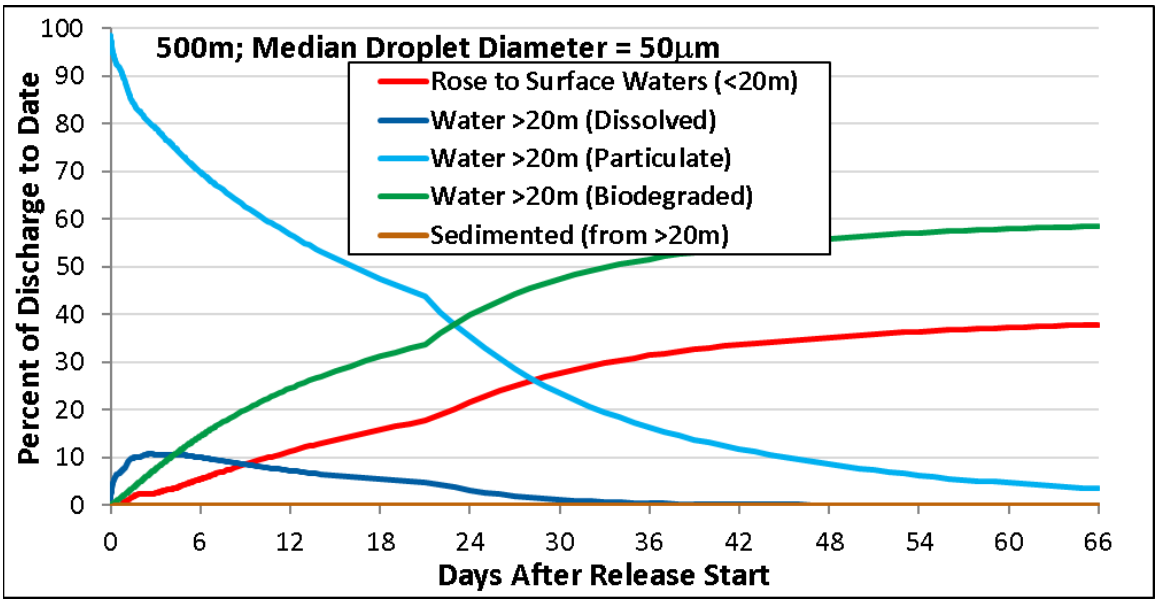

Figure 37. Percent of spilled mass to date by environmental compartment below 20m, as compared to percentage that rose into waters <20 m, for case #26: 500-m spills with intrusion at 220 m below surface, assuming d_{50} = 50 µm and s_d = 0.5, and other inputs as in Table 1.

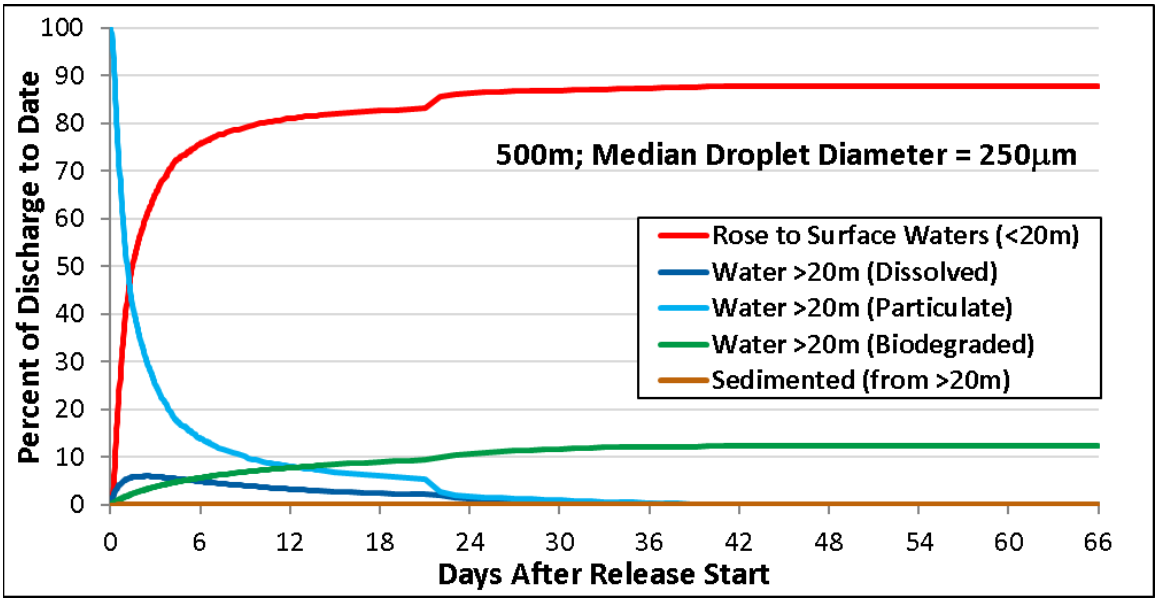

Figure 38. Percent of spilled mass to date by environmental compartment below 20m, as compared to percentage that rose into waters <20 m, for case #13: 500-m spills with intrusion at 220 m below surface, assuming d_{50} = 250 µm and s_d = 0.5, and other inputs as in Table 1.

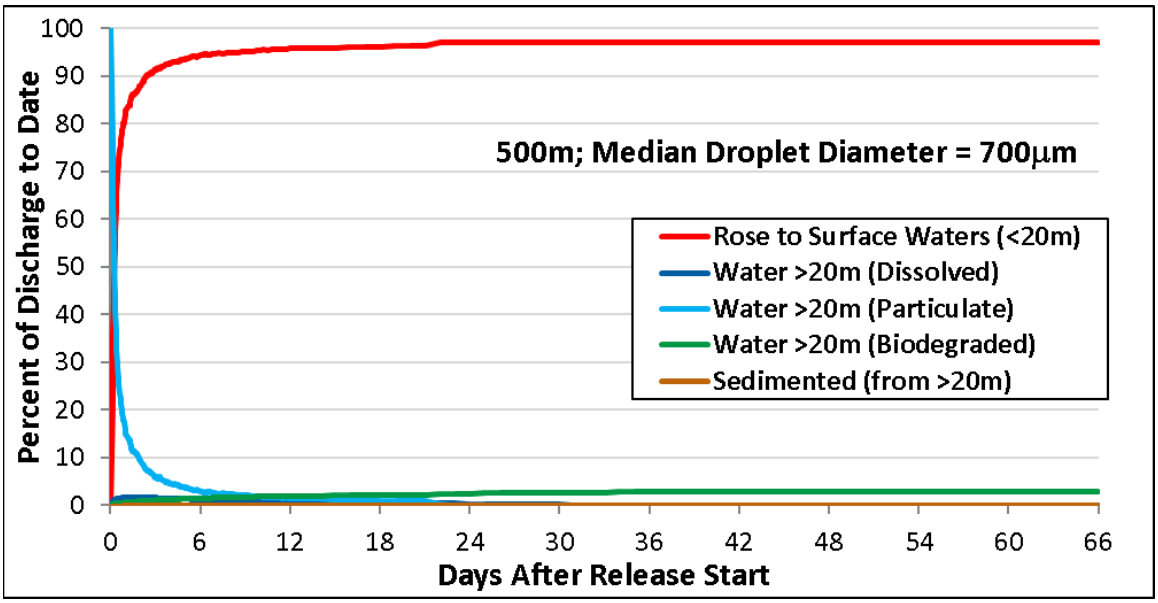

Figure 39. Percent of spilled mass to date by environmental compartment below 20m, as compared to percentage that rose into waters <20 m, for case #16: 500-m spills with intrusion at 220 m below surface, assuming d_{50} = 700 µm and s_d = 0.5, and other inputs as in Table 1.

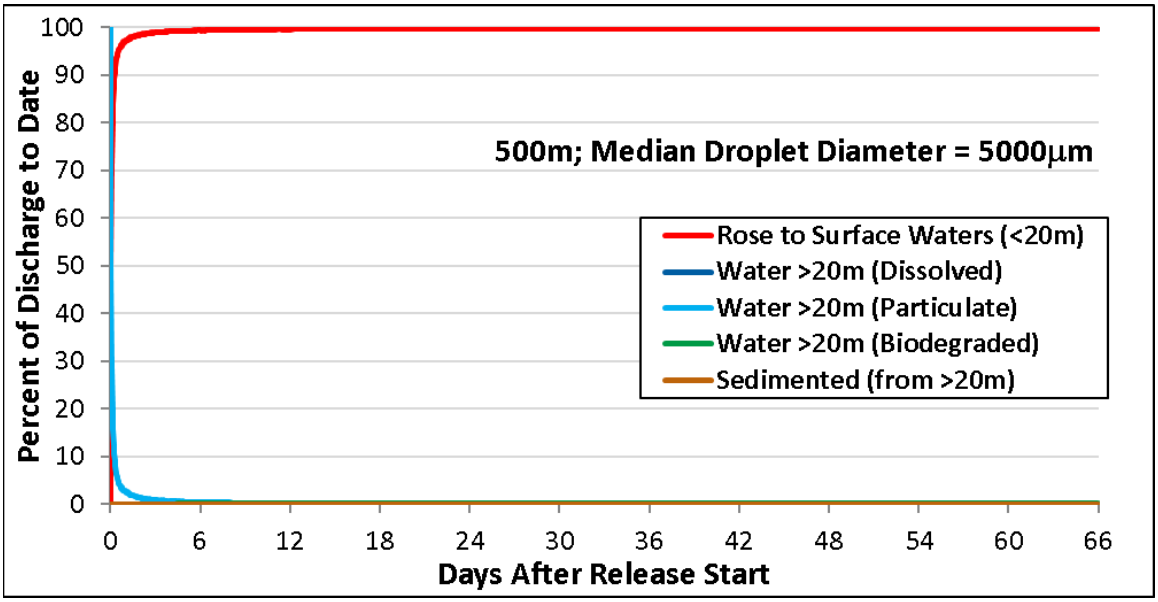

Figure 40. Percent of spilled mass to date by environmental compartment below 20m, as compared to percentage that rose into waters <20 m, for case #19: 500-m spills with intrusion at 220 m below surface, assuming d_{50} = 5000 µm and s_d = 0.5, and other inputs as in Table 1.

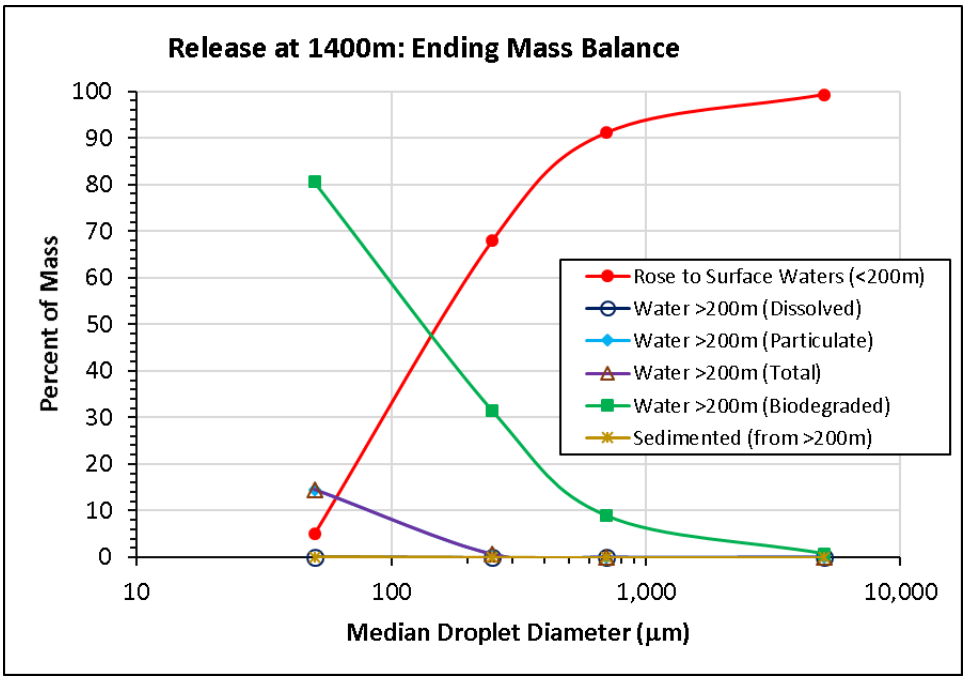

Figure 41. Percent of spilled mass by environmental compartment below 200m, as compared to percentage that rose into waters <200 m, at 66-days after spill start as a function of d_{50} – 1400-m spills with intrusion at 1100 m below surface.

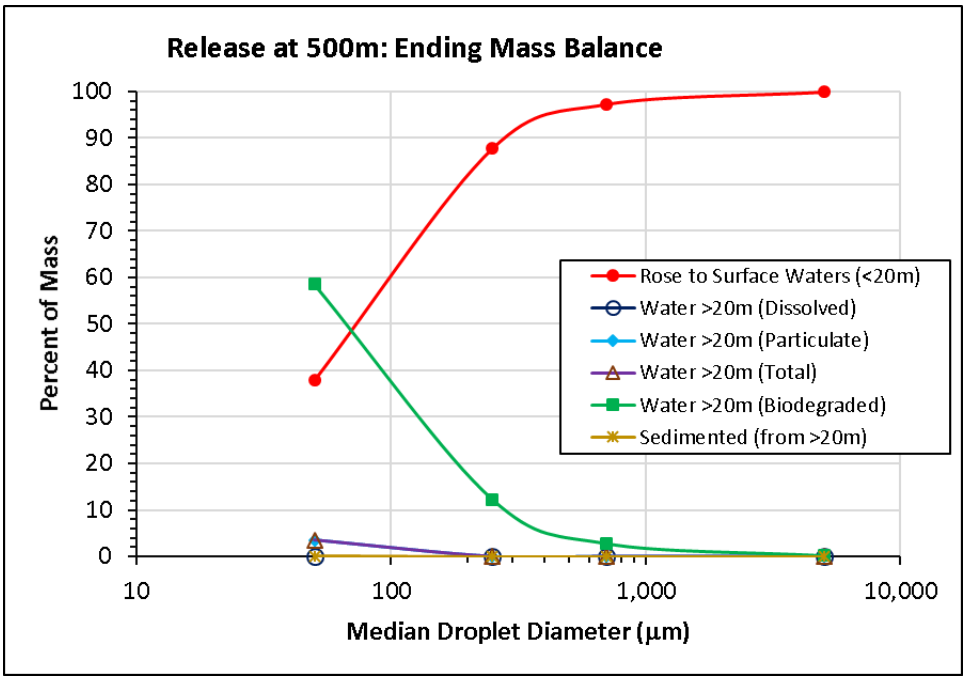

Figure 42. Percent of spilled mass by environmental compartment below 20m, as compared to percentage that rose into waters <20 m, at 66-days after spill start as a function of d_{50} – 500-m spills with intrusion at 220 m below surface.

3.4.4 Water Column Degradation Rates

Figures 43 to 45 show the sensitivity of oil fate to the assumed degradation rates of oil components in the water column. For three d_{50} cases (#13, d_{50} = 250 μm; #16, d_{50} = 700 μm; #19, d_{50} = 5000 μm), model runs were performed altering only the component-specific first-order biodegradation and photo-oxidation rates to 50% of the base case rates and to zero water column degradation. It is evident from Figures 43 to 45 that decreasing the degradation rates is reflected by an increase in the mass remaining in the water column, and that other environmental compartments are negligibly changed. In other words, for a given droplet size distribution, the total oil mass in the water column – in droplets, dissolved form, and degraded – is essentially the same with change in degradation rates. The amount of the spilled oil degraded increases with decreasing d_{50}, and so the trends are much more evident for d_{50} = 250 μm than for larger d_{50} s.

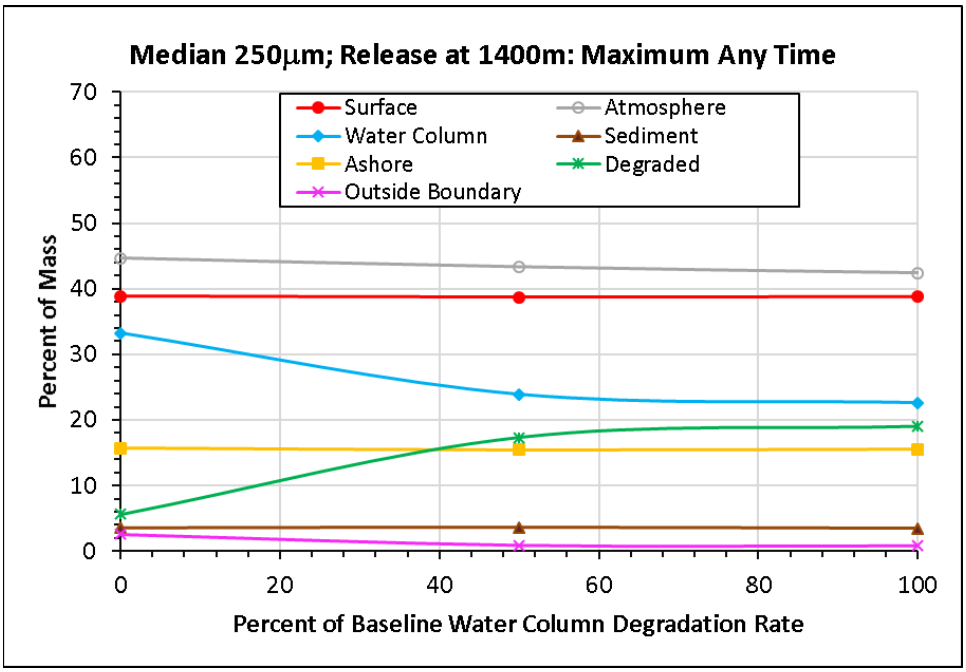

Figure 43. Maximum percent of the released oil mass in each compartment at any time after the spill as a function of the water column degradation rate set assumed, for releases with d_{50} = 250 μm –1400-m spills with intrusion at 1100 m below surface.

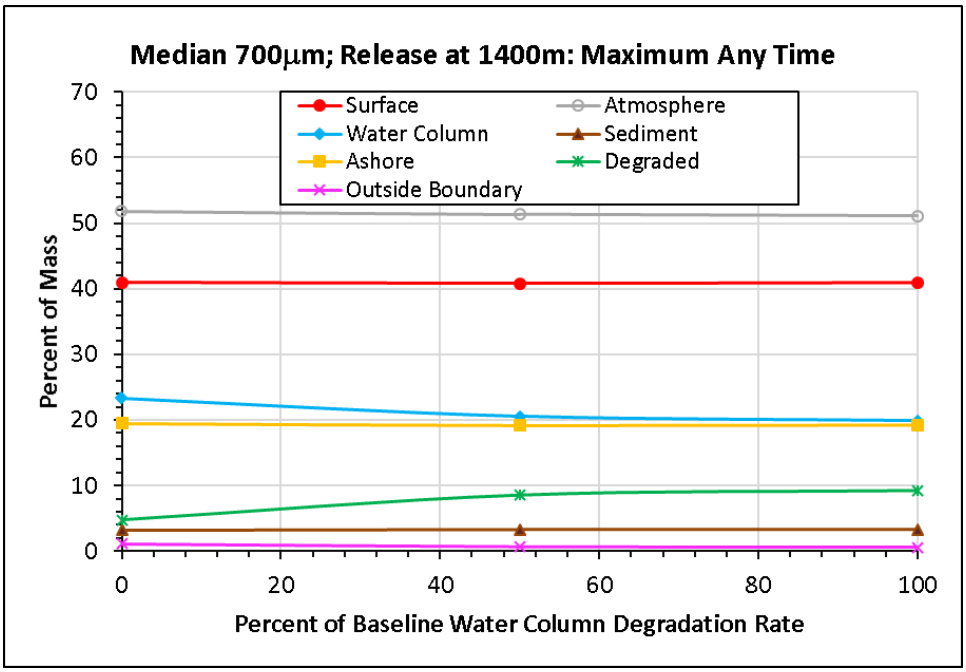

Figure 44. Maximum percent of the released oil mass in each compartment at any time after the spill as a function of the water column degradation rate set assumed, for releases with d_{50} = 700 μm –1400-m spills with intrusion at 1100 m below surface.

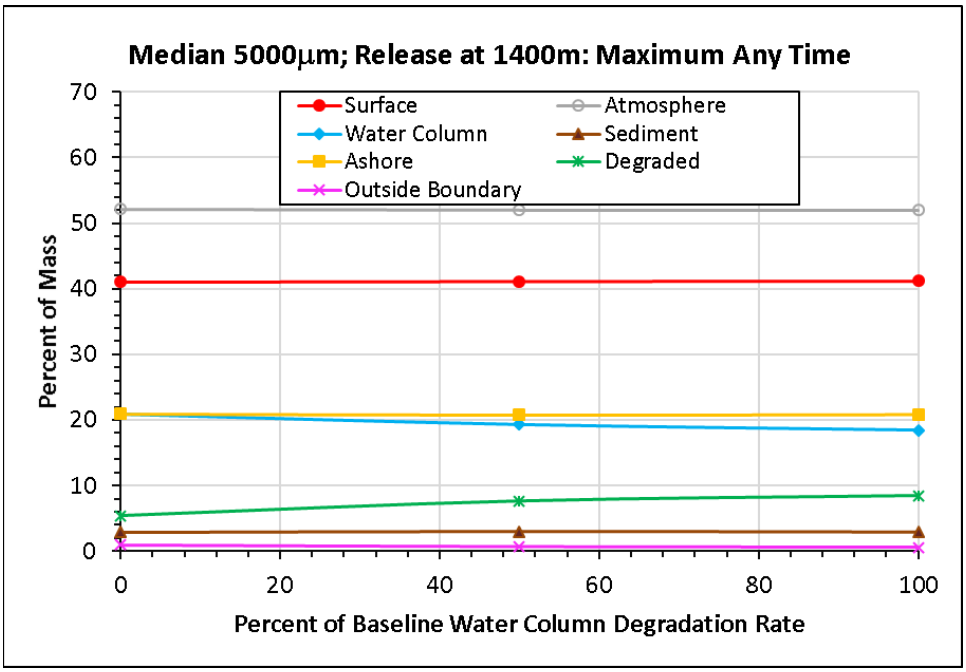

Figure 45. Maximum percent of the released oil mass in each compartment at any time after the spill as a function of the water column degradation rate set assumed, for releases with d_{50} = 5000 μm –1400-m spills with intrusion at 1100 m below surface.

4 References

Al-Rabeh, A.H., H.M. Cekirge and N. Gunay. 1989. A stochastic simulation model of oil spill fate and transport. Applied Mathematical Modelling 13, 322–329.

Bock, M., H. Robinson, R. Wenning, D, French-McCay, J. Rowe, and A. H. Walker. 2018. Comparative risk assessment of spill response options for a deepwater oil well blowout: Part II. Relative risk methodology. Mar. Pollut. Bull., http://dx.doi.org/10.1016/j.marpolbul.2018.05.032.

Boyer, T., S. Levitus, H. Garcia, R. A. Locarnini, C. Stephens and J. Antonov. 2004. Objective Analyses of Annual, Seasonal, and Monthly Temperature and Salinity for the World Ocean on a ¼ E Grid. International Journal of Climatology. 25:931-945.

Buchholz, K., A. Krieger, J. Rowe, D. Schmidt Etkin, D. French-McCay, M. Gearon, M. Grennan, and J. Turner. 2016. Worst Case Discharge Scenarios for Oil and Gas Offshore Facilities and Oil Spill Response Equipment Capabilities. Task 2: Oil Spill Response Equipment Capabilities Analysis (Volume II). Oil Spill Response Plan (OSRP) Equipment Capabilities Review, BPA No. E14PB00072, Bureau of Safety and Environmental Enforcement (BSEE), Oil Spill Preparedness Division (OSPD), Washington, D.C., February 29, 2016, 172p.[https://www.bsee.gov/site-page/worst-case-discharge-scenarios-for-oil-and-gas-offshore-facilities-and-oil-spill-response]

Chen, F. and P. Yapa, 2007. Estimating the Oil Droplet Size Distributions in Deepwater Oil Spills. Journal of Hydraulic Engineering 133(2).

Crowley, D., D. Mendelsohn, N.W. Mulanaphy, Z. Li, and M.L. Spaulding. 2014. Modeling subsurface dispersant applications for response planning and preparation. International Oil Spill Conference Proceedings, Vol. 2014, No. 1, pp. 933-948. [https://doi.org/10.7901/2169-3358-2014-1-933]

Daae, R.L., J. Skancke, P. J. Brandvik, L.-G. Faksness, 2018. The sensitivity of the surface oil signature to subsurface dispersant injection and weather conditions. Marine Pollution Bulletin 127: 175–181. https://doi.org/10.1016/j.marpolbul.2017.11.067.

ExxonMobil, 2016. Crude oil blends by API gravity and by sulfur content. http:// corporate.exxonmobil.com/en/company/worldwide-operations/crude-oils/crude- blends-by-characteristic, Accessed date: 3 May 2016.

French, D.P. and H. Rines. 1997. Validation and use of spill impact modeling for impact assessment. International Oil Spill Conference Proceedings, Vol. 1997, No. 1, pp. 829-834. [https://doi.org/10.7901/2169-3358-1997-1-829]

French, D.P., H. Rines and P. Masciangioli. 1997. Validation of an Orimulsion spill fates model using observations from field test spills. In: Proceedings of the 20th AMOP Technical Seminar, Environment and Climate Change Canada, Ottawa, ON, Canada, 20, 933-961.

French McCay, D.P. 2002. Development and application of an oil toxicity and exposure model, OilToxEx. Environmental Toxicology and Chemistry 21(10): 2080-2094.

French-McCay, D.P. 2003. Development and application of damage assessment modeling: Example assessment for the North Cape oil spill. Mar. Pollut. Bull. 47(9-12), 341-359.

French-McCay, D.P. 2004. Oil spill impact modeling: development and validation. Environ. Toxicol. Chem. 23(10), 2441-2456.

French-McCay, D.P, K. Jayko, Z. Li, M. Horn, Y. Kim, T. Isaji, D. Crowley, M. Spaulding, L. Decker, C. Turner, S. Zamorski, J. Fontenault, R. Shmookler, and J.J. Rowe. 2015. Technical Reports for Deepwater Horizon Water Column Injury Assessment – WC_TR14: Modeling Oil Fate and Exposure Concentrations in the Deepwater Plume and Cone of Rising Oil Resulting from the Deepwater Horizon Oil Spill. DWH NRDA Water Column Technical Working Group Report. Prepared for National Oceanic and Atmospheric Administration by RPS ASA, South Kingstown, RI, USA. September 29, 2015. Administrative Record no. DWH-AR0285776.pdf [https://www.doi.gov/deepwaterhorizon/adminrecord]

French-McCay, D.P. and J.J. Rowe. 2004. Evaluation of bird impacts in historical oil spill cases using the SIMAP oil spill model. In Proceedings of the 27th AMOP Technical Seminar, Environment and Climate Change Canada, Ottawa, ON, Canada, 27, 421-452.

French-McCay, D., N. Whittier, S. Sankaranarayanan, J. Jennings, and D. S. Etkin. 2004. Estimation of potential impacts and natural resource damages of oil. J. Hazardous Materials 107(1-2), 11-25.

French-McCay, D.P., N. Whittier, C. Dalton, J.J. Rowe, and S. Sankaranarayanan. 2005. Modeling fates and impacts of hypothetical oil spills in Delaware, Florida, Texas, California, and Alaska waters, varying response options including use of dispersants. International Oil Spill Conference Proceedings, Vol. 2005, No. 1, pp. 735-740. [https://doi.org/10.7901/2169-3358-2005-1-735]

French McCay, D.P, K. Jayko, Z. Li, M. Horn, Y. Kim, T. Isaji, D. Crowley, M. Spaulding, L. Decker, C. Turner, S. Zamorski, J. Fontenault, R. Shmookler, and J.J. Rowe. 2015. Technical Reports for Deepwater Horizon Water Column Injury Assessment – WC_TR14: Modeling Oil Fate and Exposure Concentrations in the Deepwater Plume and Cone of Rising Oil Resulting from the Deepwater Horizon Oil Spill. DWH NRDA Water Column Technical Working Group Report. Prepared for National Oceanic and Atmospheric Administration by RPS ASA, South Kingstown, RI, USA. September 29, 2015. Administrative Record no. DWH-AR0285776.pdf [https://www.doi.gov/deepwaterhorizon/adminrecord]

French-McCay, D.P, Z. Li, M. Horn, D. Crowley, M. Spaulding, D. Mendelsohn, and C. Turner. 2016. Modeling oil fate and subsurface exposure concentrations from the Deepwater Horizon oil spill. In: Proceedings of the 39th AMOP Technical Seminar, Environment and Climate Change Canada, Ottawa, ON, Canada, 39, 115-150.

French-McCay, D., M. Horn, Z. Li, K. Jayko, M. Spaulding, D. Crowley, and D. Mendelsohn, 2018a. Modeling distribution, fate, and concentrations of Deepwater Horizon oil in subsurface waters of the Gulf of Mexico. Chapter 31 In: S.A. Stout and Z. Wang (eds.) Case Studies in Oil Spill Environmental Forensics. Elsevier, ISBN: 978-O-12-804434-6, pp. 683-736.

French-McCay, D. K. Jayko, Z. Li, M. Horn, T. Isaji, M. Spaulding. 2018b. Volume II: Appendix II - Oil Transport and Fates Model Technical Manual. In: Galagan, C.W., D. French-McCay, J. Rowe, and L. McStay, editors. Simulation Modeling of Ocean Circulation and Oil Spills in the Gulf of Mexico. Prepared by RPS ASA for the US Department of the Interior, Bureau of Ocean Energy Management, Gulf of Mexico OCS Region, New Orleans, LA. OCS Study BOEM 20xx-xxx; xxx p.

French-McCay, D., M. Horn, Z. Li, D. Crowley, M. Spaulding, D. Mendelsohn, K. Jayko, Y. Kim, T. Isaji, J. Fontenault, R. Shmookler, and J. Rowe. 2018c. Volume III: Data Collection, Analysis and Model Validation. In: Galagan, C.W., D. French-McCay, J. Rowe, and L. McStay, editors. Simulation Modeling of Ocean Circulation and Oil Spills in the Gulf of Mexico. Prepared by RPS ASA for the US Department of the Interior, Bureau of Ocean Energy Management, Gulf of Mexico OCS Region, New Orleans, LA. OCS Study BOEM 20xx-xxx; xxx p.

French-McCay, D., D. Crowley, J. Rowe, M. Bock, H. Robinson, R. Wenning, A. H. Walker, J. Joeckel, and T. Parkerton. 2018d. Comparative Risk Assessment of Spill Response Options for a Deepwater Oil Well Blowout: Part I. Oil Spill Modeling. Marine Pollution Bulletin, https://doi.org/10.1016/j.marpolbul.2018.05.042.

Kaplan, S., and B.J. Garrick, On the Quantitative Definition of Risk, Risk Analysis, 1(1):11–27, 1981.

Lee, Kenneth (chair), Michel Boufadel, Bing Chen, Julia Foght, Peter Hodson, Stella Swanson, Albert Venosa. (2015). Expert Panel Report on the Behaviour and Environmental Impacts of Crude Oil Released into Aqueous Environments. Royal Society of Canada, Ottawa, ON. ISBN: 978-1- 928140-02-3

Li, Z., M. L. Spaulding, and D. French-McCay, D. Crowley, and J. R. Payne. 2017. Development of a unified oil droplet size distribution model with application to surface breaking waves and subsea blowout releases considering dispersant effects. Marine Pollution Bulletin 114 (1): 247–257.

Mackay, D., S. Chang, and P. G. Wells, 1982. Calculation of oil concentrations under chemically dispersed slick. Marine Pollution Bulletin, 3(8): 278-283.

McGrath J, Parkerton T, Hellweger F, Di Toro D. 2005. Validation of the narcosis target lipid model for petroleum products: Gasoline as a case study. Environ. Toxicol. Chem. 24: 2382-2394.

National Research Council (NRC). 1989. Using Oil Spill Dispersants on the Sea, National Academy Press, Washington, D.C., USA.

National Research Council (NRC). 2003. Ocean Studies, Oil in Sea III. Inputs, Fates and Effects. National Research Council, The National Academies Press, Washington, USA, 446p.

National Research Council (NRC). 2005. Understanding Oil Spill Dispersants: Efficacy and Effects, National Academy Press, Washington, D.C., USA, 277p.

Nissanka, I. D., and P. D. Yapa. 2016. Calculation of oil droplet size distribution in an underwater oil well blowout. Journal of Hydraulic Research 54 (3): 307–20. https://doi.org/10.1080/00221686.2016.1144656.

North E.W., E. E. Adams, A. Thessen, E., Z. Schlag, R. He, S. Socolofsky, A., S. Masutani, M. and S. D. Peckham, 2015. The influence of droplet size and biodegradation on the transport of subsurface oil droplets during the Deepwater Horizon spill: a model sensitivity study. Environmental Research Letters 10(2):024016.

Operational Science Advisory Team (OSAT), 2010. Summary Report for Subsea and Subsurface Oil and Dispersant Protection: Sampling and Monitoring. Prepared for: Paul F. Zukunft, RADM, U. S. Coast Guard Federal On-Scene Coordinator Deepwater Horizon MC252, Dec 17, 2010. http://www.restorethegulf.gov/sites/default/files/documents/pdf/OSAT_Report_FINAL_17DEC.pdf

Price, J.M., W.R. Johnson, C.F. Marshall, Z-G. Ji, G.R. Rainey. 2003. Overview of the Oil Spill Risk Analysis (OSRA) model for environmental impact assessment. Spill Science & Technology Bulletin 8(5–6), 529–533.

Redman A., and T. Parkerton, 2015. Guidance for improving comparability and relevance of oil toxicity tests. Marine Pollution Bulletin 98:156–170.

Reed, M., O. Johansen, P.J. Brandvik, P. Daling, A. Lewis, R. Fiocco, D. Mackay, and R. Prentki. 1999. Oil spill modeling towards the close of the 20th century: Overview of the state-of-the-art. Spill Science and Technology Bulletin 5(1): 3-16.

Skognes, K. and Ø. Johansen. 2004. Statmap – a 3-dimensional model for oil spill risk assessment. Environmental Modelling and Software 19(7), 727-737.

Socolofsky, S. A., E. E. Adams and C. R. Sherwood. 2011. Formation dynamics of subsurface hydrocarbon intrusions following the Deepwater Horizon blowout. Geophys. Res. Let., 38(9), L09602.

Socolofsky, S. A., E. E. Adams, M. C. Boufadel, Z. M. Aman, Ø. Johansen, W. J. Konkel, D. Lindo, M. N. Madsen, E. W. North, C. B. Paris, D. Rasmussen, M. Reed, P. Rønningen, L. H. Sim, T. Uhrenholdt, K. G. Anderson, C. Cooper and T. J. Nedwed. 2015. Intercomparison of oil spill prediction models for accidental blowout scenarios with and without subsea chemical dispersant injection. Marine Pollution Bulletin 96(1–2):110-126.

Spaulding, M.L., S.B. Saila, E. Lorda, H.A. Walker, E.L. Anderson and J.C. Swanson. 1983. Oil spill fishery interaction modelling: Application to selected Georges Bank fish species. Estuar., Coast. Shelf Sci. 16, 511-541.

Spaulding, M.L., P.R. Bishnoi, E. Anderson, and T. Isaji. 2000. An integrated model for prediction of oil transport from a deep water blowout. In: Proceedings of the 23rd AMOP Technical Seminar, Environment and Climate Change Canada, Ottawa, ON, Canada, 23, 611-636.

Spaulding, M.S., D. Mendelsohn, D. Crowley, Z. Li, and A. Bird, 2015. Draft Technical Reports for Deepwater Horizon Water Column Injury Assessment: WC_TR.13: Application of OILMAP DEEP to the Deepwater Horizon Blowout. DWH NRDA Water Column Technical Working Group Report. Prepared for National Oceanic and Atmospheric Administration by RPS ASA, South Kingstown, RI 02879. Administrative Record no. DWH-AR0285366.pdf [https://www.doi.gov/deepwaterhorizon/adminrecord]

Spaulding, M. Z. Li, D. Mendelsohn, D. Crowley, D. French-McCay, and A. Bird, 2017. Application of an Integrated Blowout Model System, OILMAP DEEP, to the Deepwater Horizon (DWH) Spill. Marine Pollution Bulletin 120: 37-50.

Testa, J. M., E. Eric Adams, E. W. North, and R. He, 2016. Modeling the influence of deep water application of dispersants on the surface expression of oil: A sensitivity study. J. Geophys. Res. Oceans 121: 5995–6008. doi:10.1002/2015JC011571.

Walker, A.H., D. Scholz, M. McPeek, D. French-McCay, J. Rowe, M. Bock, H. Robinson, and R. Wenning. 2018. Comparative risk assessment of spill response options for a deepwater oil well blowout: Part III. Stakeholder engagement. Mar. Pollut. Bull., available on-line.

Valentine, D. L. K., J.D.; Redmond, M.C.; Mendes, S.D.; Heintz, M.B.; Farwell, C.; Hu, L.; Kinnaman, F.S.; Yvon-Lewis, S.; Du, M.; Chan, E.W.; Tigreros, F.G.; Villanueva, C.J. 2010. Propane respiration jump-starts microbial response to a deep oil spill. Science 330: 208-211.

Venkataraman, P., Tang, J., Frenkel, E., McPherson, G.L., He, J., Raghavan, S.R., Kolesnichenko, V.L., Bose, A., John, V.T., 2013. Attachment of a Hydrophobically Modified Biopolymer at the Oil-Water Interface in the Treatment of Oil Spills. Applied Materials and Interfaces 5: 3572-3580.

Venosa, A. D. and E. L. Holder, 2007. Biodegradability of dispersed crude oil at two different temperatures. Marine Pollution Bulletin 54(5):545-553.

Zhao, Lin, Michel C. Boufadel, Scott A. Socolofsky, Eric Adams, Thomas King, and Kenneth Lee. 2014. Evolution of Droplets in Subsea Oil and Gas Blowouts: Development and Validation of the Numerical Model VDROP-J. Marine Pollution Bulletin 83 (1): 58–69. https://doi.org/10.1016/j.marpolbul.2014.04.020.

Zhao, L., M.C. Boufadel, E. Adams, S.A. Socolofsky, T. King, K. Lee, and T. Nedwed. 2015.Simulation of scenarios of oil droplet formation from the Deepwater Horizon blowout. Marine Pollution Bulletin 101(1):304–319.

Appendix A. Oil Mass by Environmental Compartment Over Time for Model Runs Varying d_{50}

Figures A.1 to A.22 show oil mass by environmental compartment over time for varying droplet size distributions and release depths (from the intrusion at the trap height). Most of these cases do not include MBSD, except for case #20 and #9 where MBSD was included. The base-case degradation rates are from French-McCay et al. 2018d.

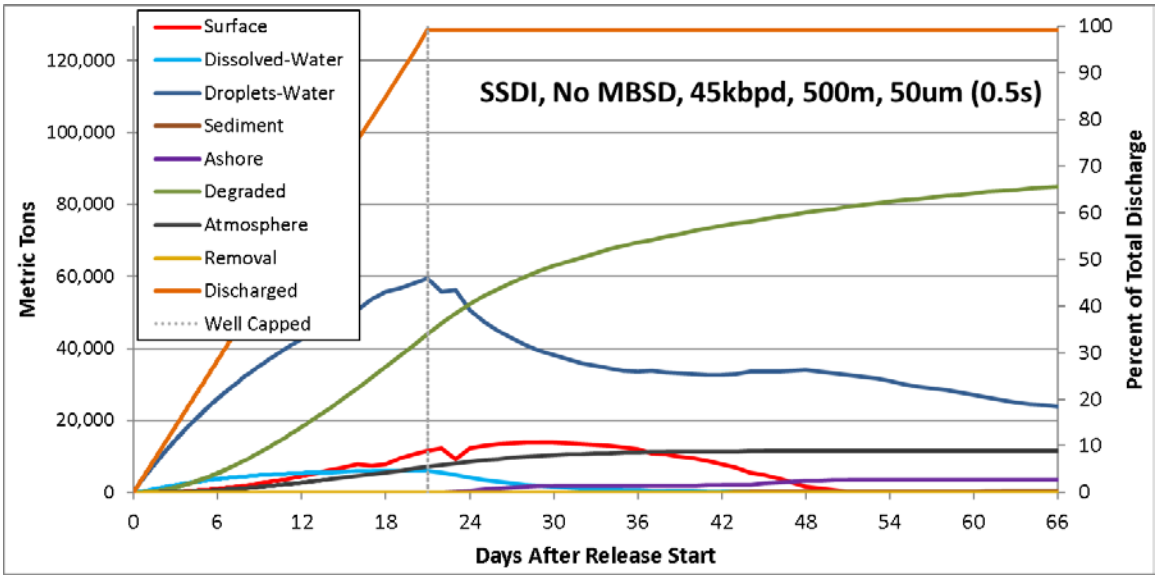

Figure A.1. Oil mass by environmental compartment over time for case #26: a spill rate of 45,000 bbl/day (7154 m^3/day) over 21 days from a 500-m intrusion depth, assuming d_{50} = 50 µm, s_d = 0.5, and base-case degradation rates.

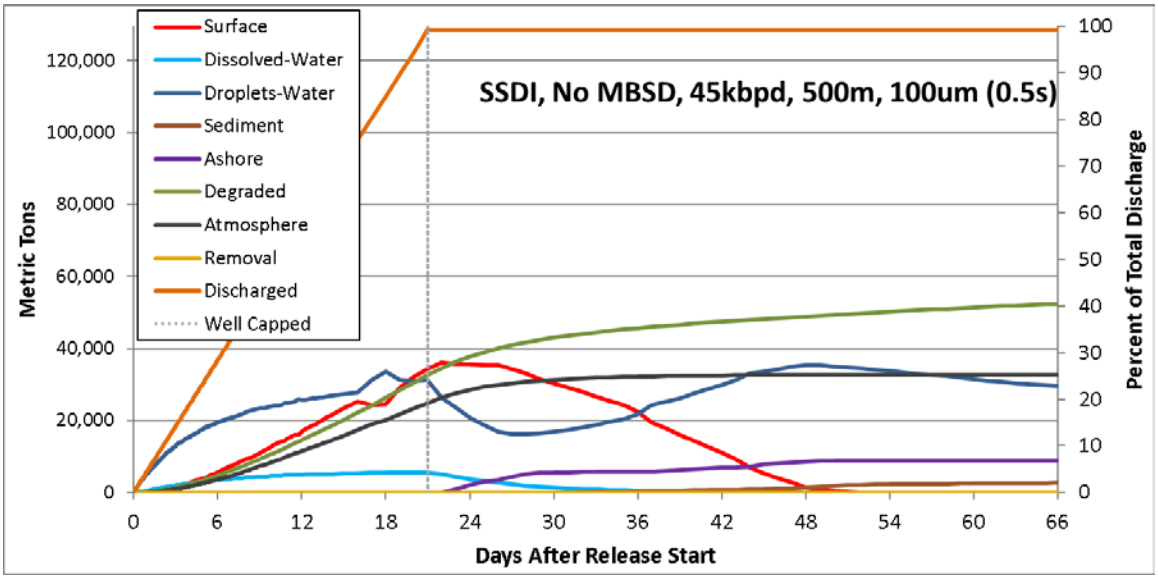

Figure A.2. Oil mass by environmental compartment over time for case #12: a spill rate of 45,000 bbl/day (7154 m^3/day) over 21 days from a 500-m intrusion depth, assuming d_{50} = 100 µm, s_d = 0.5, and base-case degradation rates.

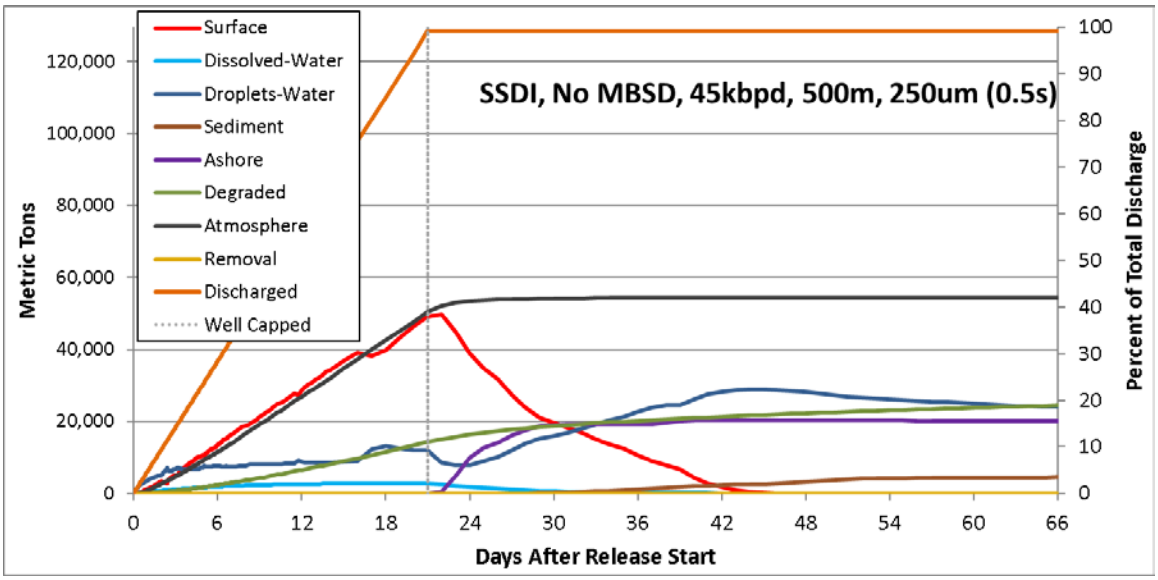

Figure A.3. Oil mass by environmental compartment over time for case #13: a spill rate of 45,000 bbl/day (7154 m^3/day) over 21 days from a 500-m intrusion depth, assuming d_{50} = 250 µm, s_d = 0.5, and base-case degradation rates.

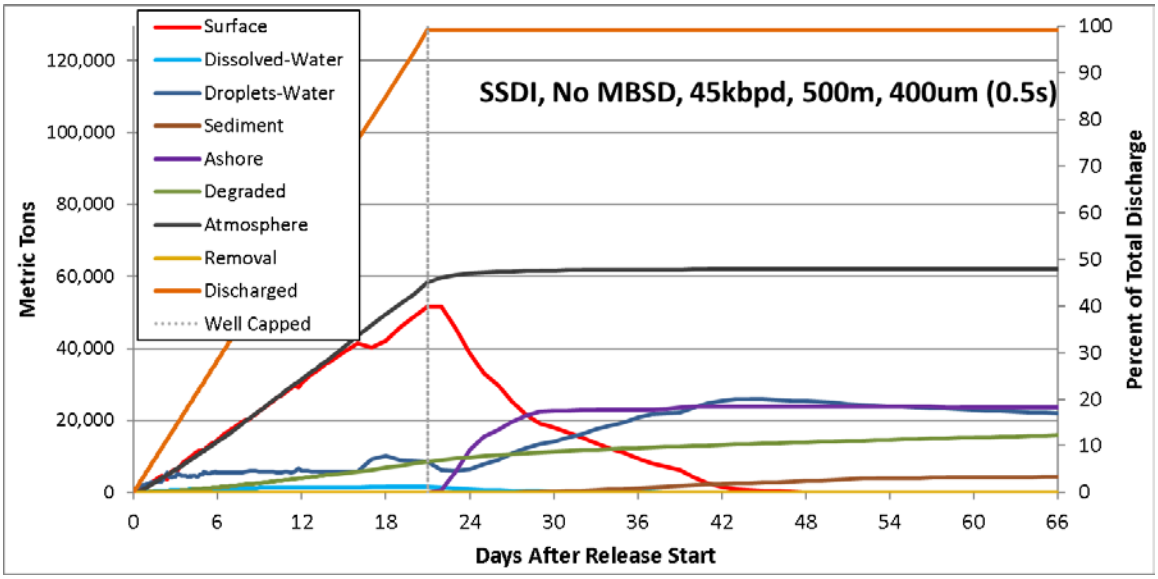

Figure A.4. Oil mass by environmental compartment over time for case #14: a spill rate of 45,000 bbl/day (7154 m^3/day) over 21 days from a 500-m intrusion depth, assuming d_{50} = 400 µm, s_d = 0.5, and base-case degradation rates.

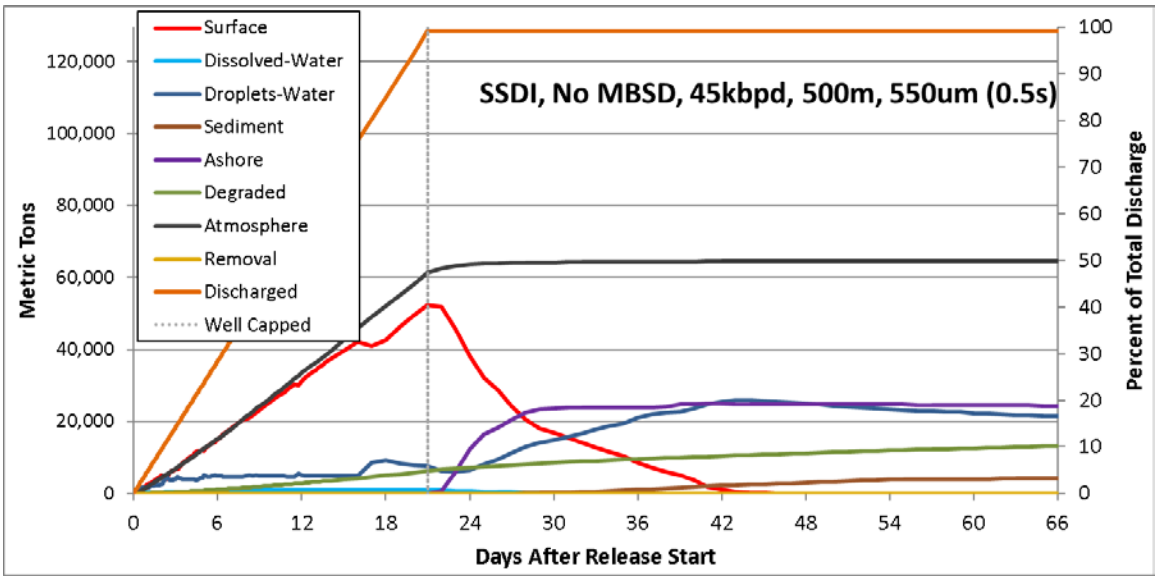

Figure A.5. Oil mass by environmental compartment over time for case #15: a spill rate of 45,000 bbl/day (7154 m^3/day) over 21 days from a 500-m intrusion depth, assuming d_{50} = 550 µm, s_d = 0.5, and base-case degradation rates.

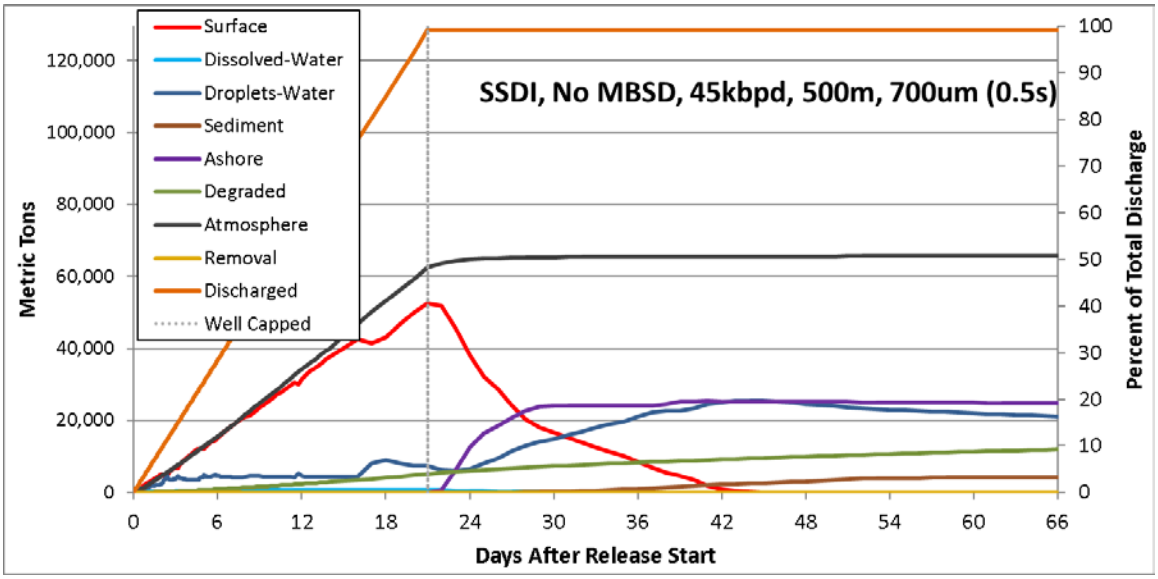

Figure A.6. Oil mass by environmental compartment over time for case #16: a spill rate of 45,000 bbl/day (7154 m^3/day) over 21 days from a 500-m intrusion depth, assuming d_{50} = 700 µm, s_d = 0.5, and base-case degradation rates.

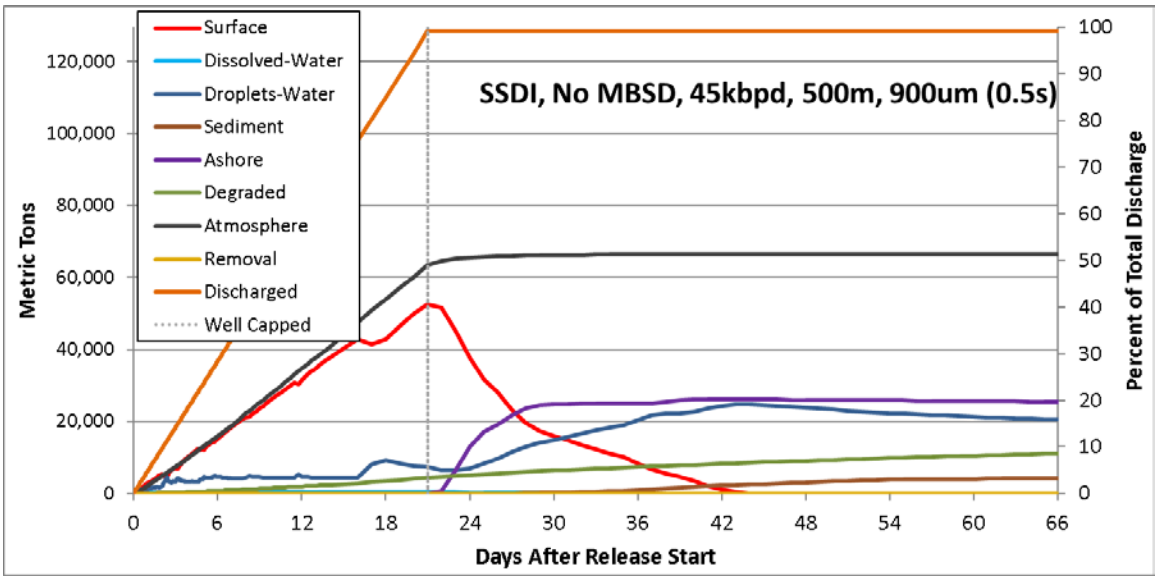

Figure A.7. Oil mass by environmental compartment over time for case #17: a spill rate of 45,000 bbl/day (7154 m^3/day) over 21 days from a 500-m intrusion depth, assuming d_{50} = 900 µm, s_d = 0.5, and base-case degradation rates.

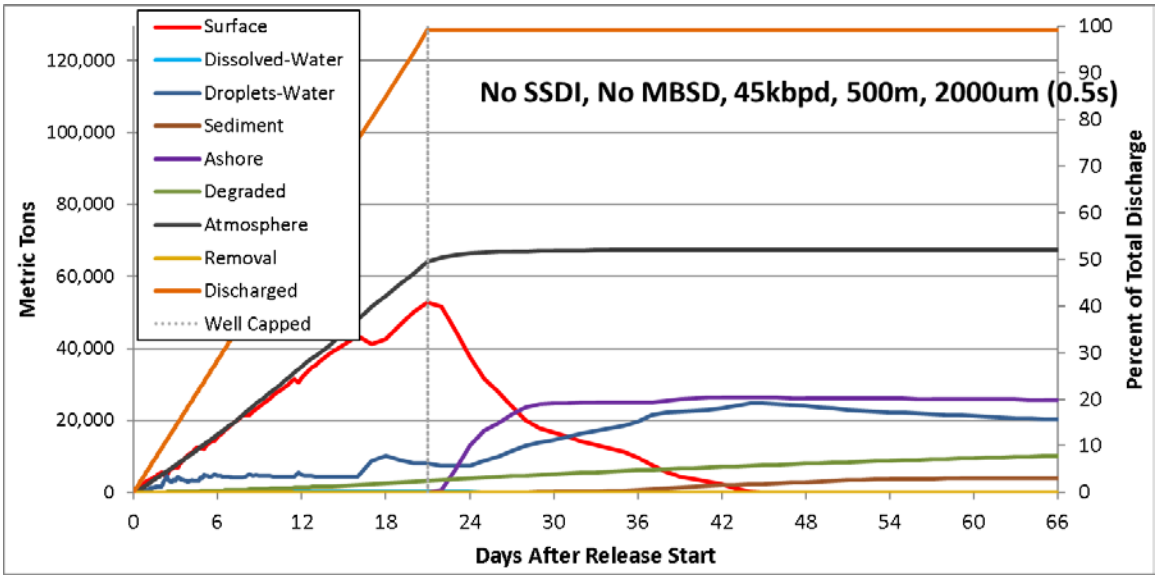

Figure A.8. Oil mass by environmental compartment over time for case #18: a spill rate of 45,000 bbl/day (7154 m^3/day) over 21 days from a 500-m intrusion depth, assuming d_{50} = 2000 µm, s_d = 0.5, and base-case degradation rates.

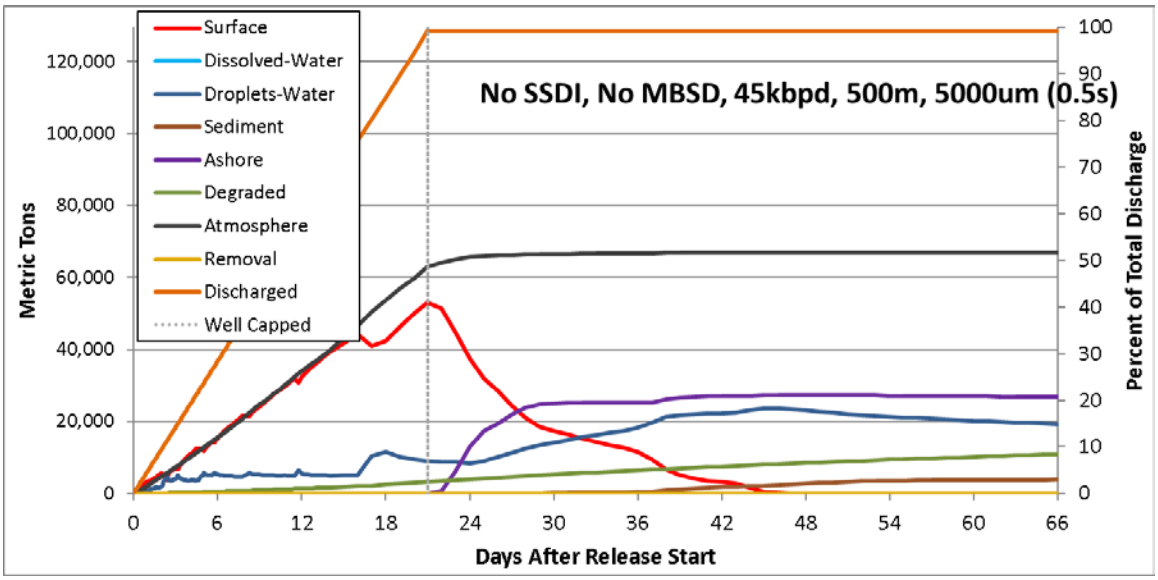

Figure A.9. Oil mass by environmental compartment over time for case #19: a spill rate of 45,000 bbl/day (7154 m^3/day) over 21 days from a 500-m intrusion depth, assuming d_{50} = 5000 µm, s_d = 0.5, and base-case degradation rates.

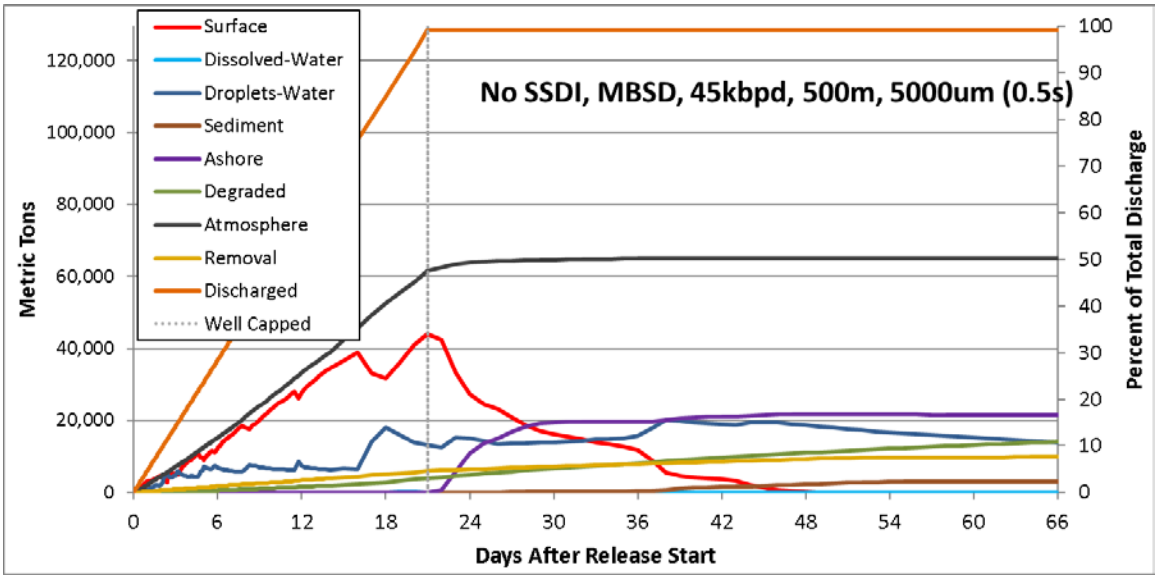

Figure A.10. Oil mass by environmental compartment over time for case #20: a spill rate of 45,000 bbl/day (7154 m^3/day) over 21 days from a 500-m intrusion depth, assuming d_{50} = 5000 µm, s_d = 0.5, and base-case degradation rates. MBSD is also included in this scenario.

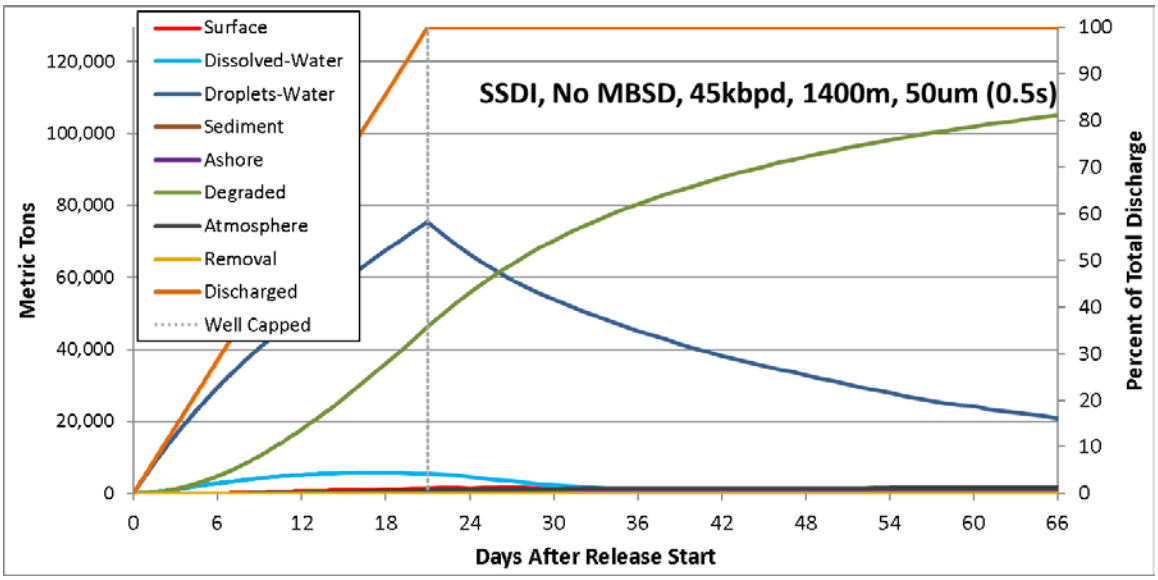

Figure A.11. Oil mass by environmental compartment over time for case #29: a spill rate of 45,000 bbl/day (7154 m^3/day) over 21 days from an 1100-m intrusion depth, assuming d_{50} = 50 µm, s_d = 0.5, and base-case degradation rates.

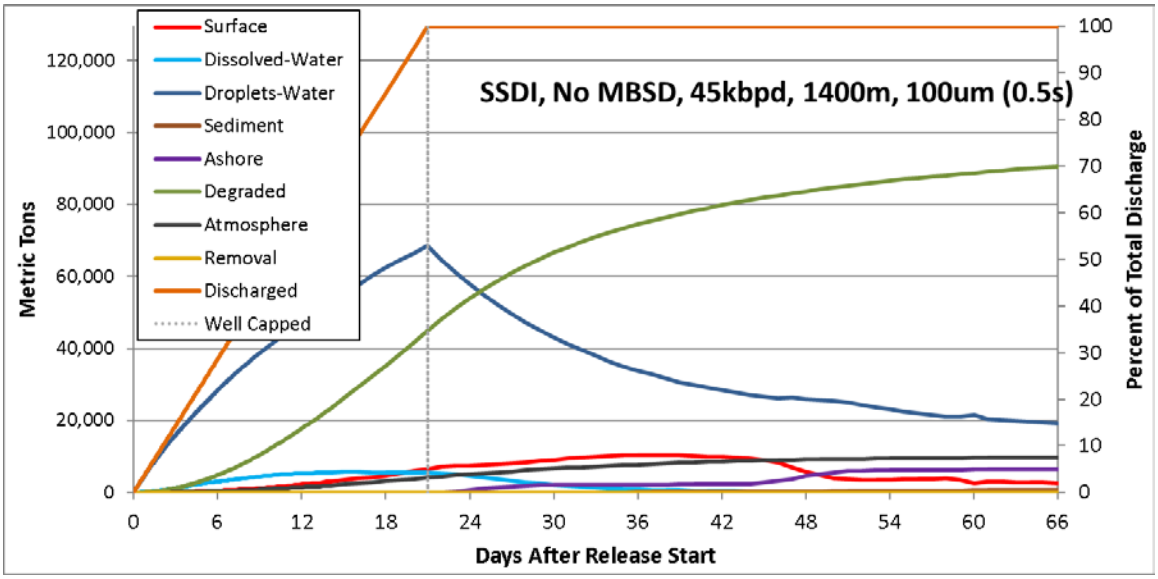

Figure A.12. Oil mass by environmental compartment over time for case #1: a spill rate of 45,000 bbl/day (7154 m^3/day) over 21 days from an 1100-m intrusion depth, assuming d_{50} = 100 µm, s_d = 0.5, and base-case degradation rates.

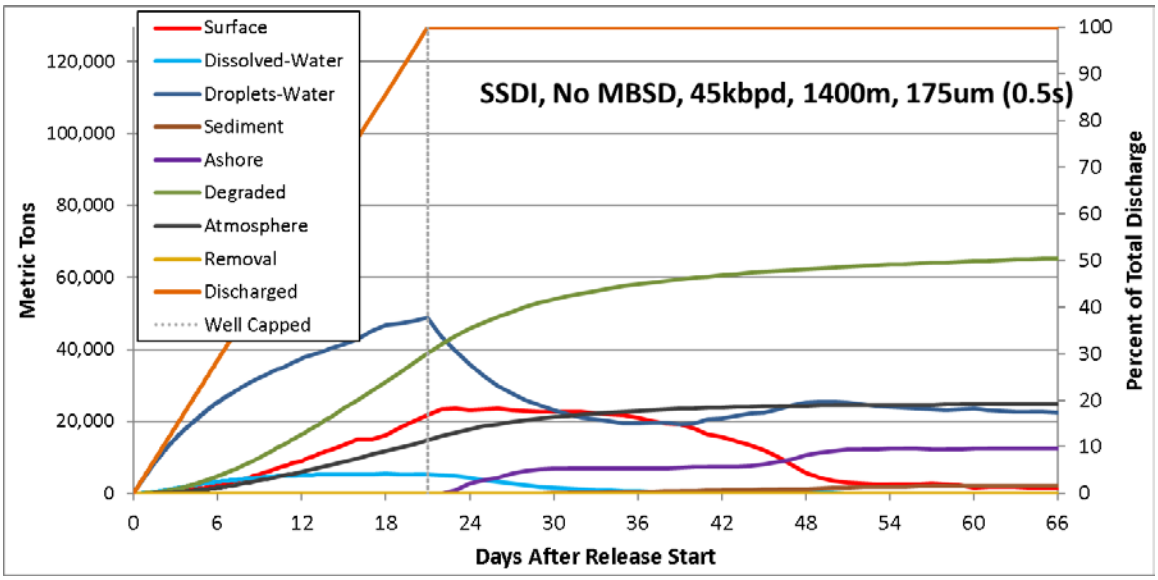

Figure A.13. Oil mass by environmental compartment over time for case #25: a spill rate of 45,000 bbl/day (7154 m^3/day) over 21 days from an 1100-m intrusion depth, assuming d_{50} = 175 µm, s_d = 0.5, and base-case degradation rates.

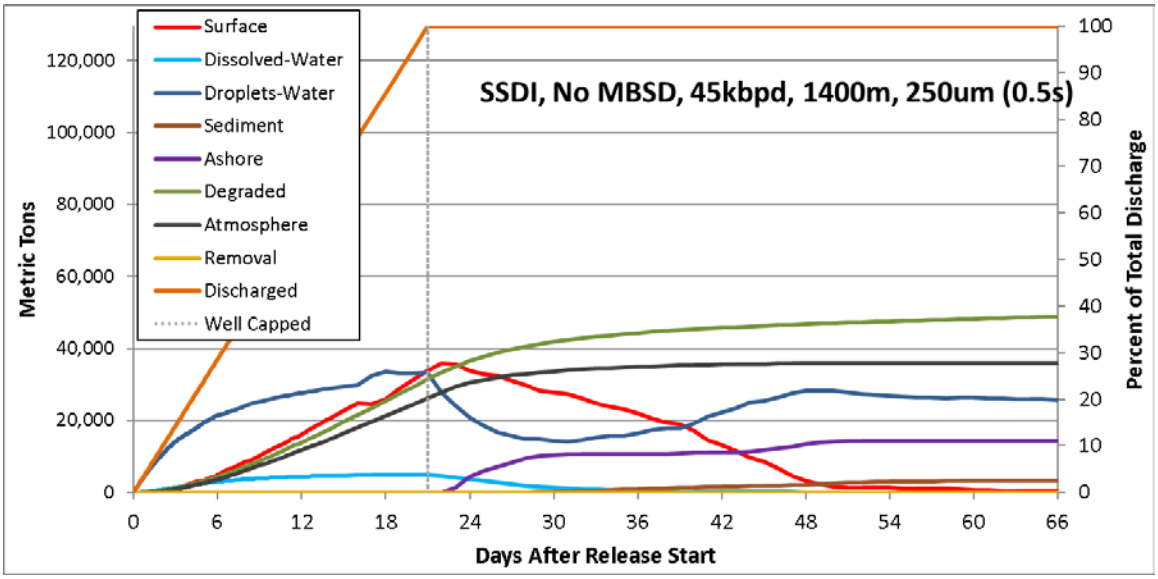

Figure A.14. Oil mass by environmental compartment over time for case #2: a spill rate of 45,000 bbl/day (7154 m^3/day) over 21 days from an 1100-m intrusion depth, assuming d_{50} = 250 µm, s_d = 0.5, and base-case degradation rates.

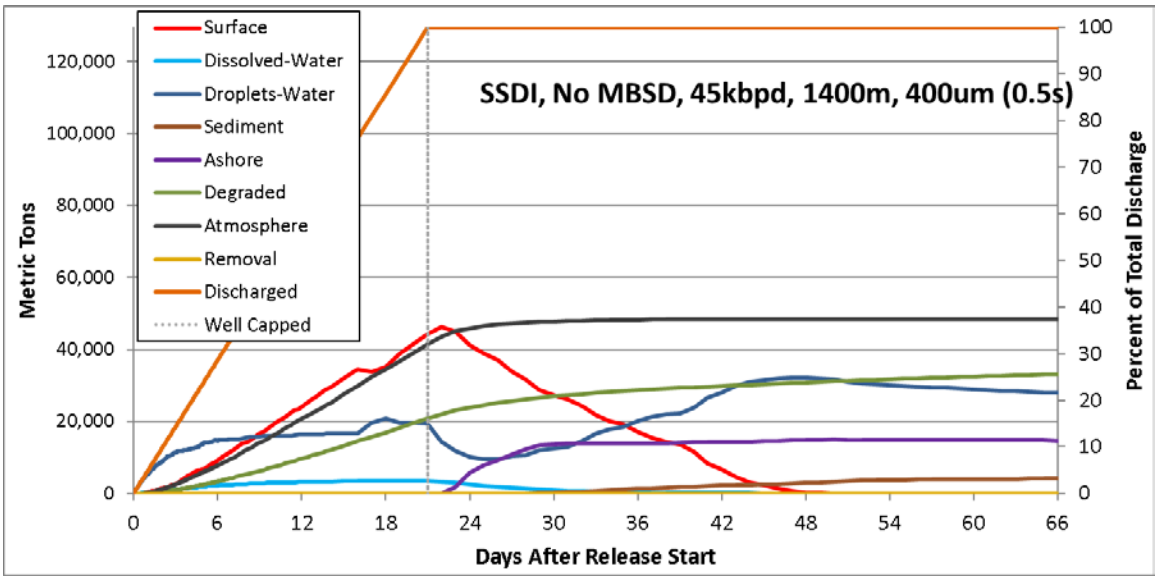

Figure A.15. Oil mass by environmental compartment over time for case #3: a spill rate of 45,000 bbl/day (7154 m^3/day) over 21 days from an 1100-m intrusion depth, assuming d_{50} = 400 µm, s_d = 0.5, and base-case degradation rates.

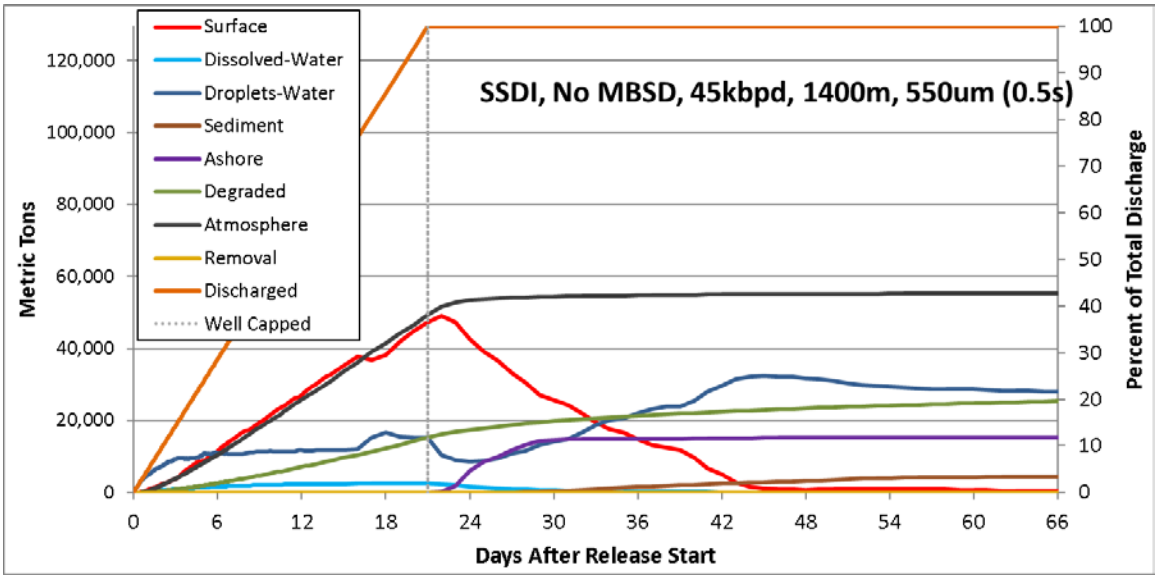

Figure A.16. Oil mass by environmental compartment over time for case #4: a spill rate of 45,000 bbl/day (7154 m3/day) over 21 days from an 1100-m intrusion depth, assuming d_{50} = 550 µm, s_d = 0.5, and base-case degradation rates.

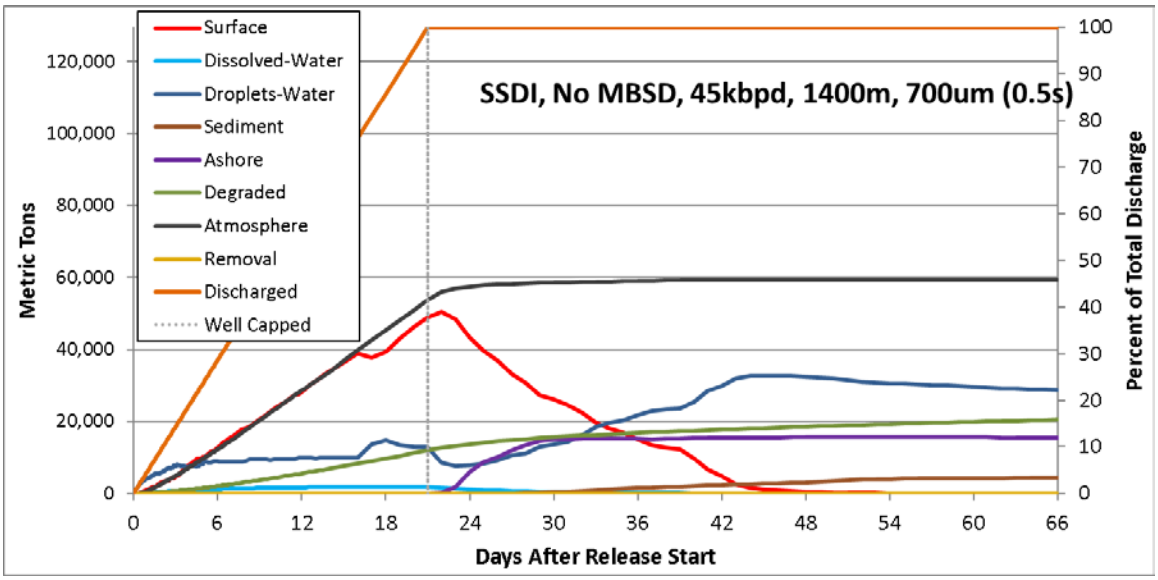

Figure A.17. Oil mass by environmental compartment over time for case #5: a spill rate of 45,000 bbl/day (7154 m^3/day) over 21 days from an 1100-m intrusion depth, assuming d_{50} = 700 µm, s_d = 0.5, and base-case degradation rates.

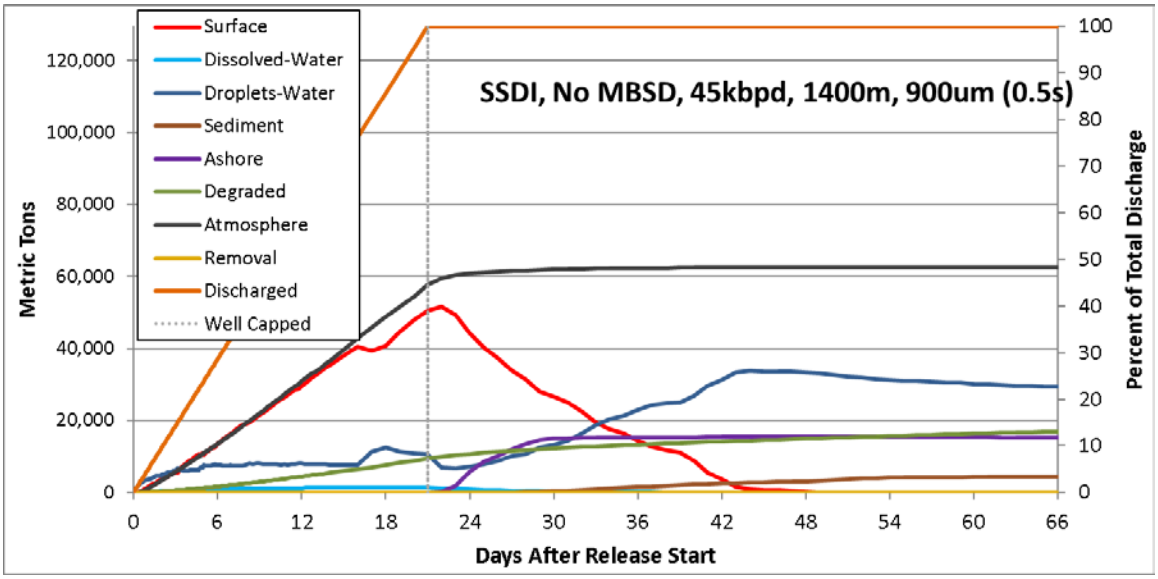

Figure A.18. Oil mass by environmental compartment over time for case #6: a spill rate of 45,000 bbl/day (7154 m^3/day) over 21 days from an 1100-m intrusion depth, assuming d_{50} = 900 µm, s_d = 0.5, and base-case degradation rates.

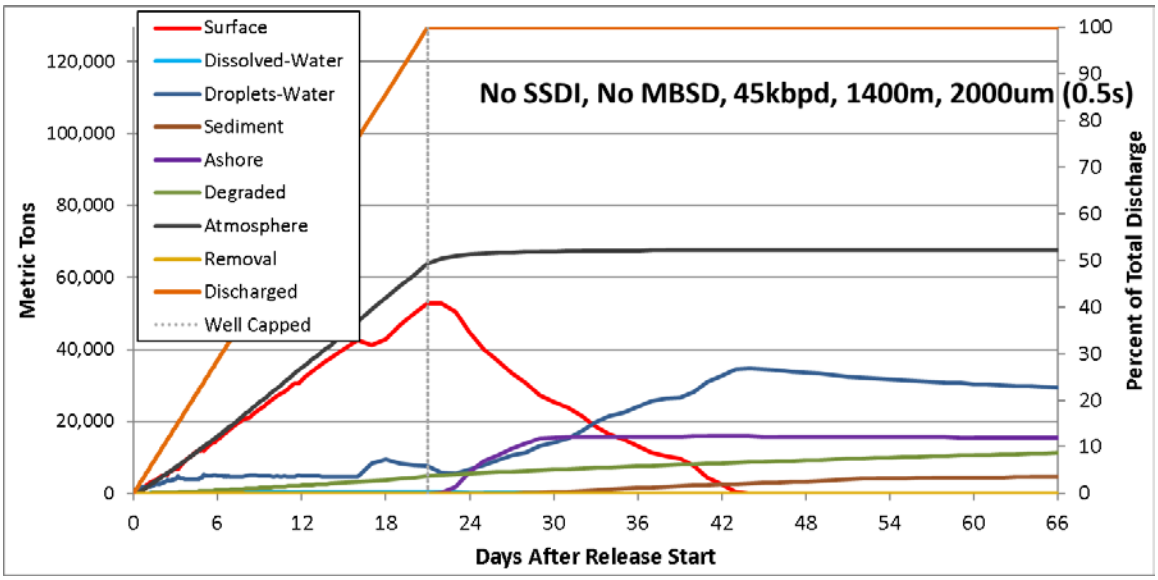

Figure A.19. Oil mass by environmental compartment over time for case #7: a spill rate of 45,000 bbl/day (7154 m^3/day) over 21 days from an 1100-m intrusion depth, assuming d_{50} = 2000 µm, s_d = 0.5, and base-case degradation rates.

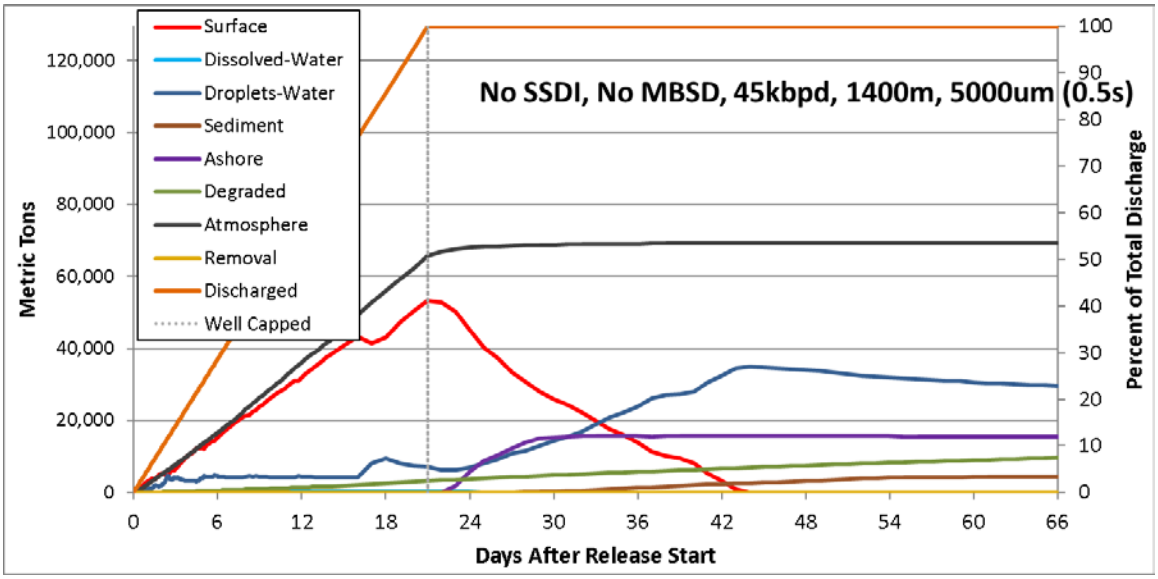

Figure A.20. Oil mass by environmental compartment over time for case #8: a spill rate of 45,000 bbl/day (7154 m^3/day) over 21 days from an 1100-m intrusion depth, assuming d_{50} = 5000 µm, s_d = 0.5, and base-case degradation rates.

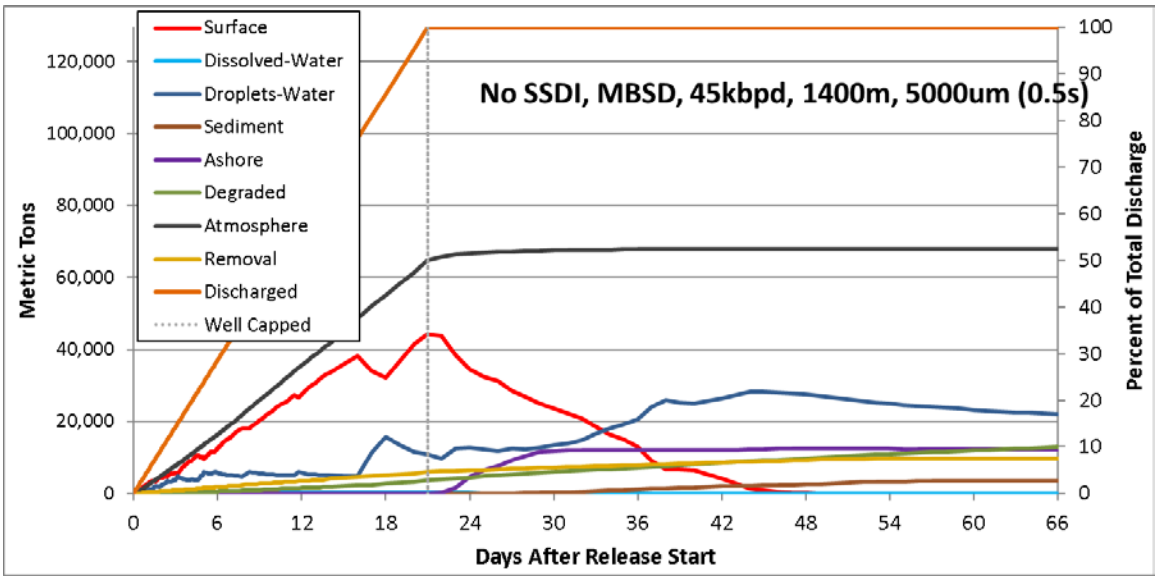

Figure A.21. Oil mass by environmental compartment over time for case #9: a spill rate of 45,000 bbl/day (7154 m^3/day) over 21 days from an 1100-m intrusion depth, assuming d_{50} = 5000 µm, s_d = 0.5, and base-case degradation rates. MBSD is also included in this scenario.

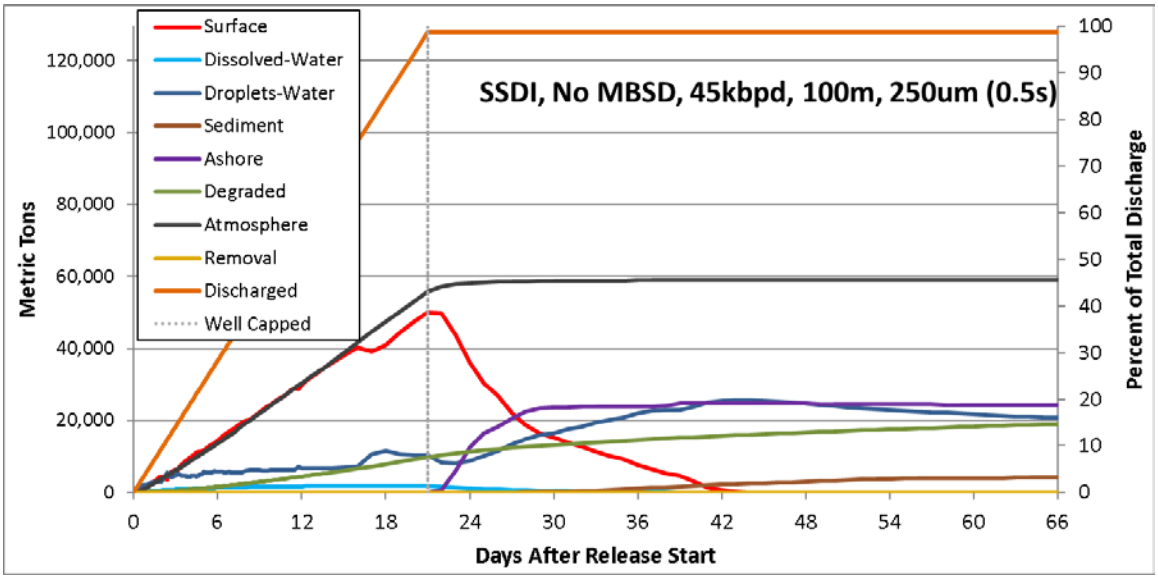

Figure A.22. Oil mass by environmental compartment over time for case #22: a spill rate of 45,000 bbl/day (7154 m^3/day) over 21 days from a 100-m intrusion depth, assuming d_{50} = 250 µm, s_d = 0.5, and base-case degradation rates.

Appendix B. Summary of Mass Balance Results for All Model Runs of the Sensitivity Analysis

Table B.1summarizes for all model cases the mass balance (percent of the released oil mass in each environmental compartment) at the end of the 66-day simulation. Also listed is the maximum percentage of the spill oil floating on the water surface and in the water column at any time after the spill. For other environmental compartments, the maximum at any time after the spill occurs at the end of the simulation.

Table B.1 Maximum percent of the released oil mass in each compartment at any time after the spill and at any time. Cases run with other than the base degradation rates (from French-McCay et al. 2018d) are designated by BD50 for 50% of base or BD0 for 0% of base degradation rates assumed.

Model Inputs						Mass Balance (Percent) at End of 66-day Model Simulation								Maximum Any Time	
Case #	Release Depth (m)	d_{50} (μm)	s_d	Include MBSD?	Oil Flow Rate (bbl/day)	Surface	Atmosphere	Water Column	Sediment	Ashore	Degraded	Outside Boundary	Removed	Surface	Water Column
22	100	250	0.5	No	45,000	0.0	46.1	16.2	3.2	18.9	14.8	0.7	0.0	39.1	20.2
27	500	50	0.25	No	45,000	0.0	4.8	17.4	0.2	1.8	71.7	4.2	0.0	7.2	56.9
26	500	50	0.5	No	45,000	0.0	9.0	18.6	0.3	2.6	66.2	3.3	0.0	10.7	51.1
28	500	50	0.8	No	45,000	0.0	11.7	18.9	0.8	3.4	62.8	2.5	0.0	12.6	47.2
12	500	100	0.5	No	45,000	0.0	25.4	23.1	2.1	6.8	40.8	1.9	0.0	28.1	30.5
13	500	250	0.5	No	45,000	0.0	42.4	18.7	3.5	15.6	19.0	0.8	0.0	38.8	22.6
13-BD50	500	250	0.5	No	45,000	0.0	43.3	19.4	3.6	15.5	17.3	0.9	0.0	38.7	23.9
13-BD0	500	250	0.5	No	45,000	0.0	44.6	27.9	3.5	15.7	5.6	2.6	0.0	38.9	33.3
31	500	250	0.8	No	45,000	0.0	41.0	18.6	3.8	14.5	21.3	0.9	0.0	37.4	22.3
14	500	400	0.5	No	45,000	0.0	48.3	17.2	3.3	18.3	12.3	0.6	0.0	40.2	20.2
15	500	550	0.5	No	45,000	0.0	50.2	16.7	3.2	19.0	10.3	0.6	0.0	40.6	20.1
21	500	550	0.8	No	45,000	0.0	48.6	16.6	3.2	18.8	12.1	0.7	0.0	39.8	19.6
16	500	700	0.5	No	45,000	0.0	51.1	16.5	3.3	19.2	9.3	0.6	0.0	40.9	19.9
16-BD50	500	700	0.5	No	45,000	0.0	51.4	17.0	3.3	19.2	8.6	0.7	0.0	40.8	20.6
16-BD0	500	700	0.5	No	45,000	0.0	51.8	19.6	3.2	19.5	4.8	1.2	0.0	40.9	23.3
17	500	900	0.5	No	45,000	0.0	51.8	15.9	3.2	19.9	8.7	0.6	0.0	40.9	19.3
18	500	2000	0.5	No	45,000	0.0	52.5	15.8	3.1	20.0	8.0	0.6	0.0	41.2	19.3
19	500	5000	0.5	No	45,000	0.0	52.1	15.0	3.0	20.9	8.5	0.6	0.0	41.2	18.4
19-BD50	500	5000	0.5	No	45,000	0.0	52.1	15.7	3.0	20.8	7.7	0.7	0.0	41.2	19.3
19-BD0	500	5000	0.5	No	45,000	0.0	52.2	17.6	3.0	20.9	5.4	1.0	0.0	41.1	20.9
20	500	5000	0.5	Yes	45,000	0.0	50.7	10.9	2.4	16.7	11.0	0.7	7.7	34.2	15.7

23	1400	50	0.25	No	45,000	0.6	0.1	16.2	0.0	0.0	83.1	0.0	0.0	0.6	64.3
29	1400	50	0.5	No	45,000	0.7	1.2	16.2	0.1	0.6	81.1	0.0	0.0	1.2	62.6
24	1400	50	0.8	No	45,000	0.9	3.7	15.9	0.2	2.1	77.2	0.1	0.0	2.9	60.2
1	1400	100	0.5	No	45,000	2.0	7.5	14.8	0.5	5.1	70.0	0.2	0.0	8.0	57.2
25	1400	175	0.5	No	45,000	1.2	19.1	17.3	1.6	9.6	50.4	0.6	0.0	18.3	41.8
2	1400	250	0.5	No	45,000	0.3	27.8	19.8	2.6	11.0	37.7	0.8	0.0	27.7	29.7
3	1400	400	0.5	No	45,000	0.0	37.4	21.6	3.2	11.3	25.6	0.9	0.0	35.7	24.9
4	1400	550	0.5	No	45,000	0.3	42.7	21.5	3.4	11.7	19.6	0.8	0.0	37.9	25.0
11	1400	550	0.8	No	45,000	0.0	40.6	21.8	3.0	11.4	22.3	0.8	0.0	35.9	24.9
5	1400	700	0.5	No	45,000	0.0	45.8	22.2	3.4	12.0	15.9	0.8	0.0	38.9	25.3
6	1400	900	0.5	No	45,000	0.0	48.2	22.6	3.4	11.8	13.1	0.8	0.0	39.9	26.1
7	1400	2000	0.5	No	45,000	0.0	52.2	22.7	3.6	12.0	8.7	0.8	0.0	40.8	26.8
8	1400	5000	0.5	No	45,000	0.0	53.5	22.9	3.4	11.9	7.4	0.9	0.0	41.1	27.0
9	1400	5000	0.5	Yes	45,000	0.0	52.4	17.0	2.7	9.4	9.9	0.9	7.6	34.2	21.8
10	1400	250	0.5	No	100,000	0.3	27.6	19.6	3.0	10.9	37.9	0.8	0.0	27.7	30.1
30	1,400	250	0.8	No	45,000	0.6	26.9	19.0	2.2	10.0	40.5	0.7	0.0	25.1	31.8

Table B.2 summarizes for all model cases exposure indices for surface floating oil and the water column.

Table B.2 Area swept by surface oil times exposure duration (km^2-days), volume of water exposed times duration of exposure (km^3-days) above the indicated thresholds. The cumulative mass exposure is listed in thousands of metric tonne-days (MT-days). (Note that the number of digits does not indicate the degree of precision, but are listed to allow smaller metrics to be displayed.)

Model Inputs						Area-days of Surface Oil Exposure (km^2-days)				Volume-days of Water Column Exposure (km^3-days)				Mass Exposure (Thousand MT-days)	
Case #	Release Depth (m)	d_{50} (μm)	s_d	Include MBSD?	Oil Flow Rate (bbl/day)	>0.1 g/m^2	>1 g/m^2	>10 g/m^2	100 g/m^2	1 μg/l	10 μg/l	1 mg/l	10 mg/l	Surface	Water Column
22	100	250	0.5	No	45,000	43,876	43,632	39,877	0	179.4	52.7	1.079	0.012	689	520
27	500	50	0.25	No	45,000	23,146	22,996	21,696	10	131.8	59.6	10.852	0.210	66	1,667
26	500	50	0.5	No	45,000	34,395	34,104	32,010	8	172.1	67.6	8.834	0.161	128	1,582
28	500	50	0.8	No	45,000	35,641	35,445	34,301	5	209.8	70.9	7.265	0.121	180	1,497
12	500	100	0.5	No	45,000	41,152	40,409	38,650	6	288.7	87.8	4.588	0.083	400	1,221
13	500	250	0.5	No	45,000	43,860	43,035	39,327	0	288.9	72.0	1.525	0.022	656	654
13-BD50	500	250	0.5	No	45,000	43,981	43,086	39,332	0	416.1	94.4	1.542	0.021	658	699
13-BD0	500	250	0.5	No	45,000	44,440	43,396	39,589	0	1,563.1	172.4	1.532	0.022	662	858
31	500	250	0.8	No	45,000	43,632	42,959	39,199	0	281.0	68.0	1.489	0.018	627	713
14	500	400	0.5	No	45,000	45,421	45,175	40,958	0	221.8	39.8	0.918	0.012	711	499

15	500	550	0.5	No	45,000	45,391	45,312	40,907	0	181.8	23.8	0.680	0.009	727	449
21	500	550	0.8	No	45,000	45,001	44,724	41,244	1	207.3	31.7	0.623	0.007	713	489
16	500	700	0.5	No	45,000	45,529	45,421	41,278	0	160.0	14.3	0.577	0.008	737	426
16-BD50	500	700	0.5	No	45,000	45,557	45,444	41,294	0	214.2	19.9	0.558	0.007	738	442
16-BD0	500	700	0.5	No	45,000	45,667	45,564	41,387	0	568.4	33.5	0.562	0.007	742	487
17	500	900	0.5	No	45,000	45,551	45,470	41,816	0	132.6	6.7	0.501	0.005	742	406
18	500	2000	0.5	No	45,000	45,248	45,231	43,585	0	46.7	0.4	0.374	0.002	756	395
19	500	5000	0.5	No	45,000	43,445	43,432	43,133	0	14.3	0.0	0.371	0.001	763	406
19-BD50	500	5000	0.5	No	45,000	43,433	43,418	43,114	0	19.2	0.0	0.427	0.001	764	421
19-BD0	500	5000	0.5	No	45,000	43,427	43,414	43,106	0	36.5	0.1	0.412	0.001	762	450
20	500	5000	0.5	Yes	45,000	39,690	39,671	39,265	1	14.7	0.0	0.378	0.001	638	431
23	1400	50	0.25	No	45,000	1,470	1,470	1,382	0	40.4	14.2	6.671	1.220	2	1,784
29	1400	50	0.5	No	45,000	6,407	6,340	5,861	0	86.8	28.4	8.841	0.930	17	1,758
24	1400	50	0.8	No	45,000	15,531	15,406	14,384	0	100.7	38.1	9.862	0.636	53	1,695
1	1400	100	0.5	No	45,000	32,587	32,332	30,102	0	137.0	47.2	10.133	0.472	106	1,632
25	1400	175	0.5	No	45,000	39,761	39,611	38,454	0	257.8	58.9	7.195	0.249	262	1,402
2	1400	250	0.5	No	45,000	41,782	41,188	38,943	1	333.0	60.9	5.186	0.142	385	1,206
3	1400	400	0.5	No	45,000	43,196	42,001	38,998	0	357.9	51.8	3.304	0.057	533	944
4	1400	550	0.5	No	45,000	43,735	42,434	38,616	0	321.5	40.9	2.392	0.047	616	787
11	1400	550	0.8	No	45,000	43,038	42,278	38,927	1	290.2	41.7	2.510	0.038	580	845
5	1400	700	0.5	No	45,000	44,064	43,357	39,431	0	266.4	31.7	1.830	0.032	662	696
6	1400	900	0.5	No	45,000	44,715	44,069	39,661	0	208.6	24.8	1.536	0.023	699	626
7	1400	2000	0.5	No	45,000	45,167	45,081	40,050	0	98.3	7.3	0.653	0.011	763	496
8	1400	5000	0.5	No	45,000	45,525	45,518	40,840	0	25.4	0.3	0.245	0.004	780	463
9	1400	5000	0.5	Yes	45,000	42,546	42,539	38,829	1	25.3	0.3	0.175	0.004	664	450
10	1400	250	0.5	No	100,000	70,624	70,479	70,021	1	548.5	112.1	12.318	0.637	871	2,368
30	1,400	250	0.8	No	45,000	39,835	39,343	37,587	1	297.2	54.8	5.014	0.122	380	1,192

Appendix C. Locations and Amounts of Shoreline Oiling.

Figures C.1 to C.23 map the modeled shoreline oiling distribution after 66 days of simulation.

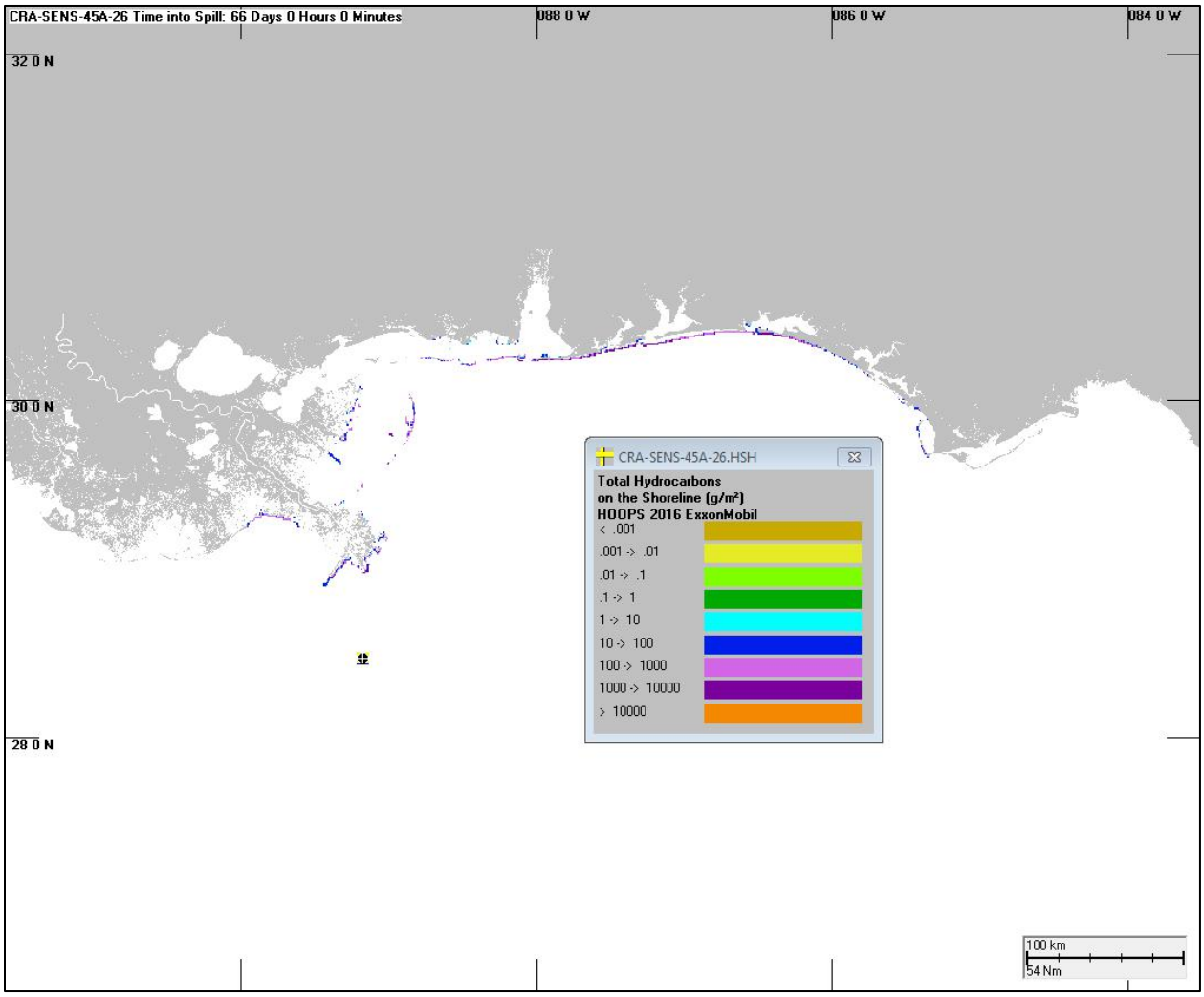

Figure C.1. Shoreline oiling at the end of the 66-day simulation for case #26: a spill rate of 45,000 bbl/day (7154 m^3/day) over 21 days from a 500-m intrusion depth, assuming d_{50} = 50 µm, s_d = 0.5, and base-case degradation rates.

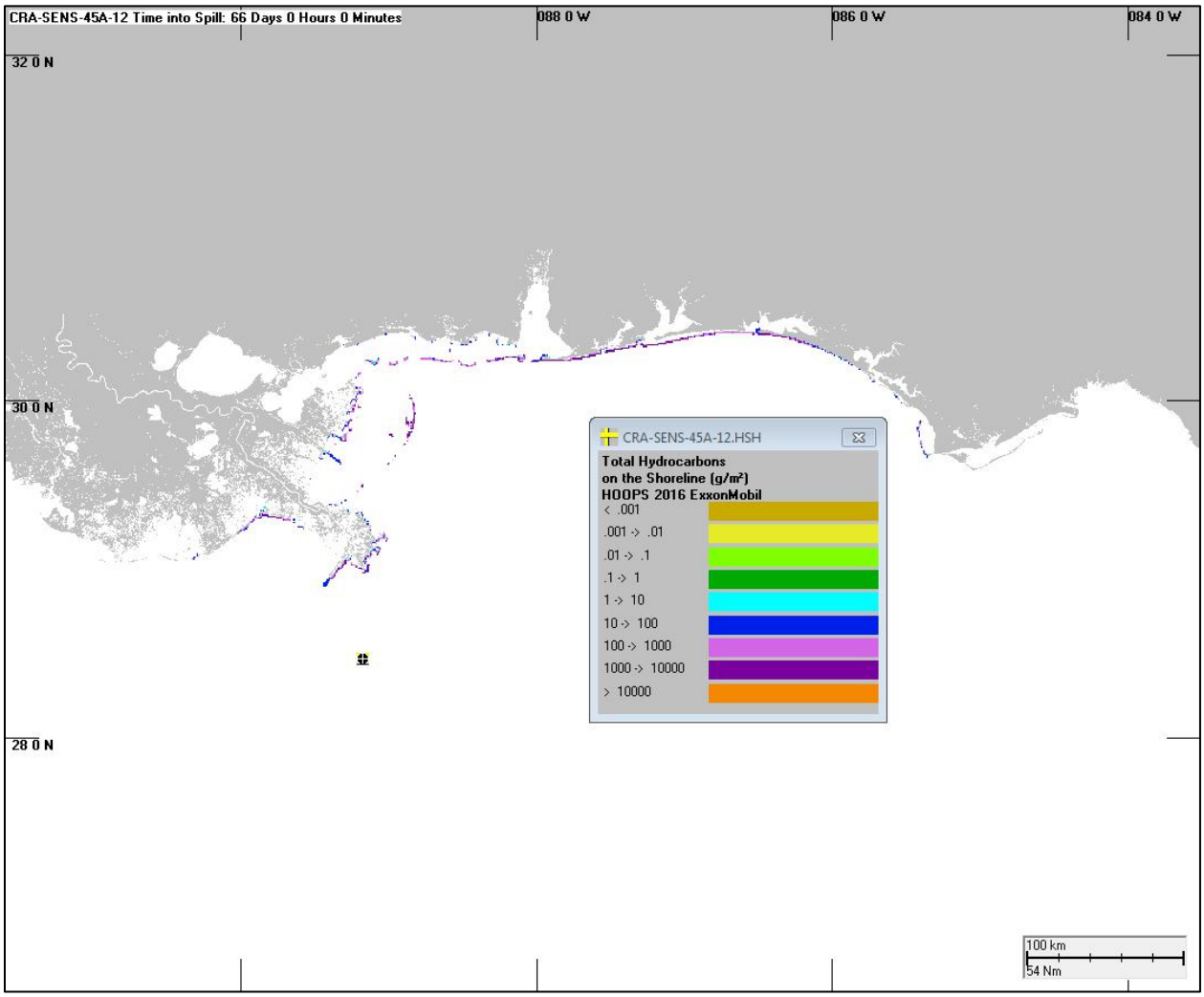

Figure C.2. Shoreline oiling at the end of the 66-day simulation for case #12: a spill rate of 45,000 bbl/day (7154 m^3/day) over 21 days from a 500-m intrusion depth, assuming d_{50} = 100 µm, s_d = 0.5, and base-case degradation rates.

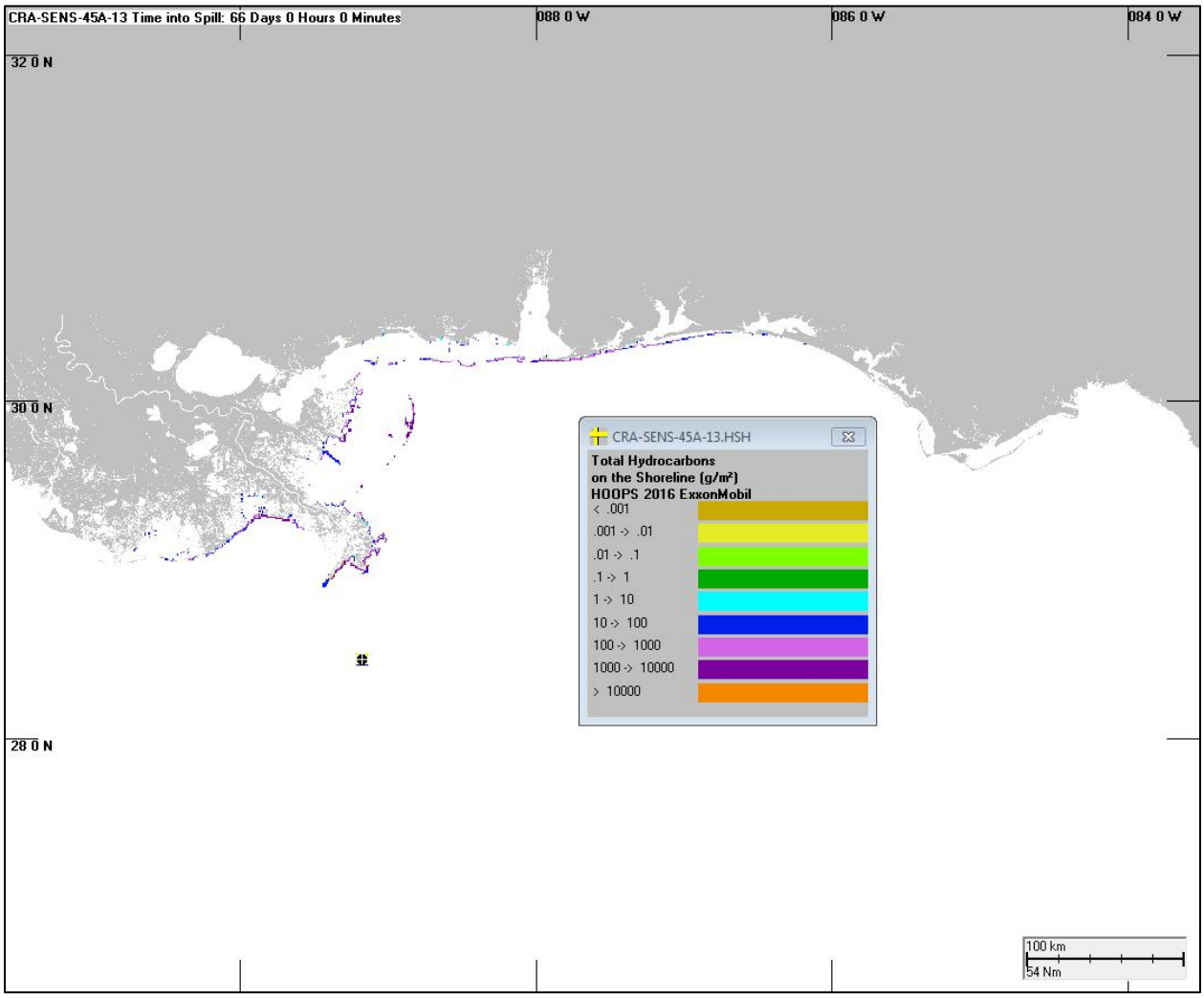

Figure C.3. Shoreline oiling at the end of the 66-day simulation for case #13: a spill rate of 45,000 bbl/day (7154 m^3/day) over 21 days from a 500-m intrusion depth, assuming d_{50} = 250 µm, s_d = 0.5, and base-case degradation rates.

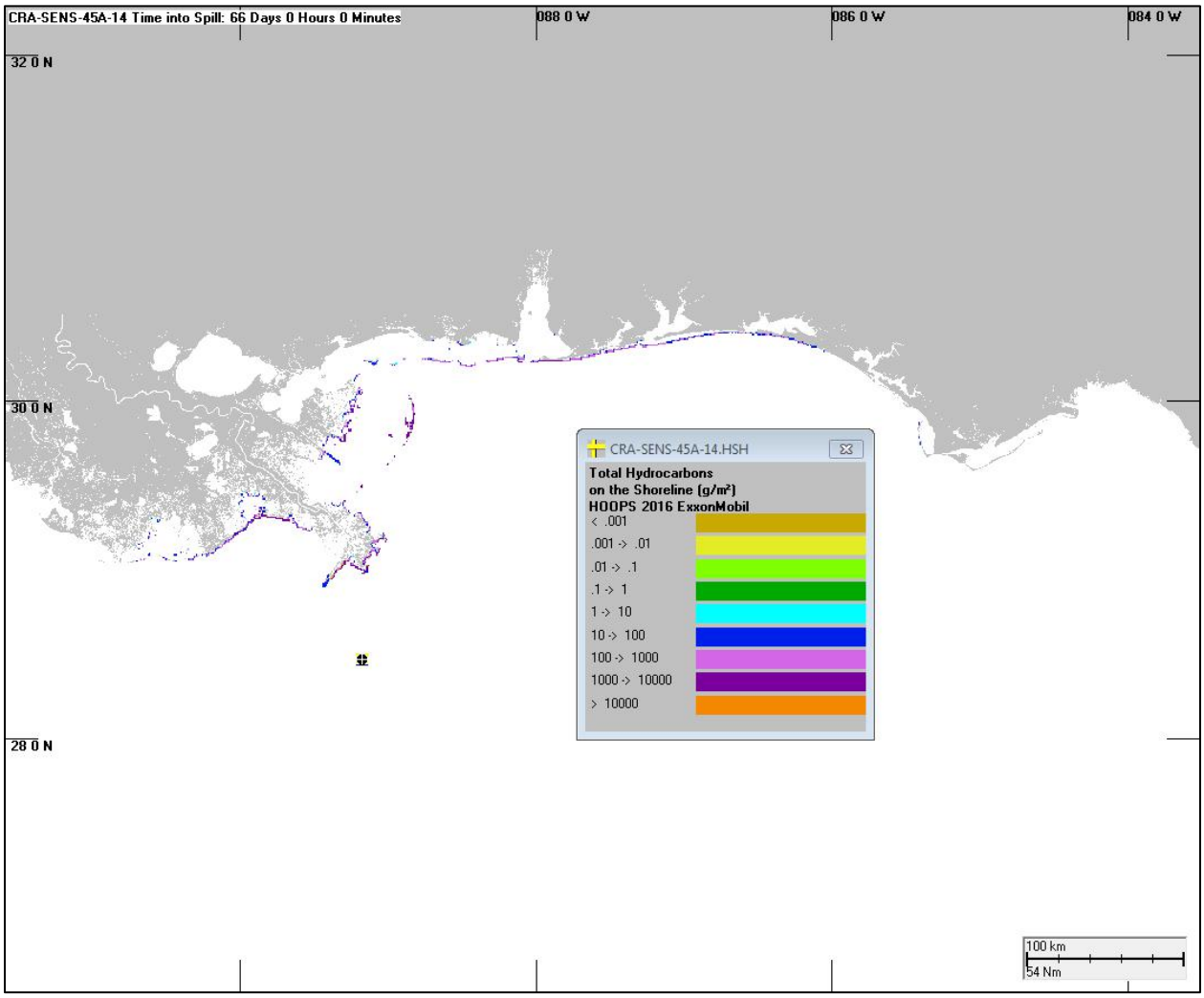

Figure C.4. Shoreline oiling at the end of the 66-day simulation for case #14: a spill rate of 45,000 bbl/day (7154 m^3/day) over 21 days from a 500-m intrusion depth, assuming d_{50} = 400 µm, s_d = 0.5, and base-case degradation rates.

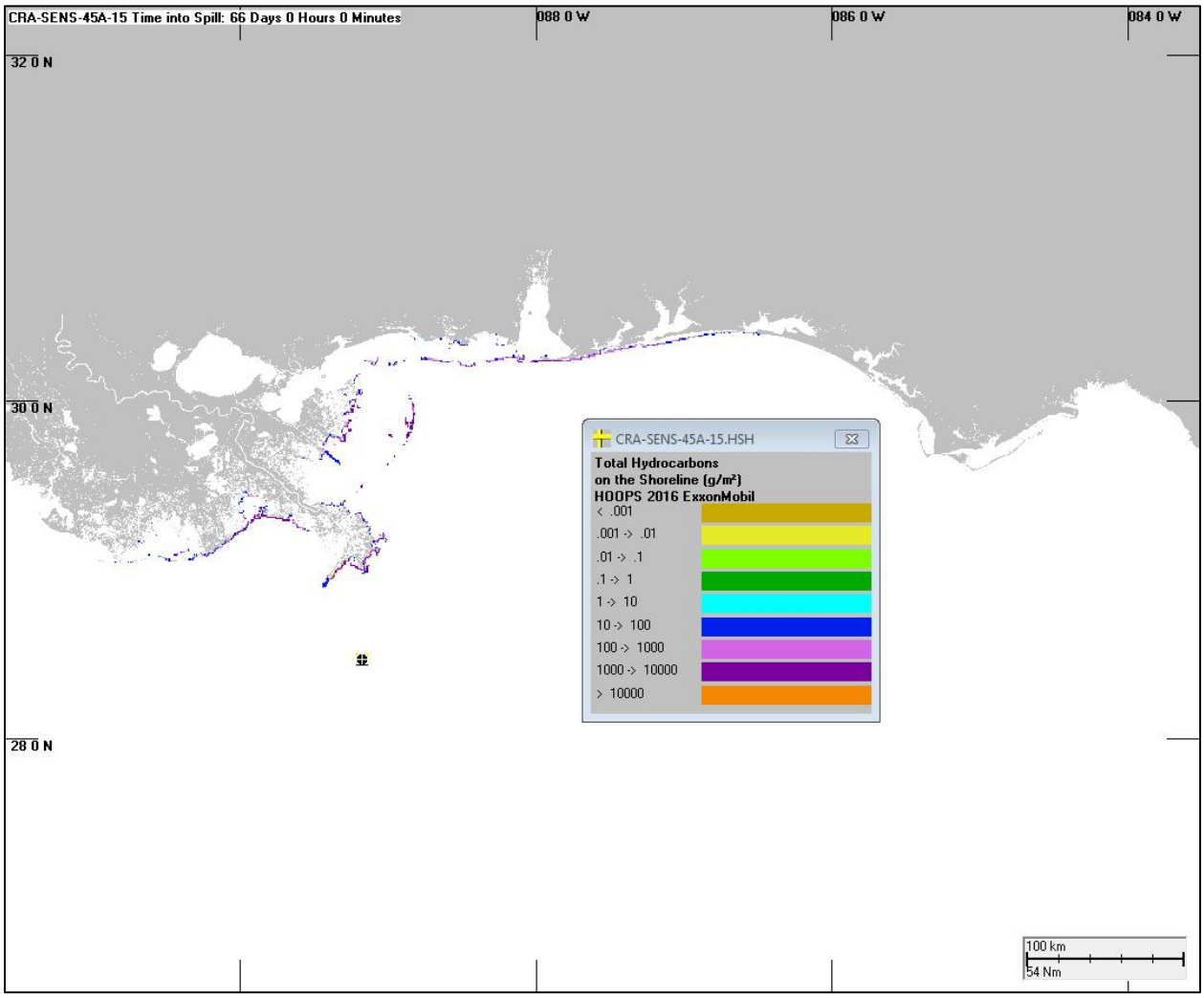

Figure C.5. Shoreline oiling at the end of the 66-day simulation for case #15: a spill rate of 45,000 bbl/day (7154 m^3/day) over 21 days from a 500-m intrusion depth, assuming d_{50} = 550 µm, s_d = 0.5, and base-case degradation rates.

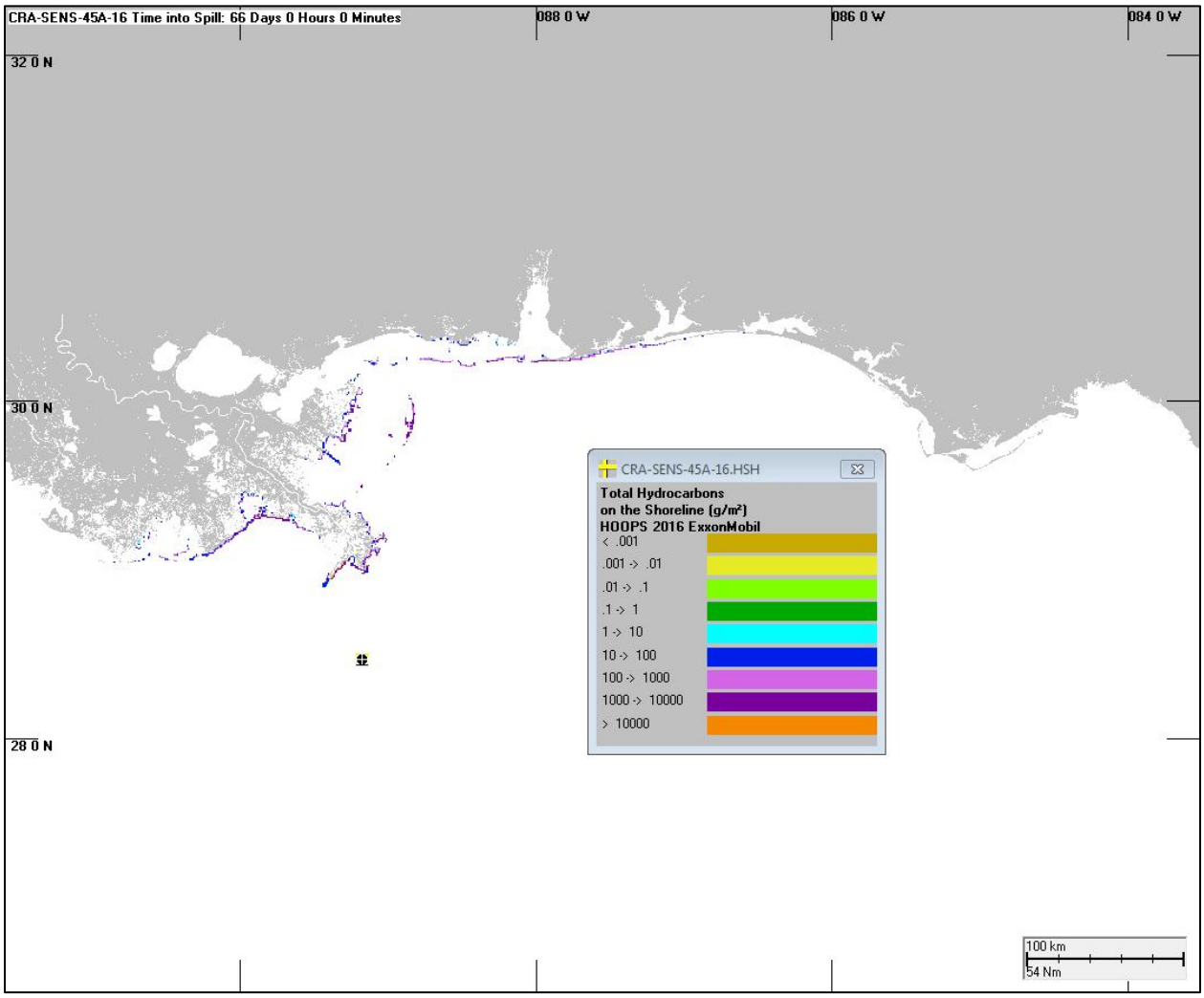

Figure C.6. Shoreline oiling at the end of the 66-day simulation for case #16: a spill rate of 45,000 bbl/day (7154 m^3/day) over 21 days from a 500-m intrusion depth, assuming d_{50} = 700 µm, s_d = 0.5, and base-case degradation rates.

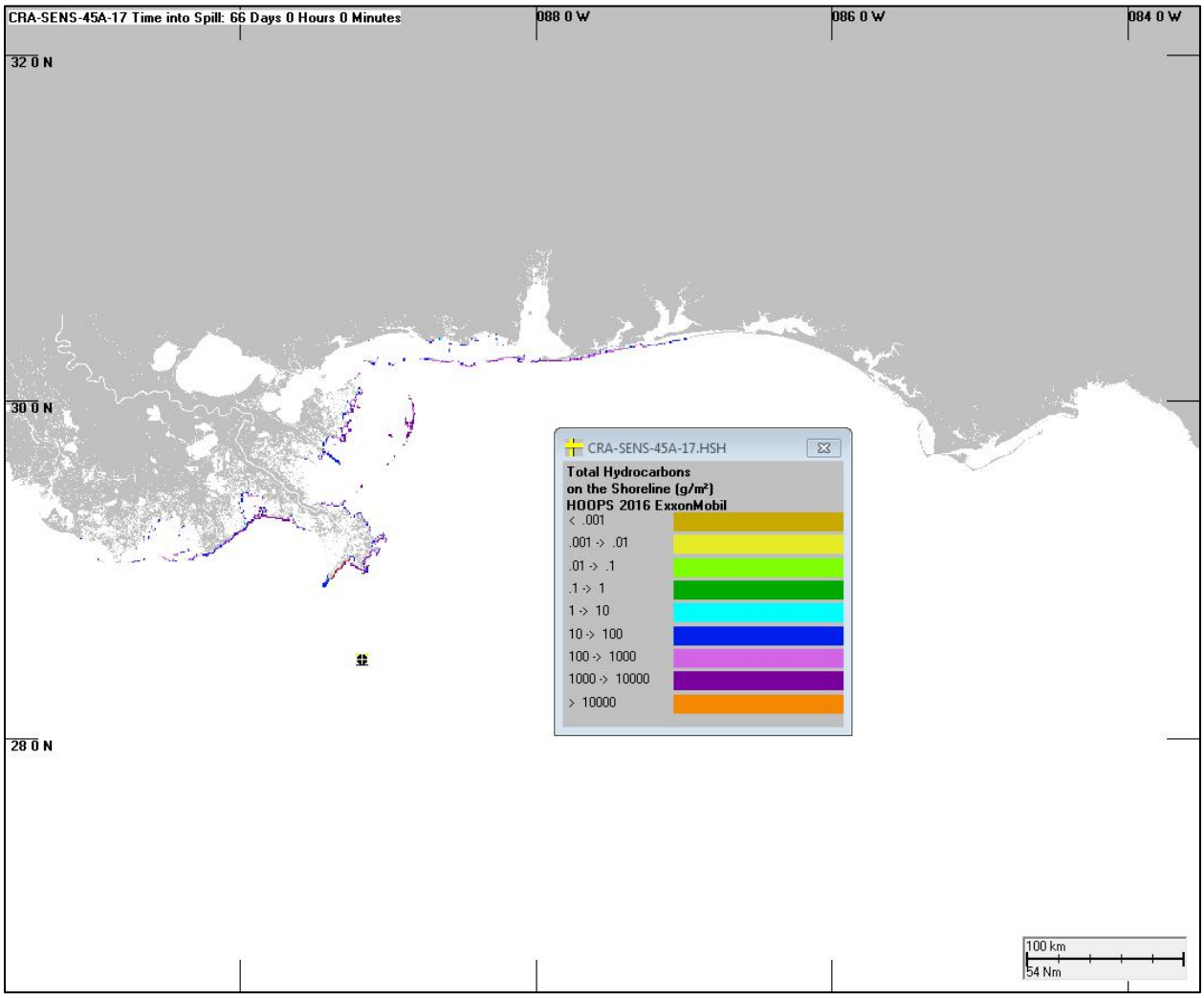

Figure C.7. Shoreline oiling at the end of the 66-day simulation for case #17: a spill rate of 45,000 bbl/day (7154 m3/day) over 21 days from a 500-m intrusion depth, assuming d_{50} = 900 μm, s_d = 0.5, and base-case degradation rates.

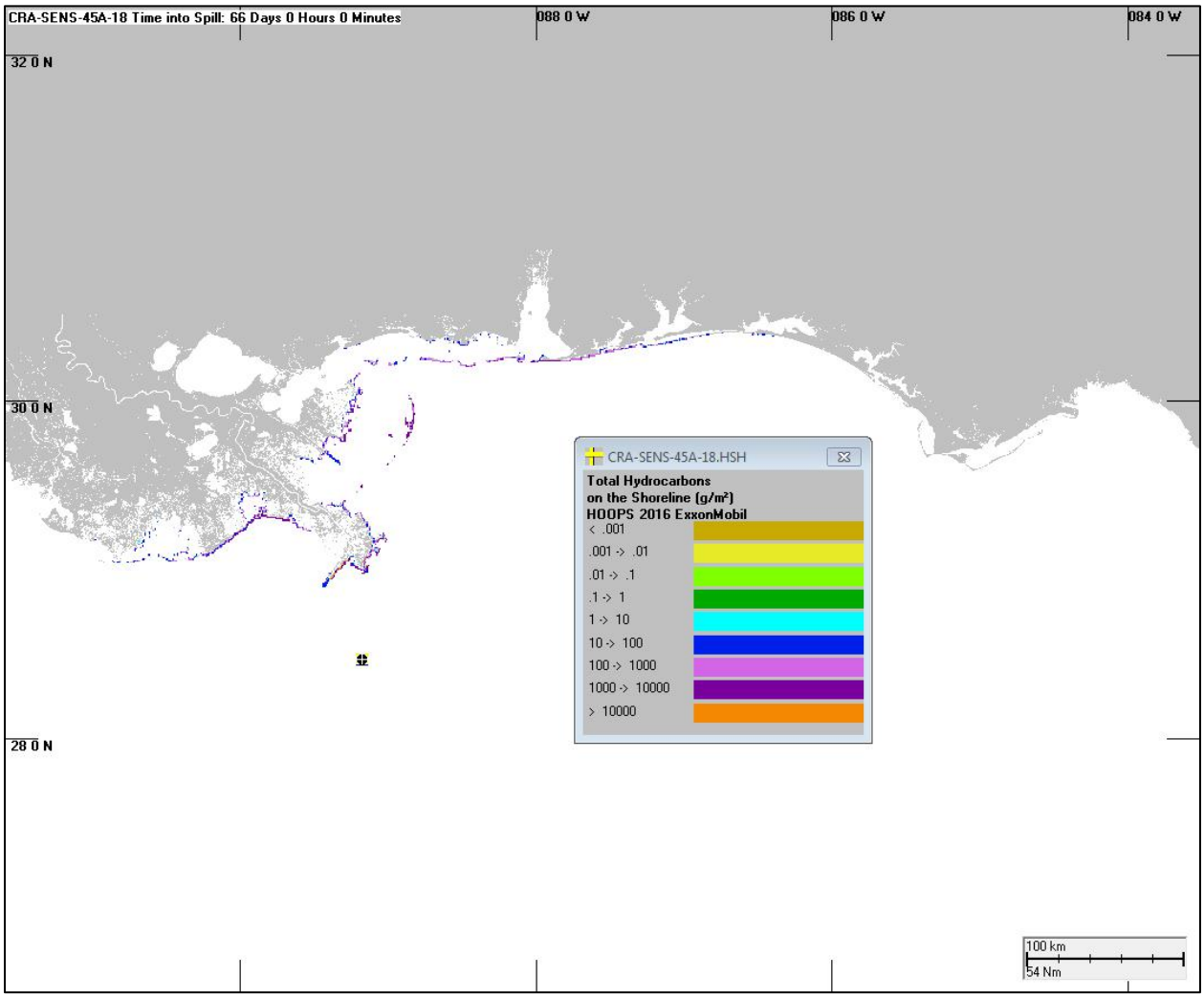

Figure C.8. Shoreline oiling at the end of the 66-day simulation for case #18: a spill rate of 45,000 bbl/day (7154 m^3/day) over 21 days from a 500-m intrusion depth, assuming d_{50} = 2000 µm, s_d = 0.5, and base-case degradation rates.

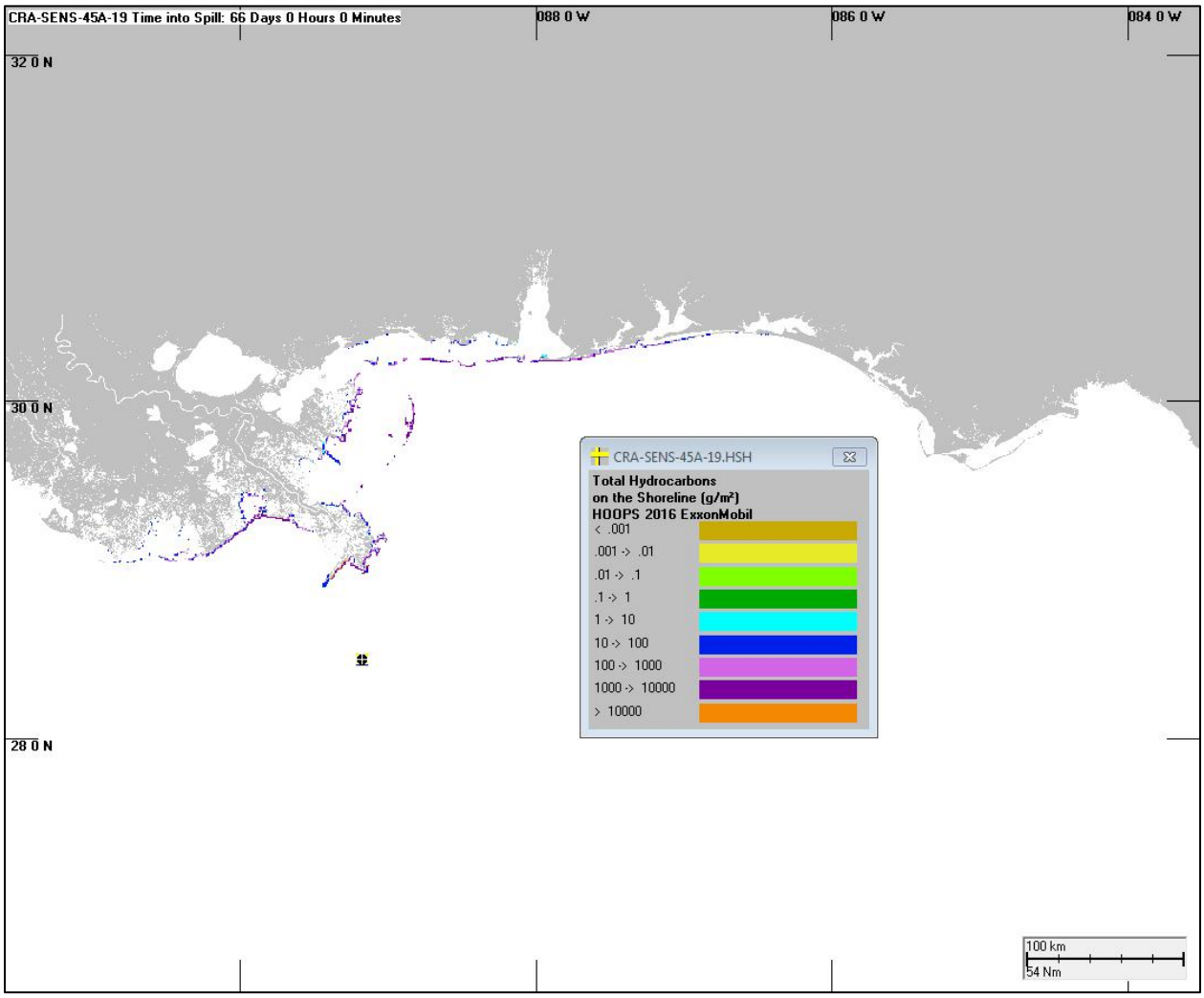

Figure C.9. Shoreline oiling at the end of the 66-day simulation for case #19: a spill rate of 45,000 bbl/day (7154 m^3/day) over 21 days from a 500-m intrusion depth, assuming d_{50} = 5000 µm, s_d = 0.5, and base-case degradation rates.

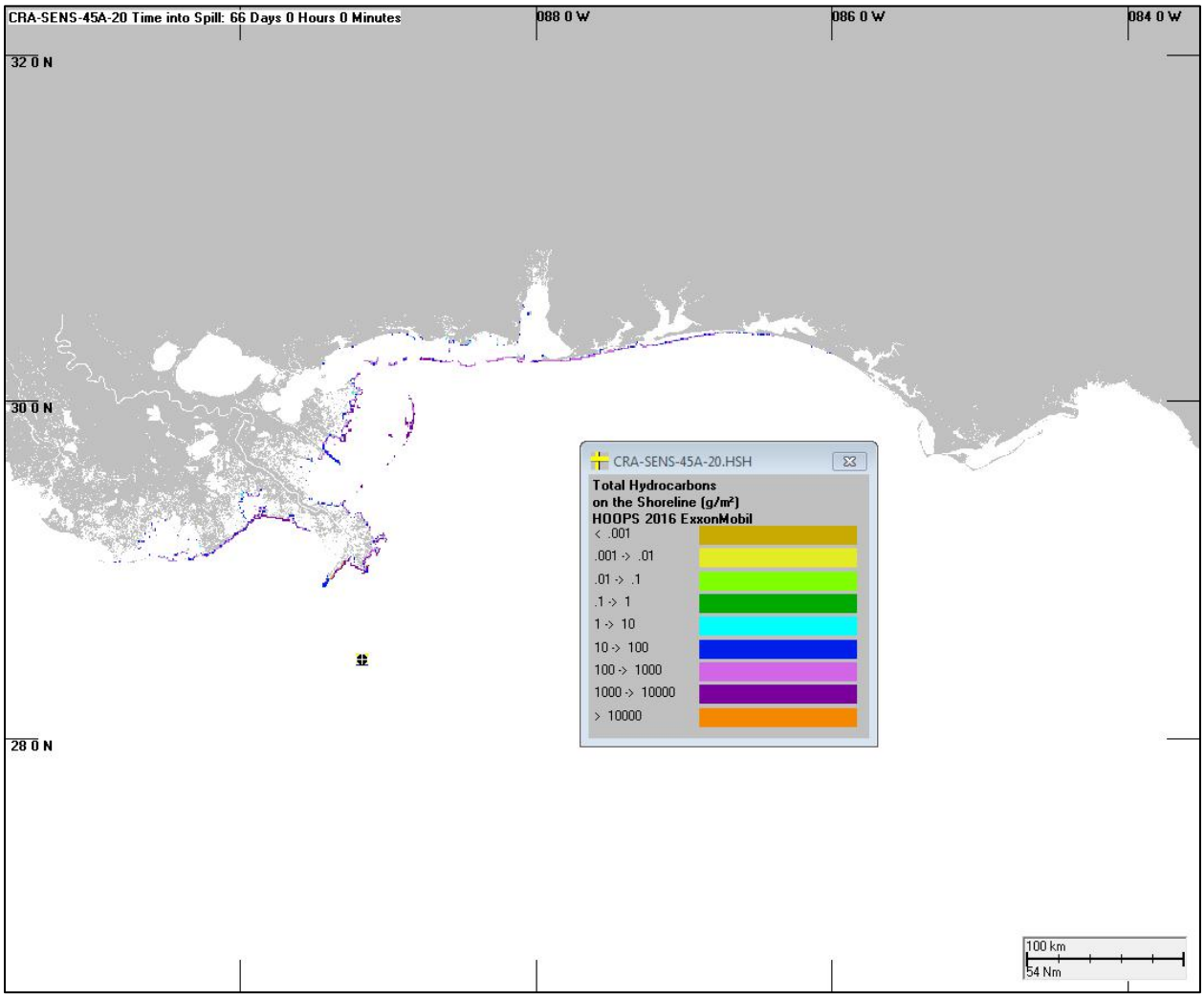

Figure C.10. Shoreline oiling at the end of the 66-day simulation for case #20: a spill rate of 45,000 bbl/day (7154 m^3/day) over 21 days from a 500-m intrusion depth, assuming d_{50} = 5000 µm, s_d = 0.5, and base-case degradation rates. MBSD is also included in this scenario.

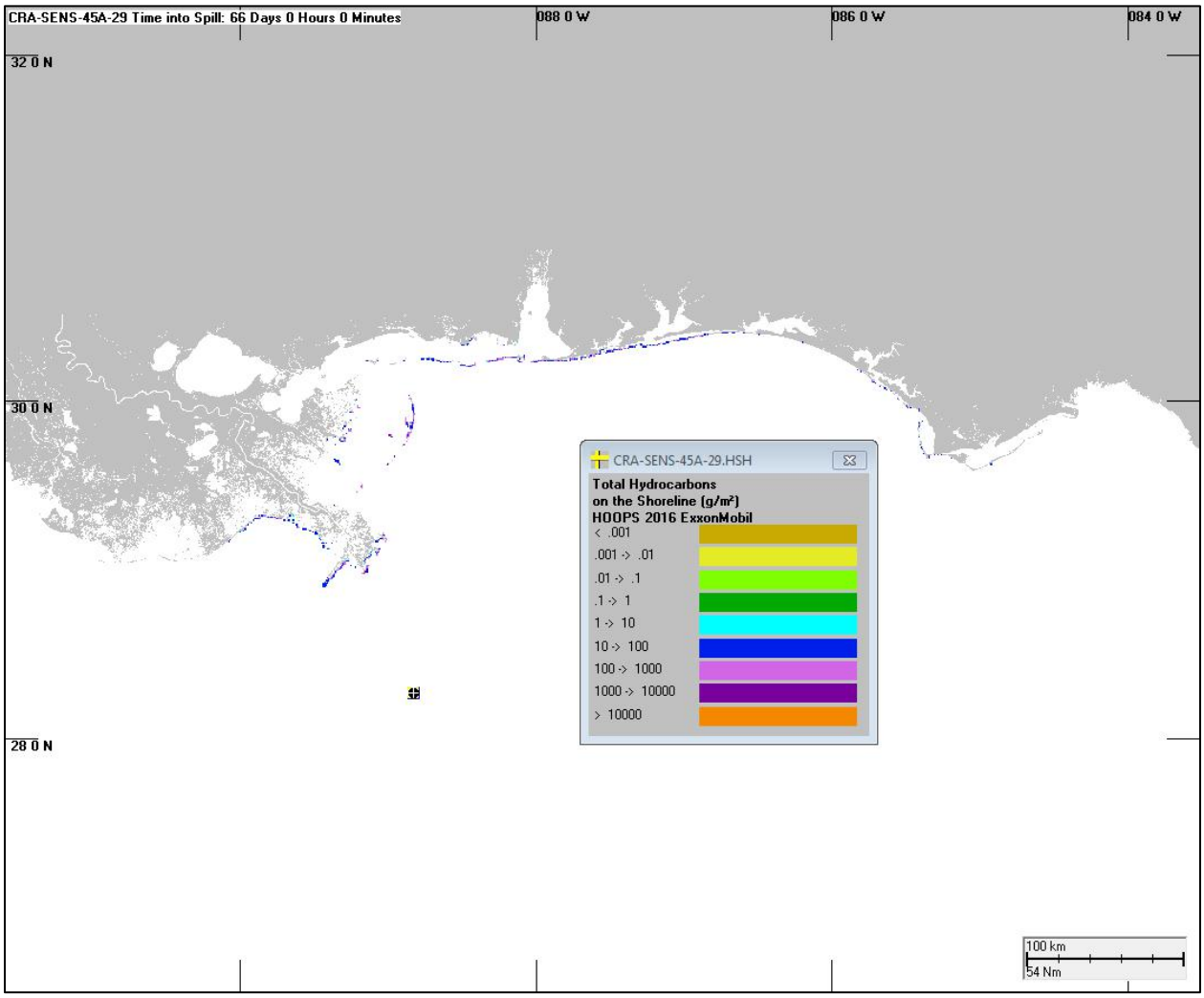

Figure C.11. Shoreline oiling at the end of the 66-day simulation for case #29: a spill rate of 45,000 bbl/day (7154 m^3/day) over 21 days from an 1100-m intrusion depth, assuming d_{50} = 50 µm, s_d = 0.5, and base-case degradation rates.

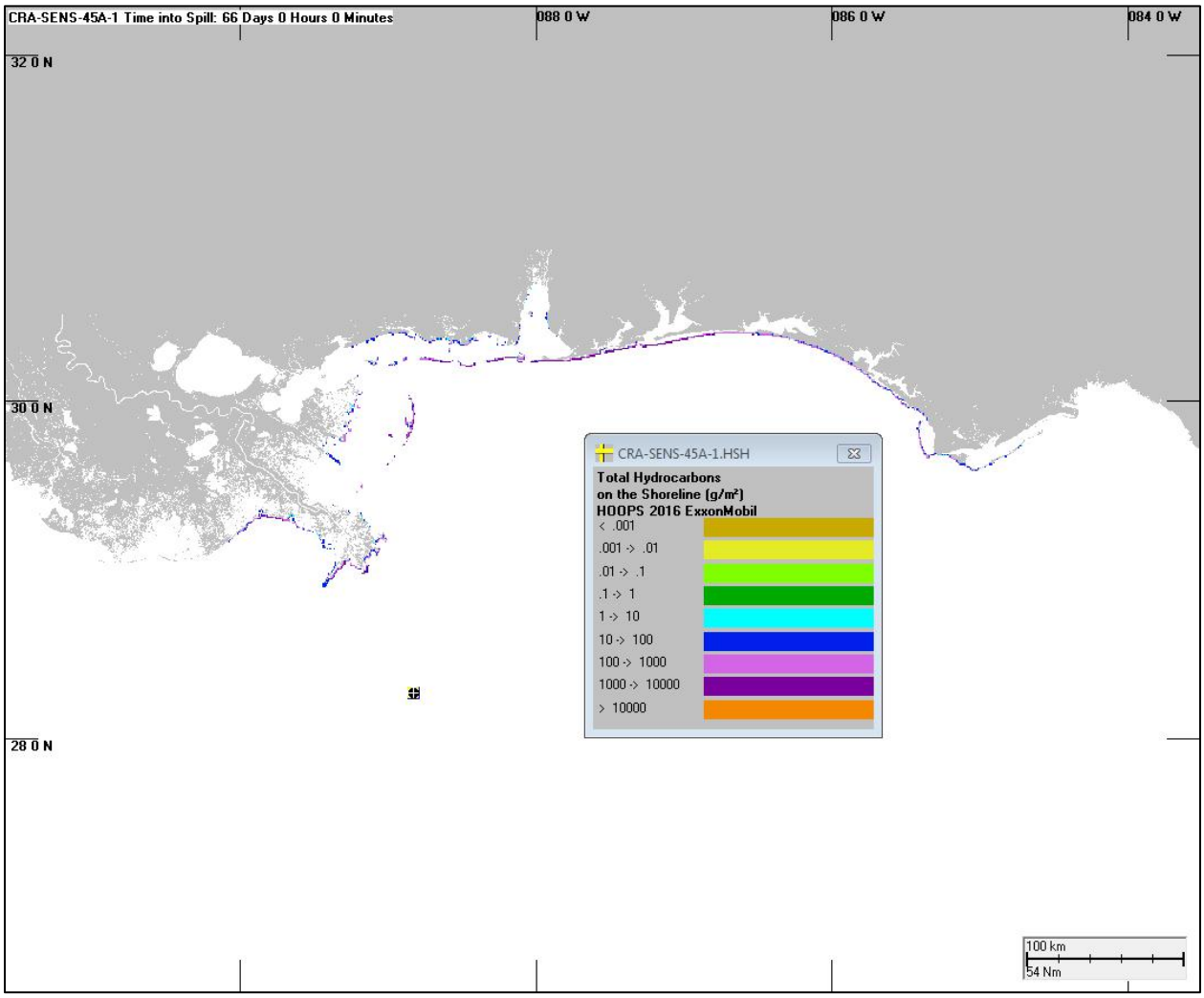

Figure C.12. Shoreline oiling at the end of the 66-day simulation for case #1: a spill rate of 45,000 bbl/day (7154 m^3/day) over 21 days from an 1100-m intrusion depth, assuming d_{50} = 100 µm, s_d = 0.5, and base-case degradation rates.

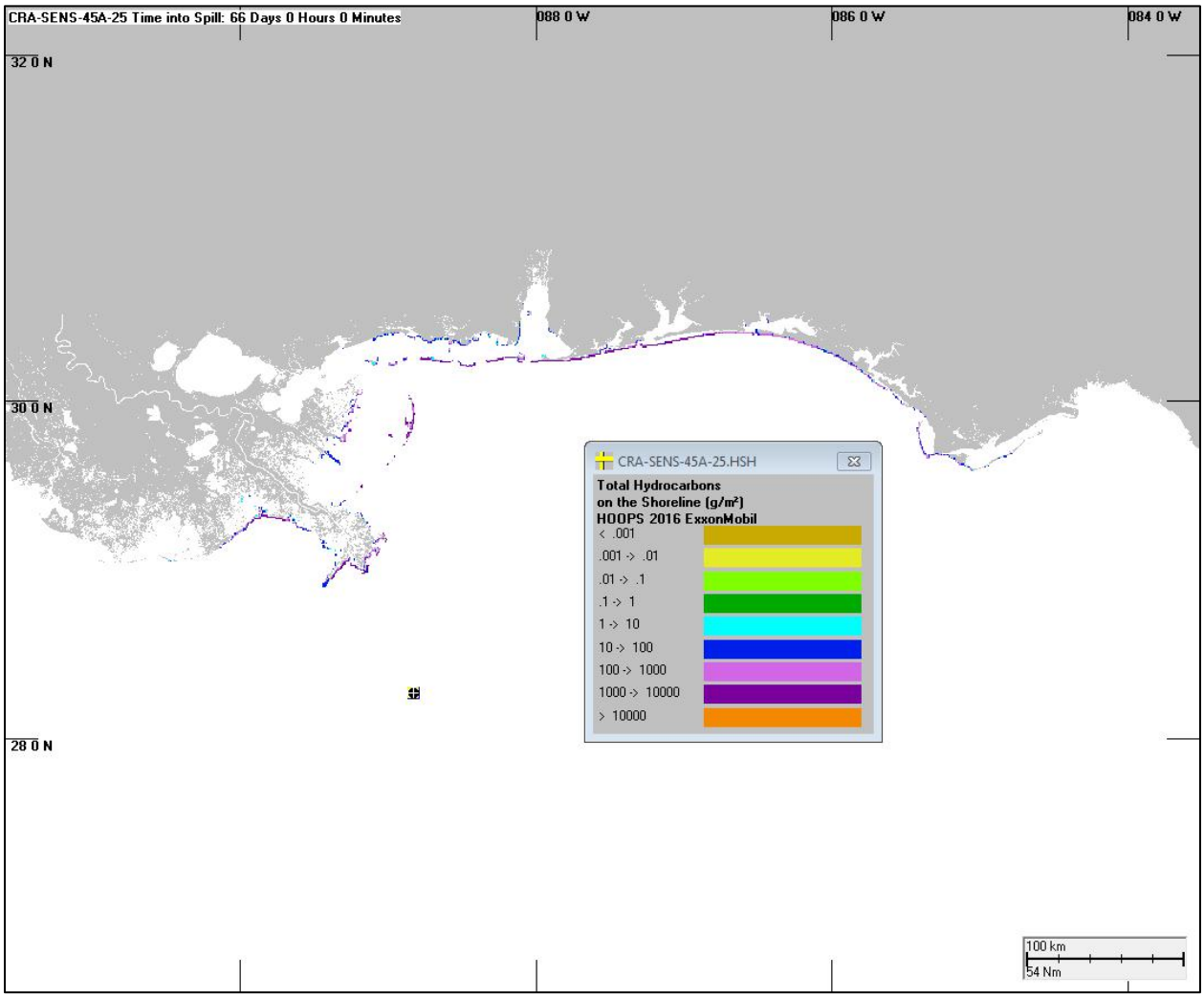

Figure C.13. Shoreline oiling at the end of the 66-day simulation for case #25: a spill rate of 45,000 bbl/day (7154 m^3/day) over 21 days from an 1100-m intrusion depth, assuming d_{50} = 175 µm, s_d = 0.5, and base-case degradation rates.

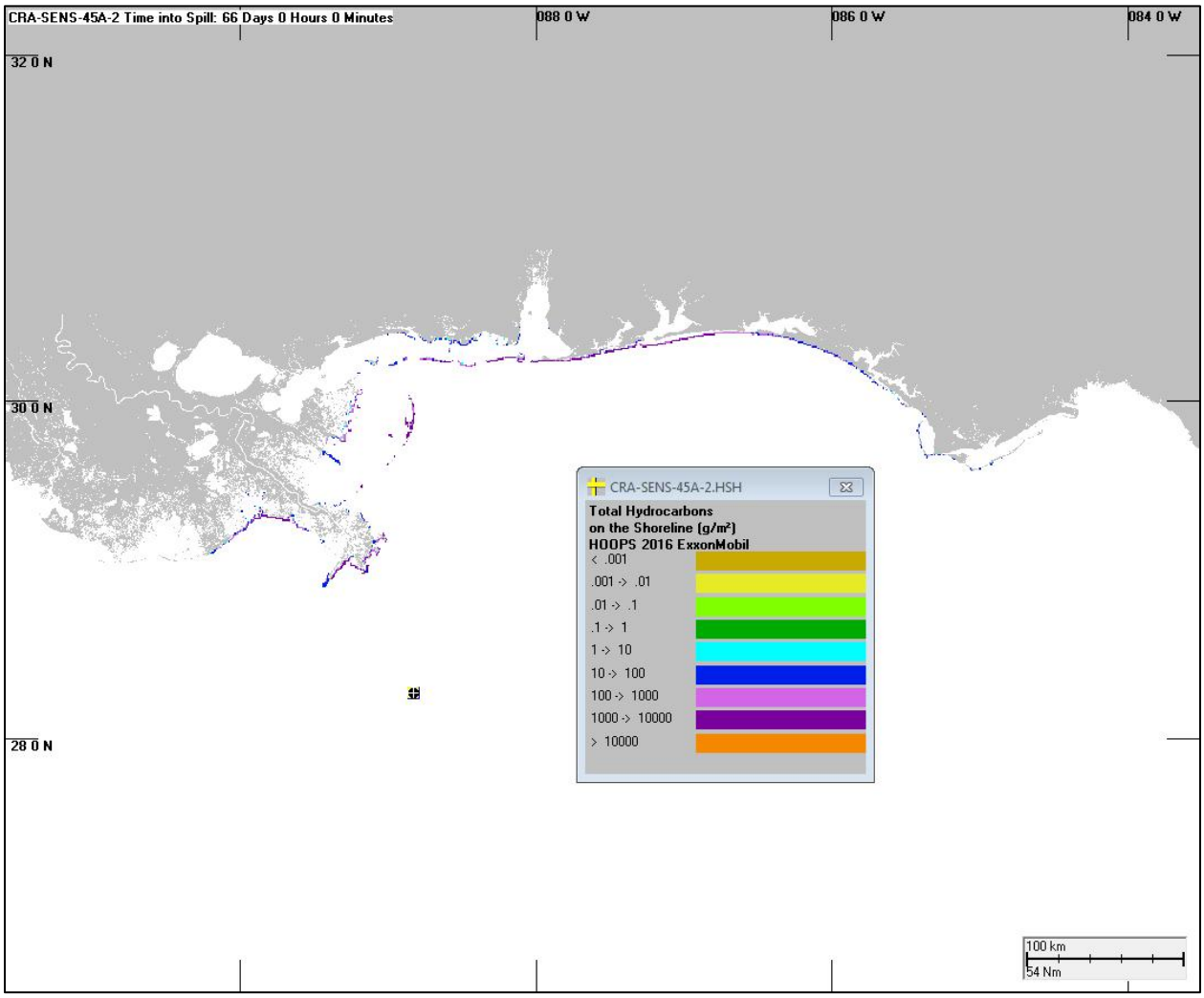

Figure C.14. Shoreline oiling at the end of the 66-day simulation for case #2: a spill rate of 45,000 bbl/day (7154 m^3/day) over 21 days from an 1100-m intrusion depth, assuming d_{50} = 250 µm, s_d = 0.5, and base-case degradation rates.

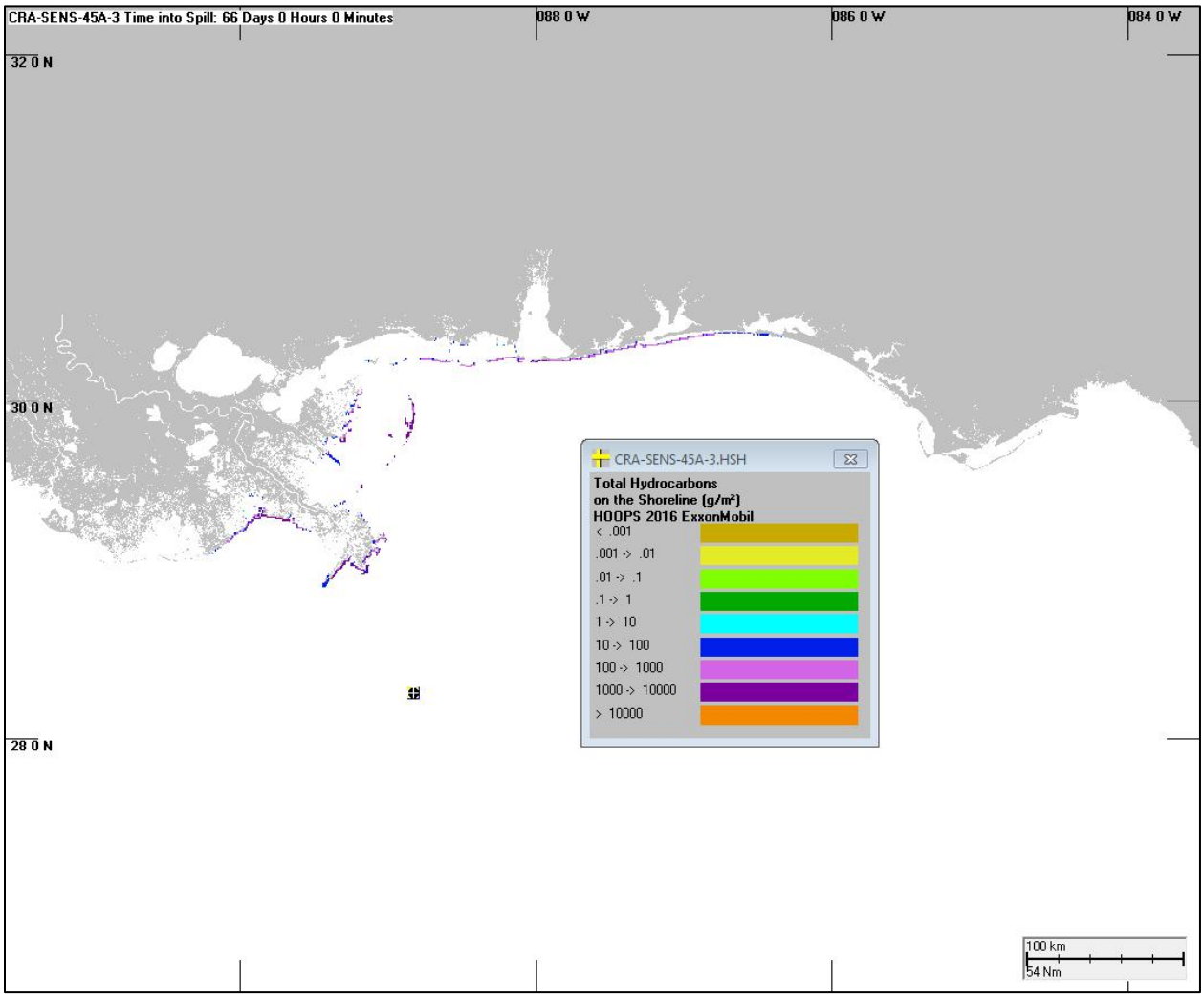

Figure C.15. Shoreline oiling at the end of the 66-day simulation for case #3: a spill rate of 45,000 bbl/day (7154 m^3/day) over 21 days from an 1100-m intrusion depth, assuming d_{50} = 400 µm, s_d = 0.5, and base-case degradation rates.

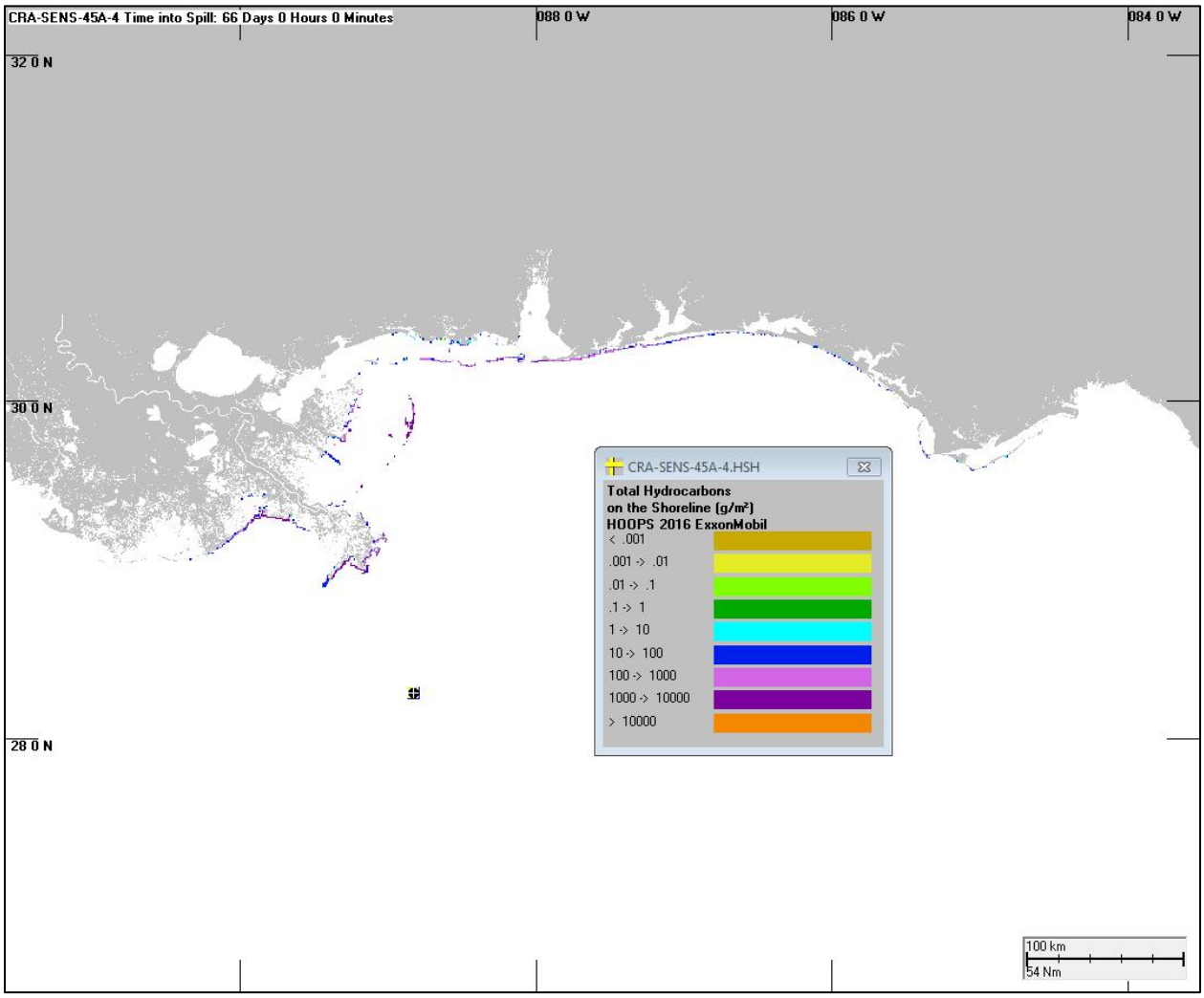

Figure C.16. Shoreline oiling at the end of the 66-day simulation for case #4: a spill rate of 45,000 bbl/day (7154 m^3/day) over 21 days from an 1100-m intrusion depth, assuming d_{50} = 550 µm, s_d = 0.5, and base-case degradation rates.

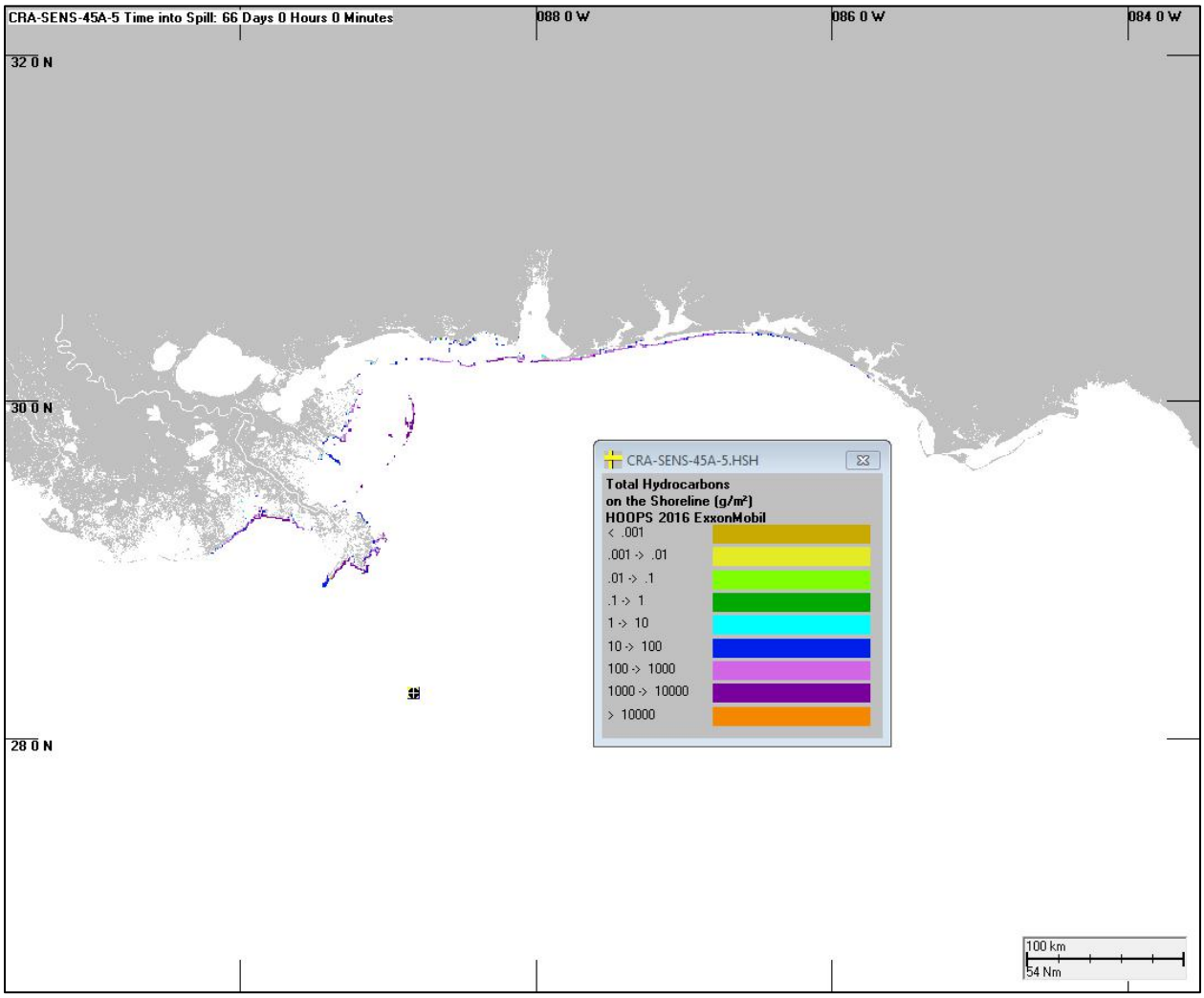

Figure C.17. Shoreline oiling at the end of the 66-day simulation for case #5: a spill rate of 45,000 bbl/day (7154 m^3/day) over 21 days from an 1100-m intrusion depth, assuming d_{50} = 700 µm, s_d = 0.5, and base-case degradation rates.

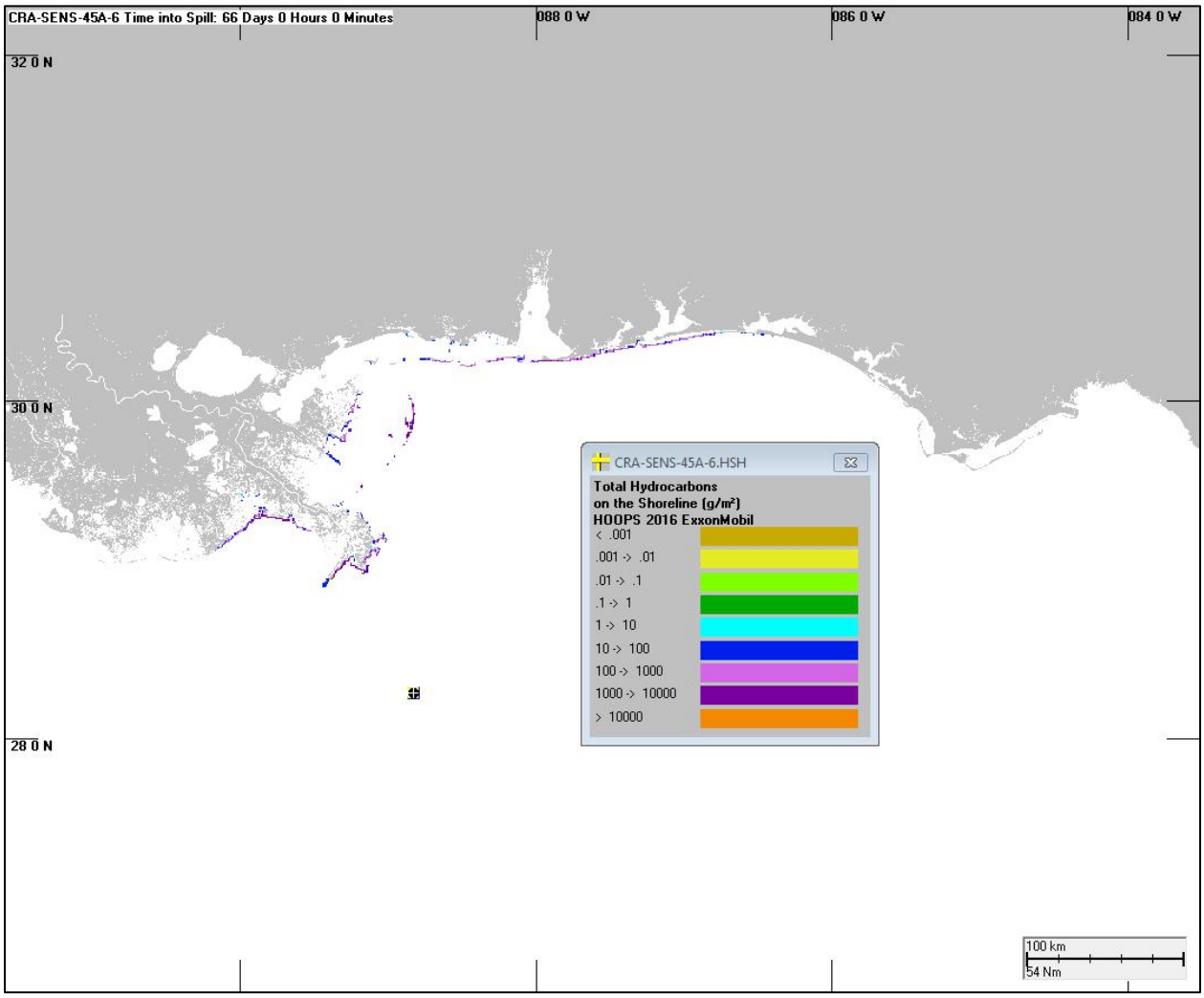

Figure C.18. Shoreline oiling at the end of the 66-day simulation for case #6: a spill rate of 45,000 bbl/day (7154 m^3/day) over 21 days from an 1100-m intrusion depth, assuming d_{50} = 900 µm, s_d = 0.5, and base-case degradation rates.

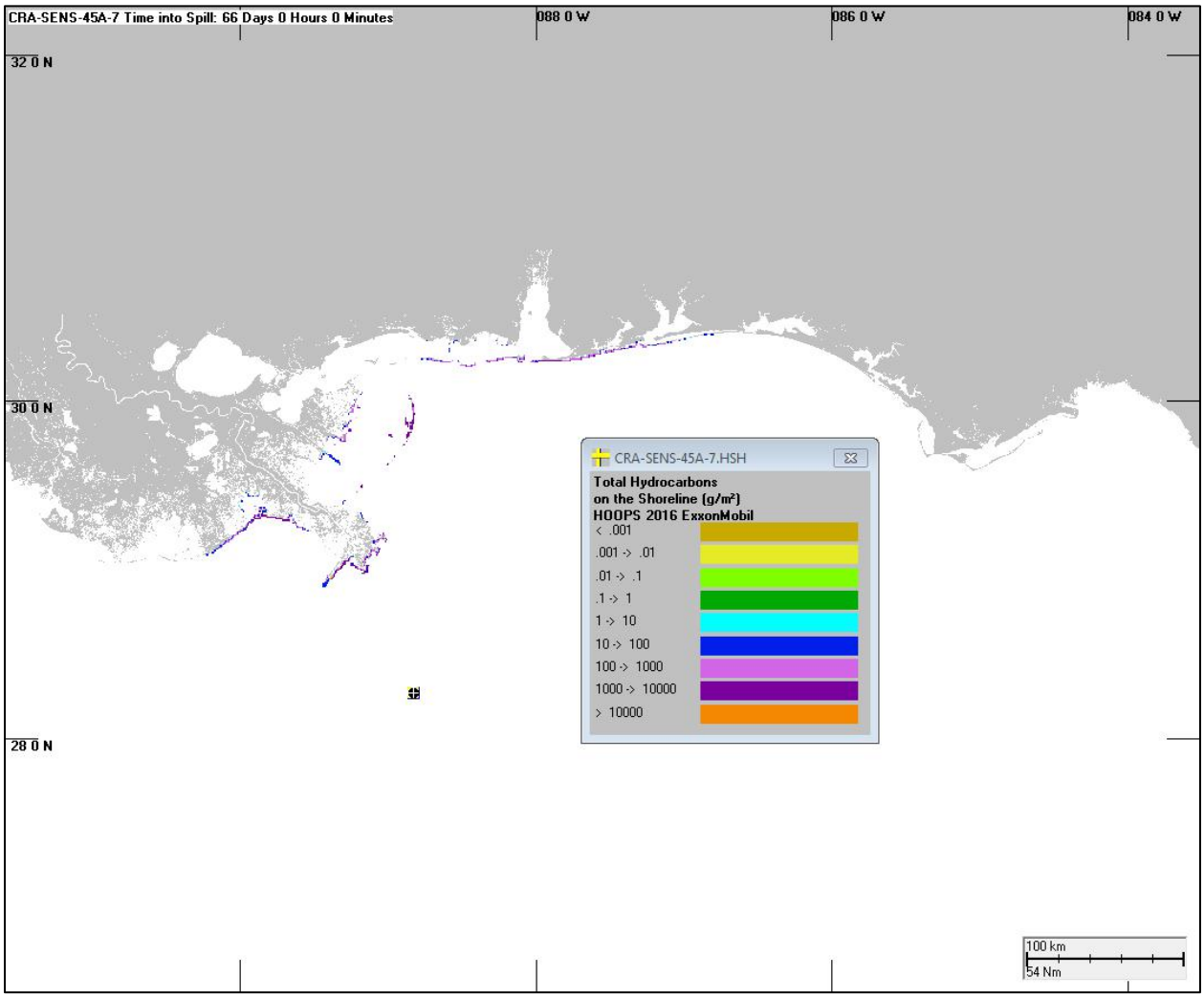

Figure C.19. Shoreline oiling at the end of the 66-day simulation for case #7: a spill rate of 45,000 bbl/day (7154 m^3/day) over 21 days from an 1100-m intrusion depth, assuming d_{50} = 2000 µm, s_d = 0.5, and base-case degradation rates.

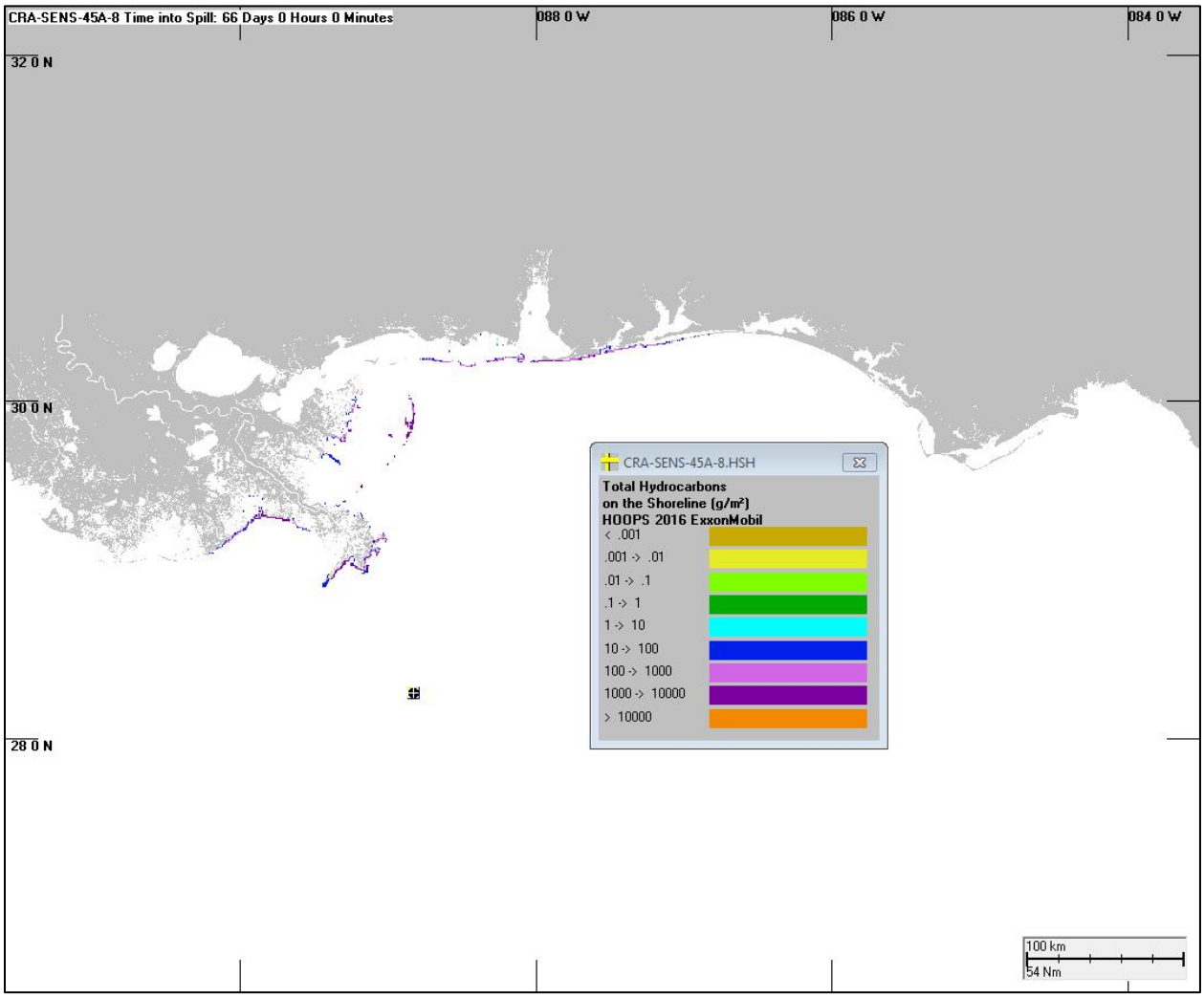

Figure C.20. Shoreline oiling at the end of the 66-day simulation for case #8: a spill rate of 45,000 bbl/day (7154 m^3/day) over 21 days from an 1100-m intrusion depth, assuming d_{50} = 5000 µm, s_d = 0.5, and base-case degradation rates.

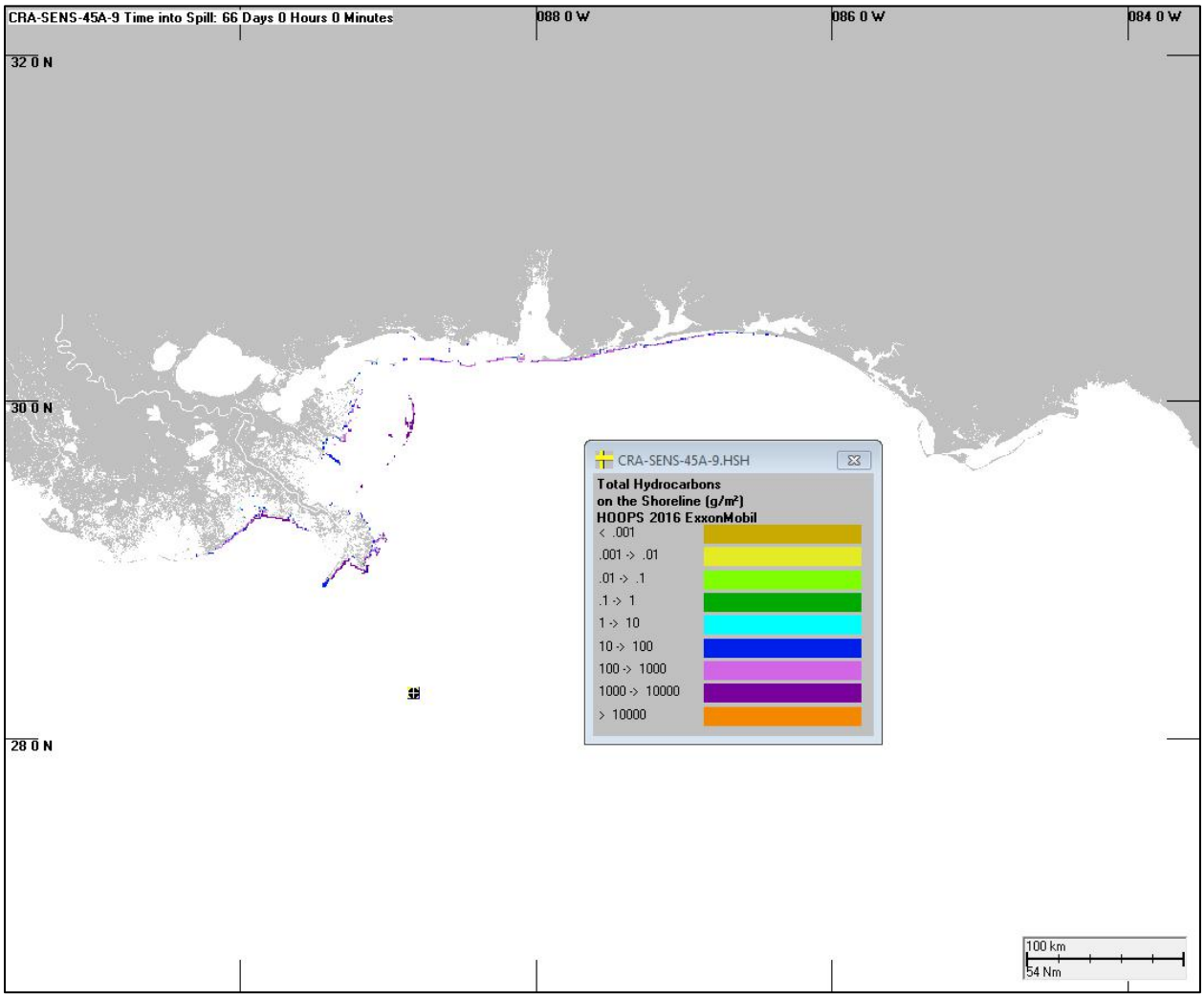

Figure C.21. Shoreline oiling at the end of the 66-day simulation for case #9: a spill rate of 45,000 bbl/day (7154 m^3/day) over 21 days from an 1100-m intrusion depth, assuming d_{50} = 5000 µm, s_d = 0.5, and base-case degradation rates. MBSD is also included in this scenario.

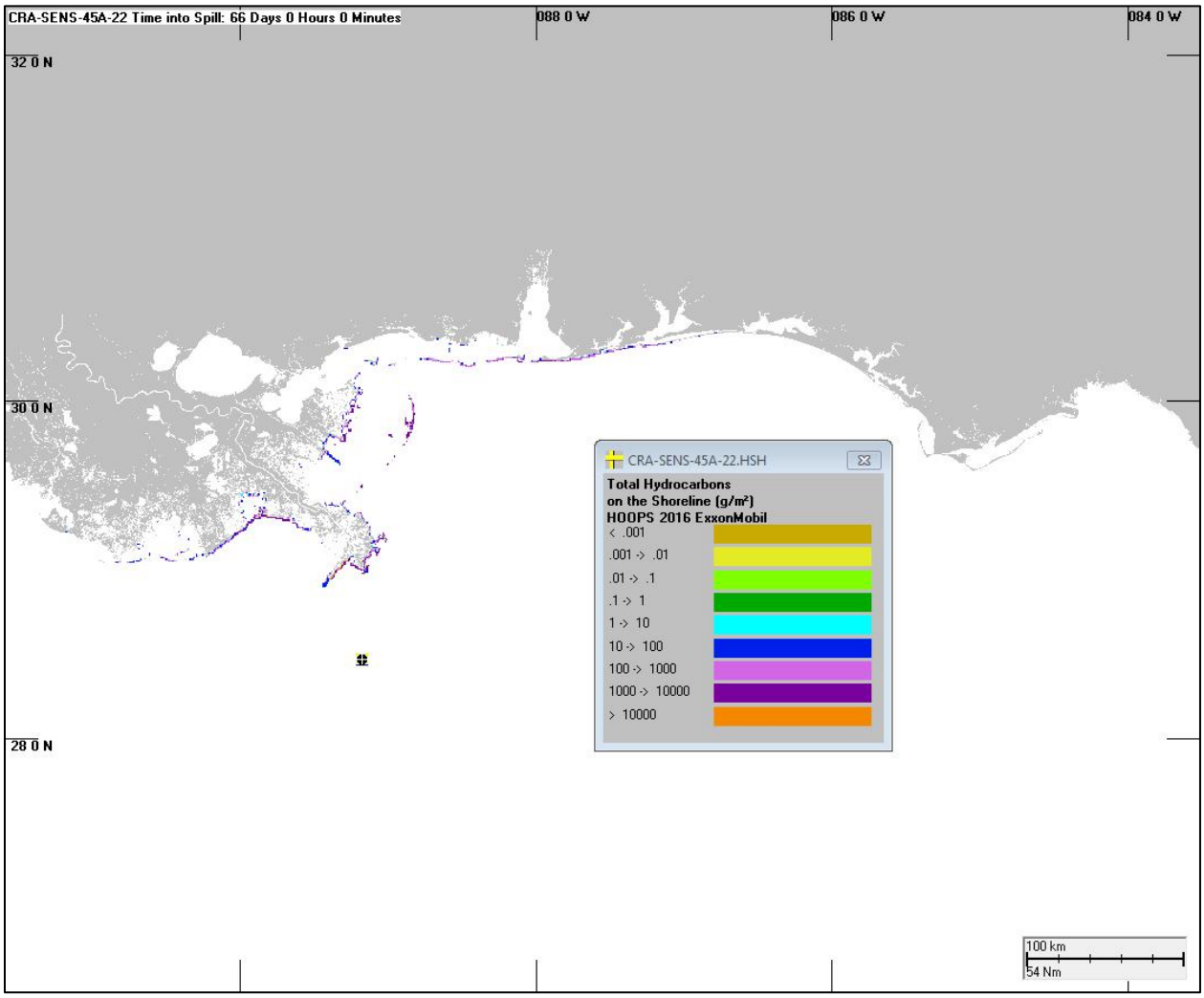

Figure C.22. Shoreline oiling at the end of the 66-day simulation for case #22: a spill rate of 45,000 bbl/day (7154 m^3/day) over 21 days from a 100-m intrusion depth, assuming d_{50} = 250 μm, s_d = 0.5, and base-case degradation rates.

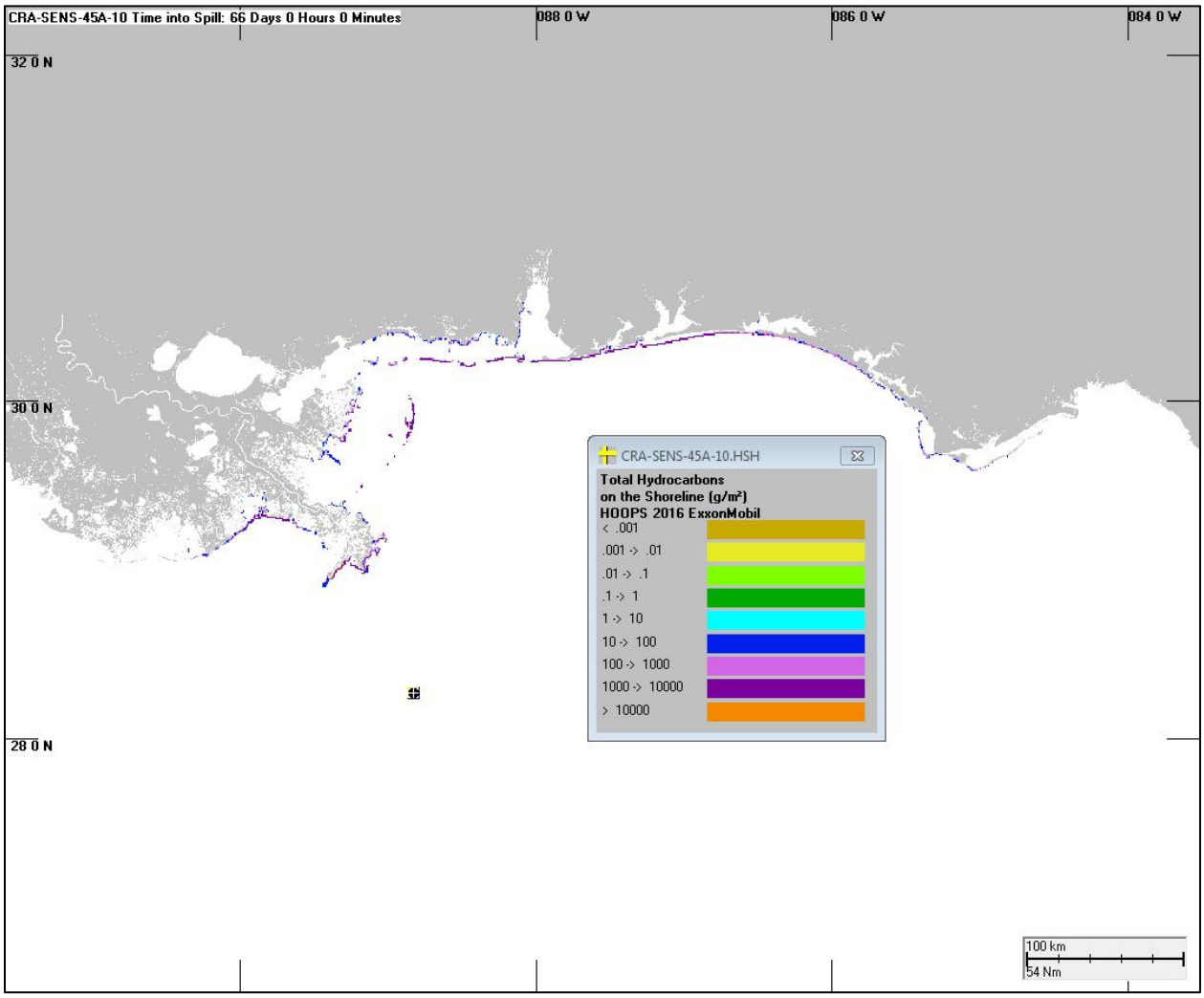

Figure C.23. Shoreline oiling at the end of the 66-day simulation for case #10: a spill rate of 100,000 bbl/day (15,899 m^3/day) over 21 days from an 1100-m intrusion depth, assuming d_{50} = 250 μm, s_d = 0.5, and base-case degradation rates.

Appendix D Definition of Oil Pseudo-Components Modeled with SIMAP

The oil pseudo-components are defined in Table D.1, as utilized in French-McCay et al. (2015, 2016, 2018a,c,d). Table D.2 lists the HOOPS oil composition (ExxonMobil 2016) assumed in the modeling.

Table D.1 Code designations and included compounds for the 19 pseudo-components. [BP = boiling point].

Code	Group	Includes
AR1	BTEX	BTEX, styrene
AR2	C3-benzenes	C3-benzenes (Trimethlybenzenes, propylbenzenes, ethyl-methylbenzenes, cumene & trimethylbenzenes, and Methyl-thiophene)
AR3	C4-benzenes	C4-benzenes (butylbenzenes, tetramethlybenzenes, tetralin)
AR4	Decalins	cis/trans decalin to C4-decalin
AR5	C0-C2 Naphthalenes	C0-C2 Naphthalenes, C0-C2 Benzothiophenes, biphenyl, acenaphthene, acenaphthylene
AR6	C3-C4 Naphthalenes	C3-C4 Naphthalenes, C3-C4 Benzothiophenes, dibenzofuran
AR7	Fluorenes & C0-C1 3-ring PAHs	C0-C3 Fluorenes, C0-C1 dibenzothiophenes, C0-C1 phenanthrenes
AR8	4-ring PAHs & C2-C3 3-ring PAHs	C0-C2 pyrenes & fluoranthenes, C2-C3 dibenzothiophenes, C2-C3 phenanthrenes, chrysene
AR9	Soluble alkanes	Low molecular weight Alkanes, Isoalkanes, Cycloalkanes
AL1	Aliphatics: BP < 150	Unmeasured compounds, using the properties of C6-C8 alkanes (n-hexane, n-heptane, n-octane)
AL2	Aliphatics: BP 150-180	Measured and unmeasured compounds, using the properties of C9-C10 alkanes (n-Nonane, and n-Decane)
AL3	Aliphatics: BP 180-200	Measured and unmeasured compounds, using the properties of C11 alkanes (n-Undecane)
AL4	Aliphatics: BP 200-230	Measured and unmeasured compounds, using the properties of C12 alkanes (n-Dodecane)
AL5	Aliphatics: BP 230-280	Measured and unmeasured compounds, using the properties of measured C13-C16 alkanes
AL6	Aliphatics: BP 280-300	Measured and unmeasured compounds, using the properties of measured C17-C18 alkanes
AL7	Aliphatics: BP 300-350	Measured and unmeasured compounds, using the properties of measured C19-C20 alkanes
AL8	Aliphatics: BP 350-380	Measured and unmeasured compounds, using the properties of measured C21-C23 alkanes
AL9	Dispersant indicator(s)	Dispersant indicator(s) on oil droplets
Residual	Residual	Other non-volatile, non-soluble hydrocarbons

Table D.2 Fraction of HOOPS oil in each pseudo-component.

Insoluble Component and Boiling Range (°C)	Fraction of Oil	S/SS HC Component (log(Kow) Range)	Fraction of Oil
AL1 (< 150°C)	0.0300	AR1: MAHs/BTEX (1.9-2.8)	0.01183
AL2 (150-180°C)	0.0308	AR2: C3-benzenes (2.8-3.6)	0.00709
AL3 (180-200°C)	0.0289	AR3: C4-benzenes (3.1-3.8)	0.00481
AL4 (200-230°C)	0.0486	AR4: Decalins (4.1-6.0)	0.00186
AL5 (230-280°C)	0.0818	AR5: C0-C2 Naphthalenes (2.3-4.3)	0.00238
AL6 (280-300°C)	0.0311	AR6: C3-C4 Naphthalenes (4.2-5.2)	0.00253
AL7 (300-350°C)	0.0827	AR7: Fluorenes & C0-C1 3-ring PAHs (4.0-5.6)	0.00149
AL8 (350-380°C)	0.0480	AR8: 4-ring PAHs & C2-C3 3-ring PAHs (4.9-6.0)	0.00247
(AL9 not applicable)	-	AR9: Low MW Isoalkanes, Cycloalkanes (2.3-5.6)	0.1522
Total	0.3819	Total	0.1867